

CZECH TECHNICAL UNIVERSITY IN PRAGUE

FACULTY OF MECHANICAL ENGINEERING  
DEPARTMENT OF POWER AND PROCESS TECHNOLOGY



**Mechanical Stability of Carbon fiber reinforced composite pipe  
for ion accelerator research facility**

BACHELOR THESIS

Supervisor: Ing. Mgr. Daniel Hadraba, Ph.D.

2022

Ali Sadig



# BACHELOR'S THESIS ASSIGNMENT

## I. Personal and study details

Student's name: **Sadig Ali Mohamed Salih** Personal ID number: **481754**  
Faculty / Institute: **Faculty of Mechanical Engineering**  
Department / Institute: **Department of Process Engineering**  
Study program: **Bachelor of Mechanical Engineering**  
Branch of study: **Power and Process Technology**

## II. Bachelor's thesis details

Bachelor's thesis title in English:

**Mechanical stability of carbon fiber reinforced composite pipe for ion accelerator research facility.**

Bachelor's thesis title in Czech:

**Mechanická stabilita kompozitních trubek z uhlíkových vláken v laboratořích pracujících s urychlovači částic.**

Guidelines:

The thesis will investigate the mechanical stability of carbon composite pipes in vacuum using strain gauges and the effect of radiation on the aging of the pipes for ion accelerator research facilities.

- 1) Review + theoretical part
- 2) Objectives + hypothesis + methods
- 3) Results
- 4) Discussion + conclusion

Bibliography / sources:

Anon., [b.r.]. Carbon Fiber - an overview | ScienceDirect Topics [online] [vid. 2022-02-24].  
FABJAN, Christian W. a Herwig SCHOPPER, ed., 2020. Particle Physics Reference Library: Volume 2: Detectors for Particles and Radiation [online]. Cham: Springer International Publishing [vid. 2022-01-26]. ISBN 978-3-030-35317-9.  
FORD, Eric, 2020. Particle Interactions with Matter. In: Eric FORD Primer on Radiation Oncology Physics [online]. 1. vyd. B.m.: CRC Press, s. 63–72 [vid. 2022-01-26]. ISBN 978-0-429-48888-7.  
HOLLINGS, Gabriel, 2022. Strain Gauges: How they Work, Applications, and Types [online] [vid. 2022-02-06].  
CHUNG, Deborah, 2012. Carbon Fiber Composites. B.m.: Elsevier. ISBN 978-0-08-050073-7.

Name and workplace of bachelor's thesis supervisor:

**Ing. Mgr. Daniel Hadraba, Ph.D. Department of Designing and Machine Components FME**

Name and workplace of second bachelor's thesis supervisor or consultant:

Date of bachelor's thesis assignment: **20.04.2022** Deadline for bachelor thesis submission: **05.08.2022**

Assignment valid until: **18.09.2022**

Ing. Mgr. Daniel Hadraba, Ph.D.  
Supervisor's signature

prof. Ing. Tomáš Jirout, Ph.D.  
Head of department's signature

doc. Ing. Miroslav Španiel, CSc.  
Dean's signature

## III. Assignment receipt

The student acknowledges that the bachelor's thesis is an individual work. The student must produce his thesis without the assistance of others, with the exception of provided consultations. Within the bachelor's thesis, the author must state the names of consultants and include a list of references.

\_\_\_\_\_  
Date of assignment receipt

\_\_\_\_\_  
Student's signature

## Annotation List

**Name:** Ali

**Surname:** Sadig

**Title Czech:** Mechanická stabilita kompozitních trubek z uhlíkových vláken v laboratorních pracujících s urychlovači částic

**Title English:** Mechanical Stability of Carbon fiber reinforced composite pipe for ion accelerator research facility

**Scope of work:**

Number of pages: 107

Number of figures: 72

Number of tables: 17

**Academic Year:** 2021 – 2022

**Language:** English

**Department:** Power and Process Engineering

**Supervisor:** Ing. Mgr. Daniel Hadraba, Ph.D.

**Reviewer:**

**Tutor:**

**Submitter:**

**Keywords:** Particle accelerator; Vacuum; Radiation; Strain gauge; Composite Material

**Affidavit**

I confirm that the diploma (bachelor's) work was disposed by myself and independently, under the lead of my thesis supervisor. I stated all sources of the documents and literature.

In Prague .....

.....

Ali Sadig

## **Acknowledgements**

I would like to express my gratitude towards my supervisor Ing. Mgr. Daniel Hadraba, Ph.D. for his expert guidance throughout this thesis. I would also like to thank Ing. František Lopot, Ph.D. and RNDr. Petr Chudoba, Ph.D. for their assistance during the experiments, and my family for their constant support.

## **Abstract**

This thesis is aimed at understanding the stability of carbon fiber composite pipe under the effects of vacuum and ionizing radiation. General information about vacuum, radiation, carbon fiber, composites, pipe under mechanical loading, strain gauges and selection methods are presented. Essentially, carbon fiber composite pipes manufactured from COMPOTECH with applied strain gauges are evacuated using a vacuum pump and irradiated by TR-24 Cyclotron in Nuclear Physics Institute Irradiation chamber, the experiment includes a control pipe for reference purposes. Data from strain gauges is processed using MATLAB, FEA (Finite Element Analysis) is done through ABAQUS to model composite material stresses and experiment is repeated in CTU labs after radiation dose decreases to safe levels to check effect of strain gauge responses before and after irradiation by subjecting the pipes to vacuum pressures only.

# Table of Contents

Table of Contents .....	7
1. Introduction.....	9
2. Literature Review.....	10
2.1. Particle Research Facilities (Particle accelerators) .....	10
2.2. Vacuum .....	11
2.2.1. Principle of Vacuum pumps.....	13
2.2.2. Effect of Vacuum on materials .....	14
2.3. Radiation .....	15
2.3.1. Ionizing radiation and public exposure .....	16
2.3.2. Radiation Damage on Materials.....	17
2.4. Materials used in Particle accelerators .....	19
2.5. Composites.....	21
2.5.1. Carbon Fiber Reinforced Polymers (CFRP) Composites.....	21
2.5.2. Advantages and Disadvantages CFRP .....	22
2.5.3. Hand Lay-up Process .....	22
2.5.4. Filament Winding Process .....	23
2.5.5. Injection Compression Molding and Reaction Injection Molding.....	25
2.6. Carbon fiber .....	25
2.6.1. Classification and types.....	26
2.6.2. Mechanical properties of Carbon Fiber.....	27
2.6.3. Manufacturing Carbon Fiber from PAN .....	28
2.6.4. Rationale of Composite material use over conventional.....	30
2.7. Composite Pipes.....	34
2.8. Pipes under mechanical load.....	36
2.8.1. Thin wall cylinder stresses .....	38
2.8.2. Lamé's Theory .....	42
2.8.3. Thick cylinders with internal and external pressure.....	45
2.8.4. Thick Cylinder strain and change in dimensions .....	48
2.8.5. Finite Element Analysis (FEA) for Composites .....	49
2.9. Strain gauge.....	50
2.9.1. Selection of a strain gauge .....	52
2.9.2. Strain Gauge types .....	56
2.9.3. Metal foil strain gauge .....	57
2.9.4. Fine Wire strain gauge .....	58
2.9.5. Semiconductor strain gauge .....	59
2.9.6. Strain Gauge configurations.....	60
2.9.7. Quarter-bridge strain gauge Type I and II.....	61

2.9.8.	Half-bridge strain gauge Type I and II.....	62
2.9.9.	Full-Bridge Strain gauge .....	63
2.9.10.	Compensation of Temperature drift of sensor.....	64
2.9.11.	Errors Caused by Lead resistances.....	66
<b>3.</b>	<b>Experiments .....</b>	<b>67</b>
3.1.	Methodology .....	68
3.1.1.	Preparing the mounting Surface.....	70
3.1.2.	Bonding the Strain gauge and Functionality test .....	70
3.1.3.	Cyclotron TR 24 and Turbomolecular pump .....	73
3.1.4.	Sealing Covers assembly and set up in Irradiation Chamber .....	77
3.1.5.	Strain Gauge Data .....	79
3.1.6.	Strain Gauge responses after irradiation .....	84
3.1.7.	Finite Element Analysis (FEA) simulation .....	88
3.1.8.	Theoretical deformation due to internal Vacuum pressure .....	92
4.	Discussion and Conclusion .....	95
<b>5.</b>	<b>References.....</b>	<b>98</b>
	List of Abbreviations .....	105
	List of Tables .....	106
	List of Figures .....	107



# 1. Introduction

Understanding material's behavior under the conditions of operation and environment is a crucial step in ensuring the safe operation of a part and its service lifetime. The motivation behind this thesis is the increase of applications adopting carbon fiber composite parts. This thesis targets a carbon fiber composite pipe that is planned to be used in an accelerator facility.

Where the experiment is focused on subjecting the carbon fiber (CF) composite pipe to vacuum and ionizing radiation. The ionizing radiation dosage may cause some changes in the microstructure of the material and due to the aging from radiation damage, possible alterations in the mechanical properties of the part can occur affecting its service lifetime. In addition to the fact that the pipes are long and subjected to high vacuum pressure they are susceptible to buckling which is not a well-known phenomenon in composite materials.

Firstly, a literature search is described about Particle accelerators and their necessity of vacuum followed by an introduction about Vacuum, Vacuum pumps, and effect of vacuum on materials. Additionally, radiation concept, ionizing radiation, and its damage on materials. Along with brief description about materials applied in particle accelerator facilities. Moreover, an introduction to composite materials as it became a modern-day replacement for conventional materials and specially carbon fiber composites considering their growing rate in different applications utilizing their remarkable properties including its advantages and disadvantages.

Furthermore, a description of typical manufacturing methods for composite materials and an overview of carbon fiber, types, properties, production, and rationale of composite material replacement to conventional is presented. In addition to composite pipe, thin and thick wall cylinder stress theory is stated. With regard to the experiment performed, strain gauges selection, types, configuration along with errors compensation is described summing up the literature review of this thesis.

Lastly, a demonstration of the experiments performed with steps involving application of strain gauge, assembly of covers, evacuation of the assembly, radiation source specification, experiment set up and plots of filtered data obtained from strain gauge outputs. In conclusion, three sets of data are acquired where stresses due to internal vacuum pressure and outside ambient pressure is analyzed through finite element analysis (FEA) as well as buckling analysis. Along with critical buckling pressure with a theoretical approach including dimensional deformations.

## 2. Literature Review

### 2.1. Particle Research Facilities (Particle accelerators)

A particle accelerator is a machine that raises the energy of small particles like electrons or protons. Fundamentally, particle accelerators create charged particle beams that can be applied to a variety of scientific research purposes. Particle accelerators can be divided into two categories: linear accelerators and circular accelerators. Particles are propelled down a linear, or straight, beam line, by linear accelerators. While in circular accelerators particles are propelled in a circle. While circular accelerators can be utilized for both colliding beam and fixed target studies, linear accelerators are employed for fixed-target investigations. [55].

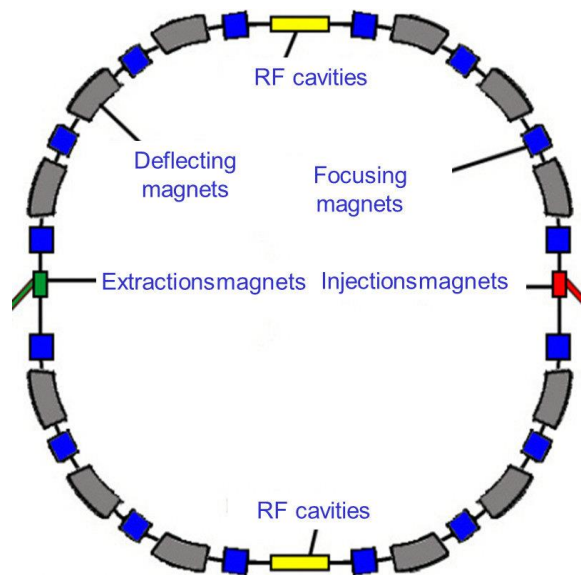


Figure 1: Typical Components of a circular accelerator , RF (Radio-frequency) cavities [56].

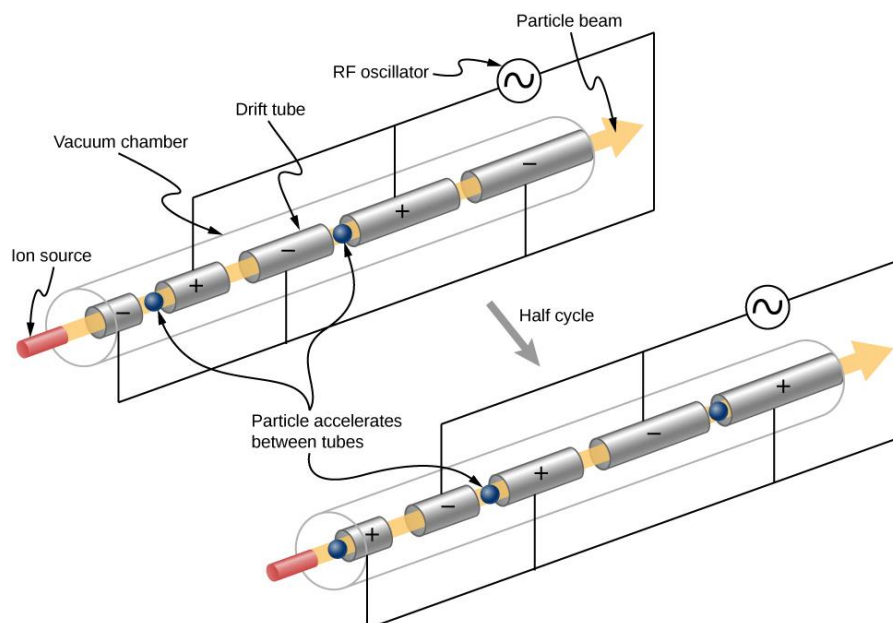


Figure 2: Linear accelerator with charged tubes [57].

Particle beams are directed and concentrated by magnetic fields, while particle accelerators use electric fields to accelerate and boost the energy of the beam. The protons or electrons that need to be accelerated come from the particle source. The metal beam pipe carries the particle beam as it moves through vacuum. In order for the particle beam to move freely, there needs to be no air or dust in the area of travel[55].

The beam of particles is directed and focused by electromagnets as it passes through the vacuum tube. Radiowaves are produced when the electric fields positioned around the accelerator switch from positive to negative at a specific frequency, accelerating particles in bulks. Two particle beams can collide or be directed at a fixed target, such as a thin strip of metal foil. Particle detectors capture and reveal visible radiation and particles created when a beam of particles collides with a target [55].

## 2.2. Vacuum

Vacuum is defined as a partially empty space, where some of the air and other gases have been removed from a gas containing volume. In other terms, vacuum is any volume containing less gas particles, atoms, and molecules (lower particle density and gas pressure), than there are in the surrounding outside environment. Hence, vacuum is the gaseous environment at pressures lower than atmospheric level. A characterization of vacuum can be made by measuring the force per unit area where particles are in constant motion when they are contained, hitting the walls of the container and this force per unit area is known as pressure. By comparing the pressure caused by the contained particles to the atmospheric pressure, one can determine the number and the intensity of particle impacts on a unit of surface area [58].

In Figure 3, Absolute, gauge, atmospheric and vacuum pressures are depicted by lines to show the difference of the pressures and how they are achieved. Initially, the zero reference to a perfect vacuum is known as absolute pressure which exists in the air free space of the universe denoted by Abs. Absolute pressure is the sum of gauge pressure and atmospheric pressure [59].

$$P_{abs} = P_{gauge} + P_{atm}$$

Gauge pressure ( $P_{gauge}$ ) is the pressure zero referenced against ambient pressure. Also known as overpressure. Gauge pressure is positive whenever it is higher than atmospheric pressure and negative when lower [59].

$$P_{gauge} = P_{abs} - P_{atm}$$

Atmospheric pressure is known as the pressure exerted by the weight of the atmosphere also referred to as ambient pressure (pressure around any person on earth). The standard value of air pressure at sea level is approximately 101,325 Pa. Finally, as mentioned before the vacuum

pressure is the pressure below atmospheric pressure measured by vacuum gauges, indicating the difference between atmospheric pressure and absolute pressure [59].

$$P_{vacuum} = P_{atm} - P_{abs} \quad or \quad P_{vacuum} = -P_{gauge}$$

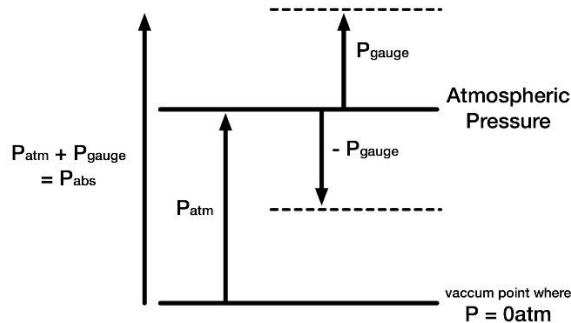


Figure 3: Absolute, Gauge, Atmosphere, and vacuum pressure [59].

Evacuation is the process of emptying a physical space of any gas until a desired target pressure is reached. In Most Industrial cases this gas is ambient air [61]. Different levels of vacuum are achievable by different pumps and the levels of industrial vacuum systems can be classified into the following groups [62]:

- Rough/Low Vacuum: 1000 to 1 mbar
- Fine/ Medium Vacuum: 1 to  $10^{-3}$  mbar
- High Vacuum:  $10^{-3}$  to  $10^{-7}$  mbar
- Ultra-High Vacuum:  $10^{-7}$  to  $10^{-11}$  mbar
- Extreme High Vacuum:  $< 10^{-11}$  mbar

Vacuum pressure is measured relative to ambient atmospheric pressure [63]. Absolute pressure is not the same as vacuum pressure as it is measured with respect to an absolute zero point. On the other hand, Vacuum pressure is expressed negatively with respect to atmospheric pressure [64]. Pressure sensors are used in many applications like automotive, medical, industrial, and building devices as they rely on precise and stable pressure measurements to operate reliably [65]. A pressure sensor has a measuring cell that transduces mechanical strain due to pressure applied and transmutes the force into an electrical signal which can then be scaled into pressure units. Whether pressure in a pipe, duct or hose applied force on the measuring cell of a sensor causing deflection which is measured by the electrical circuit and hence the output is recorded [66].

The Most prevailing method of creating a vacuum is by pumping gas out of a vessel that is initially at atmospheric pressure. There exist many ways of pumping on a vessel, nevertheless all of them have a limiting pressure below which they are ineffectual. The lowest achievable pressure by a

particular pump is called the ultimate pressure of the pump. Some pumps also have a limiting pressure ( $> 1$  atm) above which they are ineffective. Therefore, such pumps are preceded by another pump called a forepump which achieves the pressure in the vessel within the operating range. Usually pumps which require a fore pump require a backing pump as well. The backing pump is used to extract residual gases from the main pump to keep it at low enough pressure to operate. The pressure of the backing pump is known as the backing pressure [61].

Different Pumps will evacuate a vessel in different ranges of time. The time for a pump to achieve its ultimate pressure relies on not only the type of a pump, but also the volume of the vessel to be evacuated and the size of the tubing connecting the pump to the vessel. The pump down speed (S) of a complete vacuum system (Pump +tubing +vessel) is defined by [61]:

$$S = \frac{Q}{P}$$

Where Q is the volume of the gas leaving the system per unit of time, and P is the pressure of the system. There are two basic categories of vacuum pump: Gas transfer pumps and entrapment or capture pumps (see figure 4) [62].

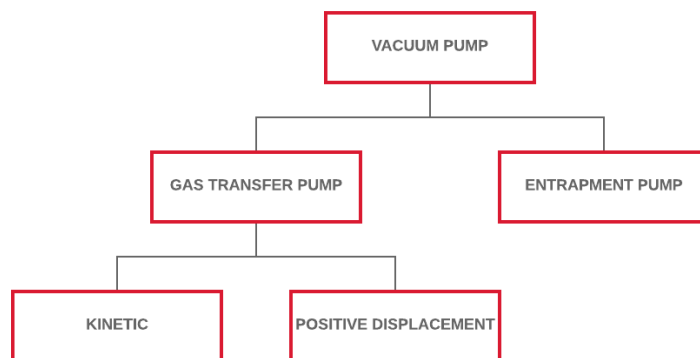


Figure 4: Classification of vacuum pumps [62]

### 2.2.1. Principle of Vacuum pumps

The basic operating principle of industrial vacuum pumps is comparatively the same when it comes to different types of pumps. Vacuum pumps extract air molecules (and other gases) from the vacuum chamber (or the outlet side in the case of a higher vacuum pump connected in series). As the pressure in the chamber is reduced, removing additional molecules becomes increasingly harder to remove. Therefore, industrial vacuum systems should be able to operate over a portion of a large pressure range, depending on the level of vacuum needed the vacuum pump selection is based on the effective operating range of the pump [68].

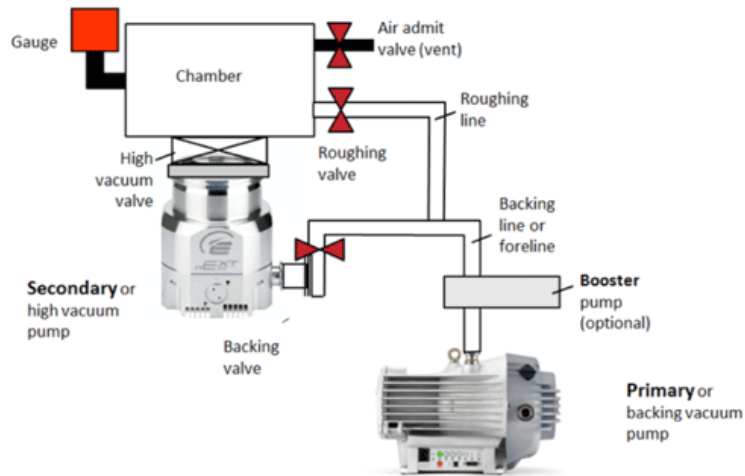


Figure 5: Typical industrial vacuum system[68]

Kinetic transfer pumps work on the principle of momentum transfer. Guiding gas towards the pump outlet to provide an increasing probability of molecule traveling towards the outlet via high-speed blades or instigated vapor. Kinetic pumps can achieve high compression ratios at lower pressures but does not have sealed volumes. On the other hand, Positive displacement pumps operate mechanically by enclosing a volume of gas and moving it through the pump. They are usually designed with multiple stages on the same drive shaft. The separated volume is compressed to an even smaller volume at a higher pressure where the compressed gas is expelled to the atmosphere [68].

Entrapment pumps seize the gas molecules on the surfaces within the vacuum system [68]. This type of pump operates at lower flow rates than transfer pumps but can provide ultra-high vacuum to  $10^{-11}$  mbar and produce an oil-free vacuum. Entrapment pumps operate utilizing cryogenic condensation, ionic reaction or chemical reaction and have no moving parts [68].

### 2.2.2. Effect of Vacuum on materials

When a material is exposed to high vacuum, there are two effects which require main consideration [67]:

- I. The enhancement of sublimation and evaporation processes.
- II. The removal of physically adsorbed layers of gas from the surface of the material.

The ancillary effects on subsurface transport should be considered even though they are less important. Any material, especially organic materials like polymers and plastics, is more severely impacted by vacuum conditions when thermal variables are added (i.e., thermal cycling between 0 and 100 °C). Furthermore, there are at least two general methods in which the release of adsorbed gases and vapors might speed up the deterioration of materials. First, by altering concentrations or

creating color centers, desorption can have a direct impact on a material's optical characteristics. Second, the passage of gases through the material (diffusion) may result in structural flaws like cracks and pores or it may disrupt the contact between the surface material and the substrate. Another observation was the acceleration of chemical activity in vacuum, which makes sense given the absence of a protective surface coating to prevent oxidation. In addition, molecular oxygen is already dissociated by the ultraviolet space into atomic oxygen which is more reactive than molecular version [67].

The actual process of evaporation is fundamentally a true surface phenomenon, even though its rate may be controlled by other factors. Since evaporation is from localized planes of high surface energy which tends to be greater than that of points with lower surface energy, microscopic etching of the surface occurs. This can be most detrimental in the case of thin metallic films, however, because of the self-balancing of surface-tension forces and grain-boundary energies the problem is not particularly severe in bulk materials but can cause stress concentration problems and eventually crack initiation. In most metals, sublimation losses are negligible. However, the extraction of surface layers of gas, especially oxygen, may seem to be very beneficial to the mechanical properties of the metal in some cases. In other instances where oxide films can move into incipient cracks and thus promote crack growth, it may be expected that the lack of oxygen on the surface may decrease the risk of crack growth and therefore result in greater fatigue life. Other effects such as changes in surface energy and internal diffusion in the vicinity of a stress concentrator may become significant at extremely low pressures [67].

### 2.3. Radiation

The definition of the ability to do work is energy [73], radiation is a form of energy transmitted from a source and travels via space at the speed of light including an electric field and a magnetic field analogous to it giving radiation wave-like properties [75]. There are two types of radiation : non-ionizing radiation and ionizing radiation. Non-ionizing radiation has energy giving it the capability to cause vibrations on atoms of a molecules or move them around within the molecule. Visible light, infrared rays, microwaves and radio waves are examples of non ionized radiation [73].

Ionizing radiation has enough energy to knock electrons outside an atom, this process is known as ionization. Atoms in living things can be affected by ionizing radiation, hence making it a health risk through damaging tissues or altering DNA in genes [75]. Alpha, beta , gamma and x-rays are examples of Ionizing radiation. Ionizing radiation can be categorized as electromagnetic or particle radiation [73].

The term "electromagnetic spectrum" refers to the whole distribution of electromagnetic radiation according to frequency or wavelength. Although all electromagnetic waves have a broad range of frequencies, wavelengths, and photon energies, they all move at the speed of light in a vacuum. The

electromagnetic spectrum comprises the entire range of electromagnetic radiation and is divided into numerous subranges, generally known as portions, like visible light and ultraviolet radiation [74].

The various portions have different names depending on variations in the emission, transmission, and absorption of the corresponding waves as well as on the many practical uses for which they are put to use. The ranges frequently overlap since none of these contiguous segments have clear, established borders. The full range of electromagnetic radiation, from lowest to highest frequency (longest to shortest wavelength), which includes all radio waves (such as those used in microwaves, radar, commercial radio, and television), as well as visible light, ultraviolet light, X-rays, and gamma rays. Spectroscopy can be applied to almost all electromagnetic radiation wavelengths and frequencies [74].

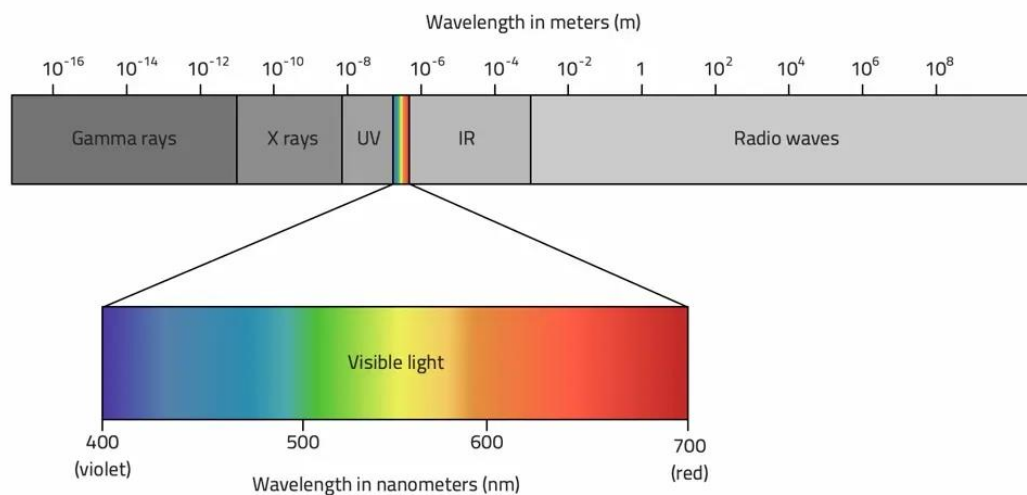


Figure 6: Components of electromagnetic spectrum[69]

### 2.3.1. Ionizing radiation and public exposure

Ionizing radiation is a type of energy that affects atoms and molecules of substances like air, water, and living tissue by removing electrons from them. These materials are permeable to invisible ionizing radiation. Ionizing radiation is in the radio waves group, which includes x-rays, alpha, beta particles, and gamma rays, on the extreme right side of the electromagnetic spectrum. A common example of ionizing radiation is that of x-rays which can penetrate our body and reveal pictures of our bones. The term “ionizing” refers to the unique capability to remove electrons from atoms and molecules in the matter through which they pass. “Ionizing” activity can alter molecules within the cells of our body. That action may cause eventual harm (such as cancer). Intense exposure to ionizing radiation may produce skin or tissue damage [71].



Generally, we are surrounded by radiation. Inside, outside, and above the planet we live in. It is a natural energy force that exists around us, being part of our natural world ever since the birth of Earth. All living beings, ever since the beginning of time have been and will still be exposed to ionizing radiation. Sources of ionizing radiation can come from very high temperatures, through acceleration of charged particles in electromagnetic fields, nuclear reactions and nuclear decay. Typically, there are two wide categories of radiation sources [72]:

1. Natural Background Radiation, which includes radiation generated from lightnings, the sun, primordial radioisotopes or even supernova explosions etc.
2. Man-made sources of radiation, which includes medical utilization of radiation, residues from nuclear reactors or tests, industrial uses of radiation etc.

Since radiation can cause possible harm when humans are exposed to high doses of radiation measured in mSv (millisievert), after exposition of the pipes in this thesis's experiment to radiation they have to be stored safely until their dose decreases to safe levels . Figure 7, below shows radiation exposure levels that can be fatal when increased.

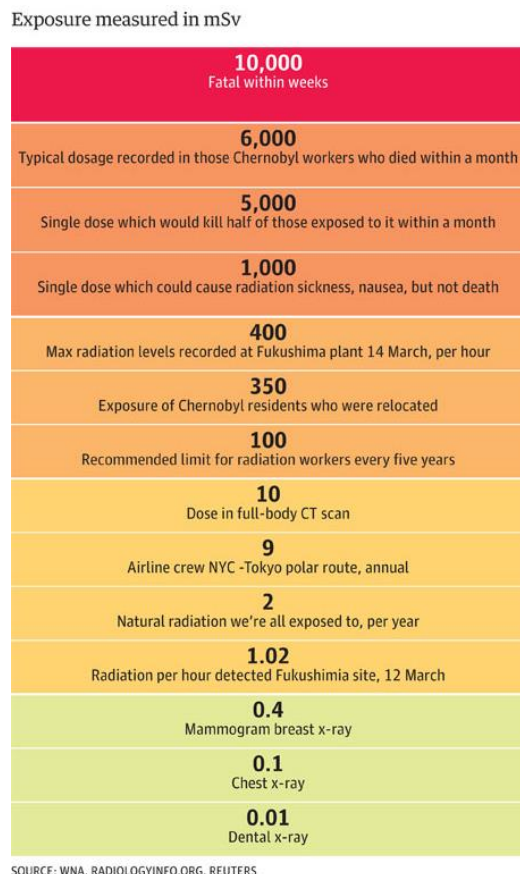


Figure 7: Comparison of radiation exposure levels [90]

### 2.3.2. Radiation Damage on Materials

Whenever a material is selected for application in a radioactive environment (i.e. ion research facilities, particle accelerators , nuclear power plant etc..) the effect of radiation on the material is

of major interest. Radiation can lead to segregation and diffusion of atoms within materials, leading to phase segregation and voids as well as enhancing the effects of possible stress corrosion cracking [70].

One of the consequences of interactions with high energy particles (photons, neutrons, ions or electrons) with crystalline materials is the formation of lattice defects resulting from the energy transfer to the atoms. Figure 8, demonstrates the process of damage initiation in a displacement cascade triggered by a neutron or an ion. This damage, and its evolution with time, determines the macroscopic response of a material to radiation. The damage production is divided into two categories [70]:

- Primary damage that is formed immediately (within few picoseconds) after the ion/neutron/electron impact by atomic collision processes far from thermodynamic equilibrium.
- Long time scale (nanoseconds to years) damage evolution caused by thermally activated processes.

If a material is irradiated under extremely low temperature condition such as less than 10K, almost all defects created by radiation are motionless. In such a case the long term damage may be approximated only by the superposition of many primary radiation damage events like the build up of the athermal damage production. In the majority of practical situations such as nuclear power plants for example, the exposure temperatures are sufficiently high for thermally activated motion of defects, leading to clustering, precipitating, segregating at dislocations and grain boundaries. Micro and often nano structural evolutions may lead in the long run to significant change of thermo-mechanical properties of materials: typically hardening and embrittlement, as well as swelling, irradiation creep and other degradation processes [70].

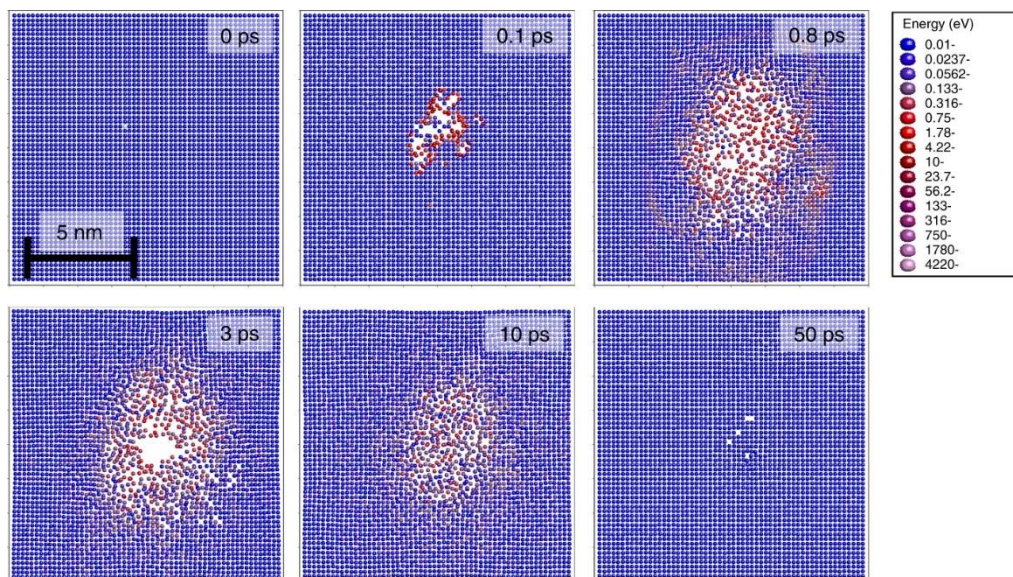


Figure 8: Displacement cascade initiated by neutron or ion impact[70]

Note that in figure 8 above the circles indicate the atom positions in a 1 unit cell thick cross-section through the center of the simulation cell, and the color scale is the kinetic energy of the atoms.

We can notice that a very large number of atoms is initially displaced, but when the cascade cools down, almost all of them return to perfect crystal positions. This is due to the athermal recombination effect. However, many atoms of the material do not return to the same position they started in, hence the number of atom replacements is much larger than the defects produced [70].

In polymeric materials, high energy radiation generates ionization and excitation in polymer molecules. Leading the high energy molecules to experience abstraction, dissociation and undergo additional reactions leading to chemical stability. The stabilization process can occur in any period of time whether immediately after, or days, weeks or even months after irradiation. Resulting in physical and chemical chain scission or cross-linking. Which can lead to degradation of the polymer's main chain [91, 92].

Radiation ordinarily affects polymers in two basic modes, both generated from excitation or ionization of atoms. The two modes are chain scission, a random fracture of bonds leading to reduction of the molecular weight (i.e, strength) of the polymer, and cross-linking of the molecules which generates a large three-dimensional molecular network [91].

When a polymer is exposed to irradiation by ionizing radiation like x-rays, gamma rays or accelerated electrons different effects can be predicted from the ionization that takes place. As the ratio of outcome recombination, cross-linking and chain scission will differ from polymer to polymer and to some extent from part to part based on the chemical composition and structure of the polymer, the total radiation dose impacted and the duration of exposition [91].

## 2.4. Materials used in Particle accelerators

Design and innovation are fundamentally reliant on choosing the best material for a given application. The quality of an engineering design is limited by the materials that are available to an engineer. Nuclear applications must consider a material's nuclear physics properties in addition to its chemical, physical, and electronic qualities. Conventional applications are primarily concerned with material's chemical, physical, and electronic properties. The extra limitation in nuclear materials engineering presents both challenges and opportunities for the field of material science [76].

Particle accelerators pose harsh conditions that its components materials should be able to endure to reliably operate and avoid compromising particle production efficiency by limiting the beam parameters [78]. As mentioned earlier, for the beam of particles to travel unobstructed, there needs to be no air or dust in the area of travel hence the beam pipe needs to have most minimalistic effects of vacuum on the material. In numerous accelerator beam lines and target facilities, Beryllium is currently the material of choice for important accelerator components including beam

windows and secondary particle production targets. The rationale of the use of Beryllium for such components is its transparency to particles, high specific stiffness and suitability with ultra-high-vacuum [79].

Beampipes present the most intimate interaction between the particle accelerator and experiments when running. In circular accelerators, where two beams of particles counter-rotate inside a continuous vacuum chamber ring and collide secondary particles are produced. All of the secondary particles perceived by the experiment pass first through the beampipe [79]. Unwanted signals in the detectors and activation of the beampipe material is caused when particles interact with the material of the beampipe. These interactions are characterized by the property of radiation length ( $X_0$ ), which is the distance a particle travels before losing  $1/e$  of its energy. This distance is inversely proportional to the product of density and atomic number hence materials with low atomic number and density are required to reduce such interactions. Chambers that are thin-walled with few mechanical supports reduced these interactions, indicating that higher the elastic modulus leads to lower interactions [80].

A demonstration of efficiency has been established considering different materials for an application considering a cylindrical, simply supported evacuated chamber which is equal to  $X_0 E^{1/3}$ . Table 1 shows these values for potential materials, where CFC (Carbon Fiber Composite) being a typical high modulus material and Be-Al which is a 62 % beryllium alloy. We can see that the material choice for these chambers is beryllium but on the other hand, beryllium is quite expensive to produce and has safety regulations when it comes to its usage. Therefore, applications are limited to critical areas specifically in the vertex region where the two beams collide [80].

Material	E (GPa)	$X_0$ (m)	$X_0 E^{1/3}$
Be	290	0.353	2.34
CFC	200	0.271	1.58
Be-Al	193	0.253	1.46
Al	70	0.089	0.37
Ti	110	0.036	0.17
Fe	210	0.0018	0.11

Table 1: Figures of Merit for Transparent Beampipes [80]

Moreover, Beam collimators which are devices that focus and direct beams in one direction [81], are made using tungsten (W) alloys. Tungsten poses high density  $19.3 (g/cm^3)$  and extremely high melting point up to  $3420 \text{ }^\circ\text{C}$  which make them suitable as well for shields [82,81]. Remarkable properties of tantalum (Ta) and niobium (Nb) metals make them suitable for superconducting material to create the electromagnetic fields that steer and accelerate the charged particles to exceedingly high speeds [83].

Particle accelerators release radiation when in operation and can produce radioactive waste. Nevertheless, rules and good safety practices make sure that operators and the public are safe when particle accelerators are running [77]

## 2.5. Composites

Composite Materials also referred to as “composites”, whether engineered or naturally occurring materials they consist of two or more constituent materials with remarkable different physical or chemical properties that remain separate and distinct at the macroscopic or microscopic scale within the finished structure [10]. Usually, the constituent materials are of different phase and when combined enhanced properties that cannot be met by a single-phase material is achieved. The constituents are classified in 3 subclasses, including particles, fibers, and structural base [11].

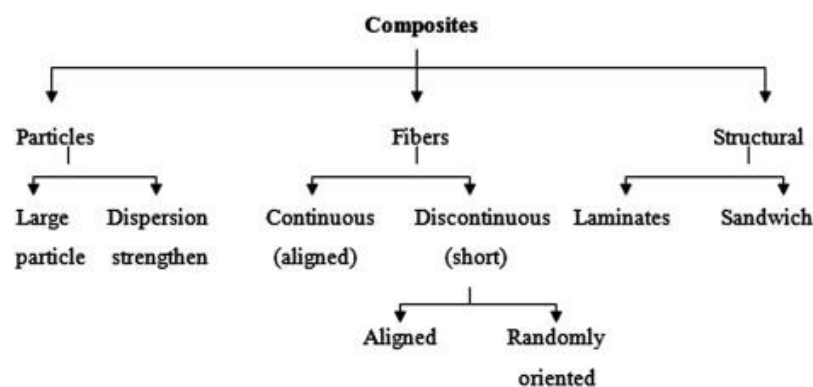


Figure 9: Classification of polymer composites[11]

Most composites are composed of a bulk material and a reinforcement material, generally fibers. The reinforcement materials usually have extremely high tensile and compressive strength, but since they are anisotropic which means it has different strength and stiffness in different directions through the material these theoretical values are not achieved in structural form alone [12].

### 2.5.1. Carbon Fiber Reinforced Polymers (CFRP) Composites

CFRP is a strong, lightweight material where CF is used as reinforcement with a resin matrix. Elevated stress capacity, durability, and best strength to weight ratio promotes it being the most reliable and efficient material in constructional engineering [14]. Continuous fibers in polyester or epoxy matrix provides peak performance. The process variables are what can be changed to vary the stiffness and strength of the CF and hence they are available in high modulus and intermediate modulus form [15]. Fibers convey the mechanical loads, while the matrix material transmits loads to the fibers and facilitating ductility, toughness, as well as protecting the fibers from damage caused by handling or the environment. The service temperature and processing conditions is limited by the matrix material [13].

Manufacturing Fiber-reinforced polymers (FRP) is a skill demanding and labor-intensive process that can be achieved in both one-off and batch production. Generally, in FRP production, the

continuous straight fibers are joined in the matrix to form individual plies, which are laminated layer above layer onto the final product. The composite properties are influenced by the materials as much as the laminating process as the way the fibers are incorporated strongly influences the performance of the part. The thermoset resins are shaped together with the reinforcement in a tool or mold and cured to form a sturdy product [16]. There are several existing laminating techniques available in this chapter common general techniques are discussed.

### 2.5.2. Advantages and Disadvantages CFRP

The well known benefit of CFRP is its strength-to-weight ratio. This characteristic is of major importance in cases where the weight of the object produced has a remarkable influence on its performance. For example, it facilitates light manufacturing vehicles which can use a less powerful engine and save more fuel. CFRP surpasses steel in strength and stiffness. To be accurate, discrete quantity of CFRP will be as strong as steel which amounts 20% of its weight [23]. Secondly, CFRP is distinguished by radiolucence which means they are transparent to x-rays allowing earlier detection of postoperative complications and local recurrence [24]. Thirdly, is the atypical durability. The structure and qualities of the material provides the stability and endurance of harsh environment conditions. Nevertheless, CF material is known for its low thermal expansion which influences the stability of the material. This characteristic matters when small changes of position matter [24].

Even though we have multiple advantages of CFRP, there are various drawbacks of this material that restricts the scope of applying it significantly. Most importantly, cost of the composite material is relatively high. As Manufacturing of CFRP is an intricate process that demands advanced technical equipment which on the other hand will result in high repair cost in case of damages as the process of renovation is complex due to the structure of the material. Each damaged fiber cannot be repaired and hence all the piece of plastic becomes not suitable for use. The cost of the material depends on factors like market situation, fiber tow size, and type of CF. Adding to that, another drawback would be the brittleness of CFRP. Even though the surface of an object may remain unaltered, inner structure can disintegrate in case of damage when being hit. Therefore, additional safety measures are required during when considering an application of CFRP [24].

### 2.5.3. Hand Lay-up Process

To fabricate FRP, Hand layup is a well-known technique and oldest open molding method for fabricating composites. At first, dry fibers in the form of woven, knitted, stitches, or bond fabrics are manually placed in the mold, and a brush is used to apply the resin matrix on the reinforcing material. Subsequently, hand rollers are used to roll the wet composite to ensure an enhanced interaction between the reinforcement and the matrix, to facilitate a uniform resin distribution, and to obtain the required thickness. Finally, the laminates are left to cure under standard atmospheric

conditions. Generally, this process is segmented into four steps: mold preparation, gel coating, lay-up, and curing. Curing is the process of hardening the fiber-reinforced resin composite without external heat. A pigmented gel coat is first applied to the mold surface to obtain a high-quality product surface [17]

The hand lay-up fabrication process is mainly used in marine and aerospace structures. Despite the flexibility in design and easy application, it is not suitable for cylindrical FRP structures such as piping pipeline, tube, casing as well as a pressure vessel [17].

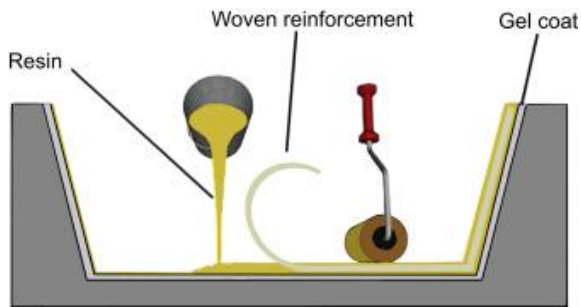


Figure 10: Hand lay-up schematic [17]

#### 2.5.4. Filament Winding Process

A more optimized fabrication method is introduced known as filament winding. This method is either fully or semi-automated depending on the design of the cylindrical structure [18].

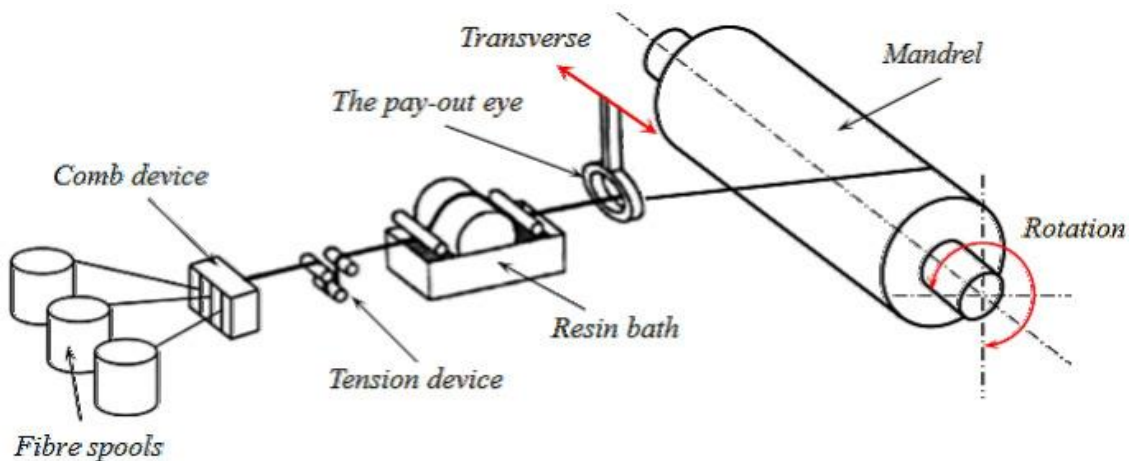


Figure 11: Schematic diagram of filament winding technique [19]

Filament winding is the process of winding advanced fiber or resin impregnated glass around a rotating mandrel, to form a composite structure. By using various fibers, resins and associating different winding techniques, filament winding creates high fiber loading with directional strength properties as it provides a high degree of manipulation over uniformity and fiber orientation. Filament winding process is suitable for highly orchestrated structures and is able to meet stern tolerances when it is computerized, the project conditions affecting productivity for filament winding is lower than that of other open molding processes. The Process is initiated by



having a continuous strand roving that is fed through a resin bath and wound onto a rotating mandrel. The mobile feed runs on a trolley that travels the length of the mandrel. The filament is laid down in a prearranged geometric pattern to provide maximum strength in the directions required. When enough required layers have been applied, the laminate is cured on the mandrel. The molded part is then taken off the mandrel [20].

Equipment are available for filament winding on a regular basis with axis winding for pressure cylinders. Filament winding can be merged with the chopping process and that is known as the hoop chop process. The use of mandrels of specific suitable size and shape, made from steel or aluminium, forms the inner surface of the hollow parts. Some mandrels are foldable to allow part removal[20].

Hence, due to the mechanical restrictions, part shapes that are manufactured with filament winding techniques are limited to mainly axisymmetric and round parts. The exact shape of the wound part depends on the shape of the mandrel. Generally, three types of winding patterns are used [21] :

- a) Circumferencial or hoop
- b) Helical
- c) Polar

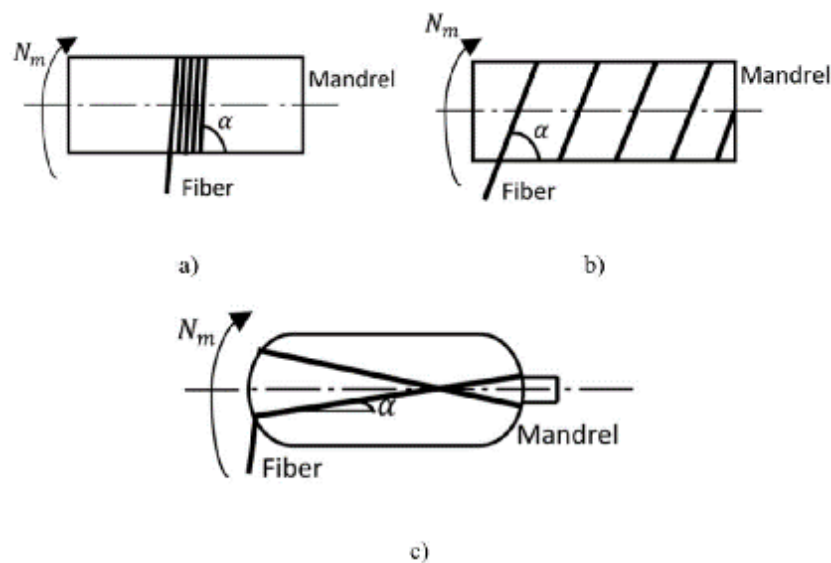


Figure 12: Schematic representation of three types of winding patterns; a) circumferencial winding; b) helical winding; c) polar winding[22]

The classification of the patterns of winding is based upon the winding **angle  $\alpha$**  which is made with the longitudinal axis as shown in figure 12. If the process has the winding angle near the  $90^\circ$ , then it is hoop or circumferencial winding process. Helical winding has constant mandrel rotation while carriage unit is moving with linear propagating motion. Polar winding is generally used for fabrication of high pressure vessels since the fiber is wrapped from one end directly to another on the mandrel, winding angle being close to  $0^\circ$  is required in this pattern [22].



### 2.5.5. Injection Compression Molding and Reaction Injection Molding

There are typically two types of injection molding processes : the screw type injection where the fiber resin mixture is moved toward the mold by the rotation of a screw, and the plunger type injection process. A hopper receives the mixed compound, which is then fed into a heated barrel. With the aid of a rotating screw, the material's viscosity decreases as it moves through the barrel. After reaching the end of the barrel high pressure in the range of 14 to 20 MPa is applied to inject the mixture into the mold. Depending on the product's wall thickness, a holding pressure ( 50% of the injection pressure) is also provided to prevent the mixture from flowing backward. Following the product's curing , the finished product is acquired after the mold is opened. To maintain good mechanical characteristics , plunger type injection molding process is accepted as the screw cuts off the fibers. The production rate of this process is relatively higher than other processes [14].

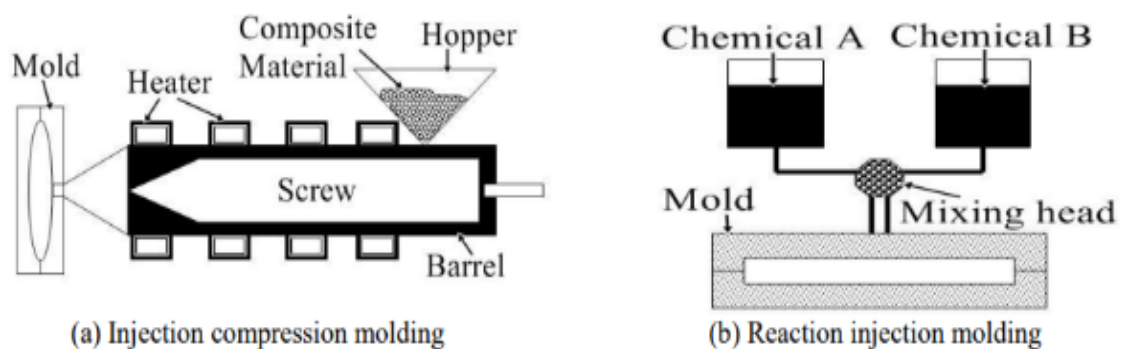


Figure 13: Schematic diagram of injection molding and reaction injection molding process [14]

In reaction injection molding (RIM) , two monomeric or oligomeric chemicals are placed in two separate tanks and combined by injection with high pressure in a mixing chamber. The polymer matrix is created when these vigorously reactive compounds clash under pressures between 10 and 40 MPa [14].

### 2.6. Carbon fiber

Carbon atoms make up most carbon fibers, which have a diameter of about 5 to 10  $\mu\text{m}$ . Along the axis of the fiber, parallel-aligned crystals of carbon atoms are linked together. The fiber's remarkable strength-to-volume ratio is due to the crystal alignment. Materials reinforced with carbon fiber are strong, lightweight, and have good shock absorption qualities. Carbon fibers, on the other hand, have poor shear strength, and when the material cracks, the fibers fall out, causing unpredictable results [1]. While Graphite and carbon fiber both have sheets of carbon atoms arranged in a regular hexagonal pattern also known as Graphene sheets, the way these sheets interlock in carbon fiber is different. In the crystalline substance known as graphite, the sheets are uniformly arranged parallel to one another. Van der Waals forces, which in molecular physics are comparatively weak attractive forces that act on neutral atoms and molecules as they emerge due to the electric polarization that is caused in each of the particles by the presence of other particles, are

the intermolecular forces between the sheets. Thus, this is what causes the soft and brittle features of graphite [2, 3].

Carbon fibers have distinct advantages such as high stiffness, high tensile strength, low weight, high chemical resistance, high temperature tolerance and low thermal expansion. These properties made carbon fiber renowned in aerospace, military, civil engineering, and motorsports. Nevertheless, they are comparatively expensive when compared with similar fibers, like plastic fibers or glass fibers [4].

### 2.6.1. Classification and types

Based on modulus, strength, and final heat treatment temperature, carbon fibers classification can be summarized in the categories shown on the tables below [4]:

<b>CF type</b>	<b>Young's Modulus (E)</b>
Ultra-high modulus (UHM)	$E > 450 \text{ GPa}$
High – modulus (HM)	$350 < E < 450 \text{ GPa}$
Intermediate modulus (IM)	$200 < E < 350 \text{ GPa}$
Low modulus (LM) and high tensile (HT)	$E < 100 \text{ GPa}$ , Tensile strength ( $\sigma_T$ ) $> 3.0 \text{ GPa}$
Super high-tensile (SHT)	$\sigma_T > 4.5 \text{ GPa}$

Table 2: Classification of carbon fiber types based on Mechanical properties

<b>Type Number</b>		
<b>I</b>	<b>II</b>	<b>III</b>
High-heat-treatment carbon fibers (HHT), where the final heat treatment temperature should be above $2000^\circ\text{C}$ and this corresponds with HM type fiber.	Intermediate-heat-treatment carbon fibers (IHT), where final heat treatment temperature is around or above $1500^\circ\text{C}$ and this corresponds with HS type fiber.	Low-heat-treatment (LHT) carbon fibers, where final heat treatment temperatures do not exceed $1000^\circ\text{C}$ . These are low modulus and low strength materials.

Table 3: Classification of carbon fiber types based on final heat treatment

<b>CF precursor fiber material</b>
PAN (polyacrylonitrile) - based
Pitch-based carbon fibers
Mesophase pitch based
Isotropic pitch-based

Rayon based
Gas - phase - grown
Mesophase pitch based

Table 4: Classification of carbon fiber based on precursor fiber material

## 2.6.2. Mechanical properties of Carbon Fiber

The parallel alignment of the carbon atoms that are bonded together in crystals along the axis of the fiber is what leads to CF high strength-to-volume ratio. This property provides CF unique characteristics like high stiffness, high tensile strength, low weight, high chemical resistance, and low thermal expansion. They also have high surface-to-volume ratio and enhanced reactivity as well as improved electrical properties.[6]

The most common precursor used today is PAN and carbon fibers extracted from it inherit the general average carbon fiber mechanical properties shown in table 5 [7]:

Mechanical Properties	
Young's Modulus (E)	200 – 399 GPa
Compressive Strength ( $\sigma$ )	~ 3 GPa
Shear Modulus (G)	~ 15 GPa
Diameter of fiber	5 – 7 $\mu\text{m}$
Density ( $\rho$ )	1.75 – 2.00 $\text{g/cm}^3$
Electrical Conductivity ( $\Upsilon$ )	50,000 $\text{kg}^{-1}\cdot\text{m}^{-3}\cdot\text{s}^3\cdot\text{A}^2$
Thermal Conductivity (k)	< 10 W/mK

Table 5: Physical and Mechanical Properties of Carbon fiber[7]

Carbon and graphite materials are superior high temperature materials, where strength and stiffness are preserved up to temperatures above 2500 K (see figure 14). A past study involved various types of this material group and their specific high-temperature properties shows the difference in their performance. This superiority brought attention to carbon fibers being the strongest form of carbon materials and to the carbon fiber reinforced composites (CFC) with carbon matrix, the carbon/carbon composites, as the most advanced high-temperature material. Moreover, CFC should not only be considered as a high-temperature material as in a combination with a carbon matrix but more often in combination with polymers as new ideal low-weight/high-stiffness structural material for general use [8].

Carbon Fiber reinforced polymers (CFRPs) are applied in a wide temperature range going from cryogenic to room temperature and moderately elevated temperatures. Polymers started to be

used in structural engineering materials because of carbon fiber reinforcement, where their mechanical properties exceed those of the conventional metals [8].

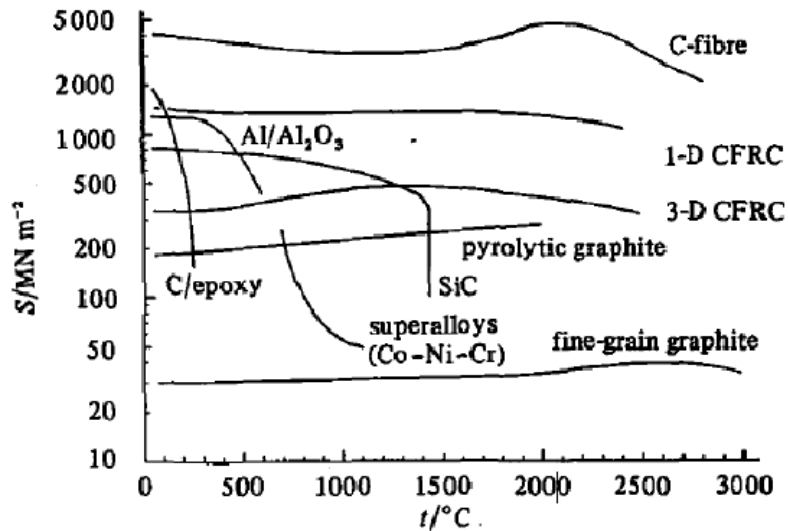


Figure 14: Study by Fitzner and Heym (1978),  $S$  - Short term Strength (stress), of Carbon materials including CFRC compared with C/epoxy and metals.[8]

### 2.6.3. Manufacturing Carbon Fiber from PAN

The raw material that CF is extracted from is called the precursor. Most carbon fibers approximately 90 % are made from polyacrylonitrile (PAN), the remaining 10 % are from rayon or petroleum pitch. All these materials are organic polymers, characterized by long strings of molecules bonded together with carbon atoms. The required composition of each precursor varies from one company to another and is generally kept as a business secret. During the manufacturing process different gases and liquids are employed, some of these substances are intended to interact with the fiber to produce a certain required effect. Other substances are not meant to react or simply prevented certain reactions with the fiber due to possible unwanted effects [4].

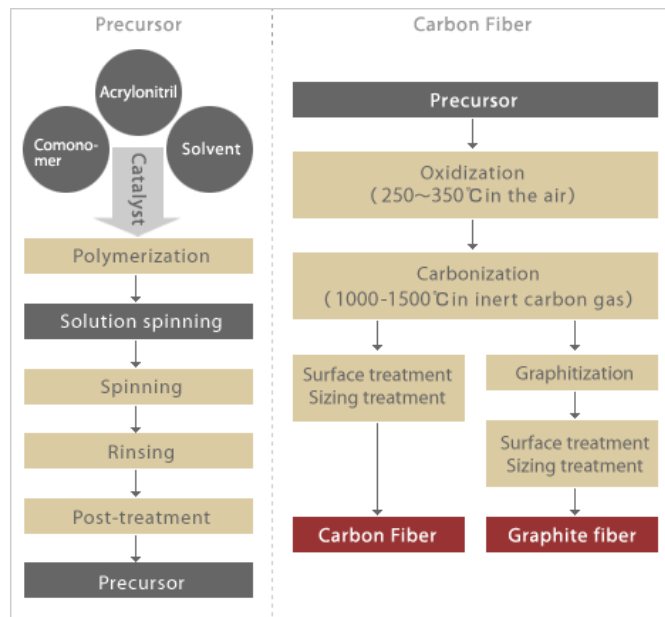


Figure 15: Manufacturing Process of Carbon Fiber (PAN-based) [5]

Firstly, in spinning process the acrylonitrile plastic powder is combined with another plastic, such as methyl acrylate or methyl methacrylate, and reacts with a catalyst in a conventional suspension or solution polymerization process to form a polyacrylonitrile plastic. The plastic is then spun into fibers using one of various methods. Indifferent methods, the plastic is mixed with specific chemicals and pumped through tiny surges into a chemical bath quenching chamber where the plastic thickens and solidifies into fibers. In alternative methods, the plastic mixture is heated and pumped through tiny surges into a chamber where the solvents evaporate, leaving a solid fiber residue. The spinning stage of processing PAN is crucial because this is where the internal atomic structure of the fiber is configured during this process. The fibers are then washed and stretched to required fiber diameter. The stretching aids alignment of molecules within the fiber and facilitates the basis for the formation of tightly bonded carbon crystals after carbonization [5].

Secondly, after the fibers stabilize, they are heated to a temperature in the range of 1000 to 3000 °C for some minutes in a furnace filled with a gas mixture that is free of oxygen to avoid burning at elevated temperatures. The gas pressure inside the furnace is maintained higher than the ambient outside air pressure and the spots in which the fibers enter and exit the furnace are tightly sealed to keep oxygen from entering the chamber. As the fiber's temperature elevate, they start to get lose their non-carbon atoms, in addition to a few carbon atoms, in the form of several gases including steam, ammonia, carbon monoxide, carbon dioxide, hydrogen, nitrogen, and others. As the non-carbon atoms are ejected, the remnants of carbon atoms create tightly bonded carbon crystals that are aligned parallel to the longitudinal axis of the fiber. In other processes, two furnaces operating at two different temperatures are utilized to better control the rate of heating during carbonization [5].

Thirdly, post carbonizing the fibers surface does not bond well with the epoxy and other materials used in composite materials. Therefore, to provide the fibers enhanced bonding properties, their surface is subjected to slight oxidation. The inclusion of oxygen atoms to the surface provides better chemical bonding properties and carves the surface to an extent roughing it up for better mechanical properties. Oxidation can be done by dipping the fibers in various gases such as air, carbon dioxide or ozone; or in different liquids such as sodium hypochlorite or nitric acid. The fibers can also be coated electrolytically by making the fibers the positive terminal in a bath filled with different electrically conductive materials. The surface treatment procedure should be conducted with care and controlled to prevent the formation of small surface defects, such as pits, which would result in fiber failure [5].

Ultimately, aftersurface treatment is sizing where the fibers are covered to protect them from disfigurement during winding or weaving. Coating materials are chosen to be compatible with the adhesive used to form composite materials. Typical coating materials include epoxy, polyester, nylon, urethane, and several others. The coated fibers are wound onto cylinders known as bobbins. The bobbins are stacked into a spinning machine and the fibers are twisted into threads of various sizes [5].

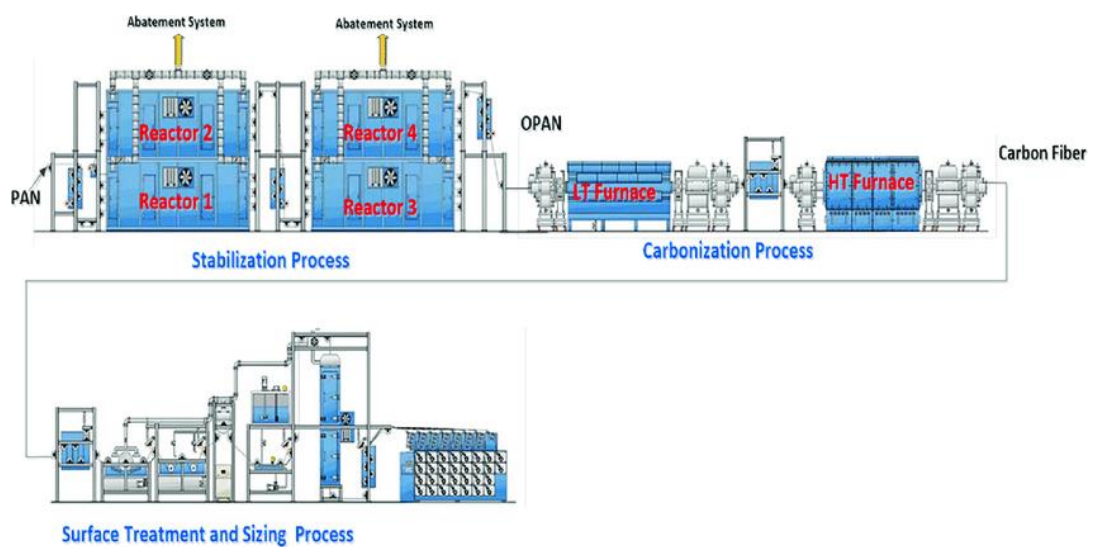


Figure 16: Industrial Carbon fiber manufacturing process [9]

#### 2.6.4. Rationale of Composite material use over conventional

Metal against plastic is a controversial decision that has been a topic considered by companies for many projects depending on the application and its environment. However, innovations in both plastic materials and process capabilities, along with evolution in industry demands have closed many of the physical and cost performance gaps that once existed between metal and plastic [84].

Several industries, such as aerospace, medical devices, and mass transit, are perceiving the potential of the evolved advantages of replacing large scale, interior, or enclosure metal parts with plastic materials and manufacturing processes, such as thermoplastic materials and the plastic

thermoforming process. In this subchapter some key aspect comparisons are mentioned to consider for Metal versus plastic selection [84].

Initially, Weight is of major importance specially from the financial point of view as heavy weight equals heavier costs. Fuel efficiency, maintenance costs, logistics, installation will experience significant cost reduction along with decreased part weight. Referring to Table 6 one can see that this is a major advantage that plastic has over metal with regard to specific gravity [84].

<b>Plastics / Composites</b>	<b>Specific Gravity</b>
Acetal copolymer	1.41
Acetal, 20% glass composite	1.55
High-impact ABS	1.03
Polycarbonate	1.19
Polyetherimide	1.27
Polymethylpentene	0.83
<b>Metals</b>	<b>Specific Gravity</b>
Aluminum	2.55 – 2.80
Carbon Steel	7.8
Cast Iron	7.03 – 7.13
Cast Rolled Brass	8.4 – 8.7
Copper	8.89
Stainless Steel	7.7
Titanium	4.5
Tool Steel	7.70 – 7.73

*Table 6 : Metals and Plastic different specific gravity indicating difference in weight [84].*

Note that the specific gravity (SG) is a dimensionless unit defined as the ratio of density of the material to the density of water at a specified temperature. There is a variety of alloys and grades for steel and aluminium, and there are just as many diverse formulations of plastic material. For a more precise weight comparison reference to the specific material manufacturer's data sheets for the applicable material for your project shall provide required material information [84].

Secondly, The strength to weight ratio is another factor to look at and account as an advantage for composites/plastics. As in the past this is one of the biggest obstacles encountered when replacing metal parts with plastic. Since plastic materials are much lighter and could not compete with the strength characteristics of metal. Nowadays, with the evolution of plastic composites and the addition of carbon fiber or other glass fibers to plastic material formulations, thermoplastic products can perform as well as and in some cases even outperform metal materials such as strength to weight and strength to stiffness. Strength to weight ratio also known as specific strength is a material's strength (force per unit area at failure) divided by its density. Referring to the chart below (figure 17) note that examples of thermoplastics reside in the composite and polymer categories and this data does not include all thermoplastic material products, many of which are specifically formulated to compete with metal and alloys in strength and stiffness [84].

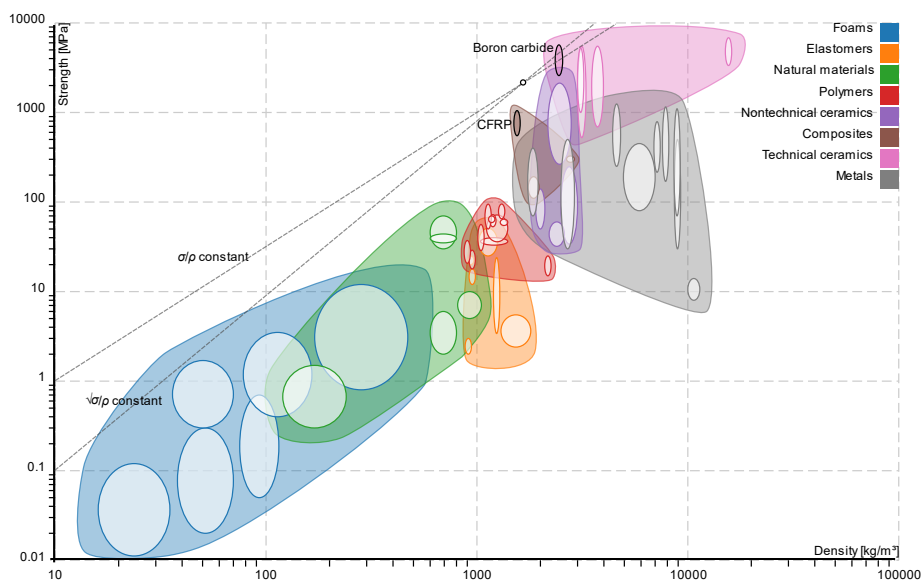


Figure 17: Material comparison Strength[84]

Thirdly, the strength to stiffness ratio also known as specific modulus which is a materials property consisting of the elastic modulus per mass density of a material. In figure 18 , we can see the significant difference of the specific stiffness that carbon epoxy over takes the conventional metallic materials as an example to show the advantage that composites have [84].



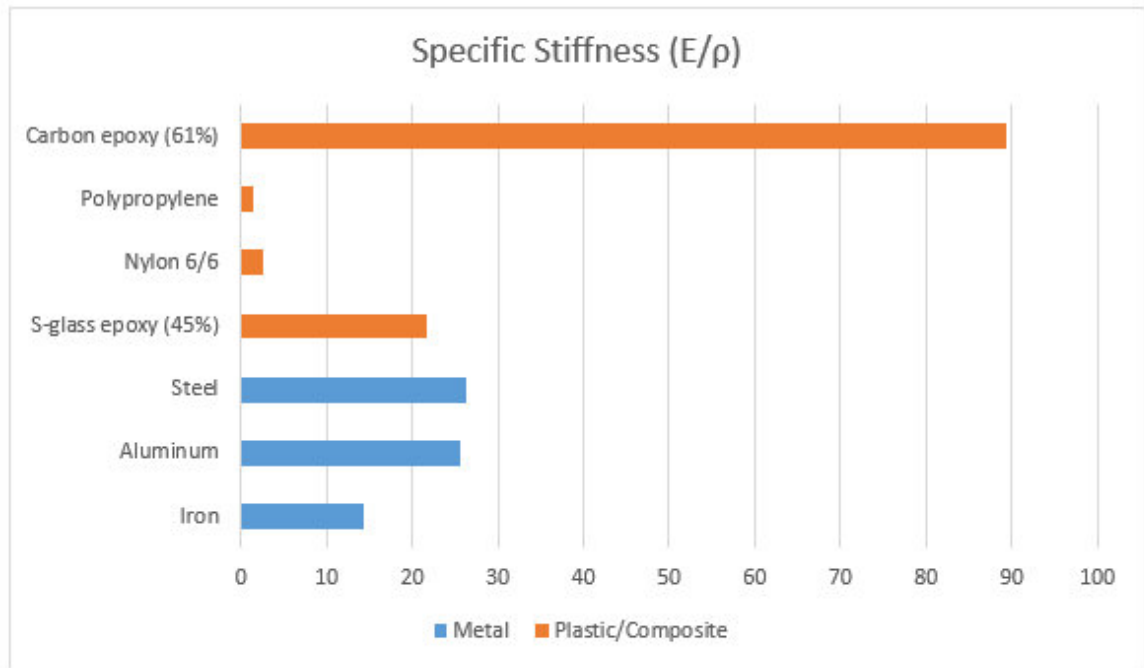


Figure 18: Specific Stiffness comparison [84]

Fourthly, Production time is an essential factor for the success of any project whether meeting a deadline or an increase in demand. In a less labor intensive process, plastic thermoforming can save production time, energy, labor and cost compared to manufacturing components from metal processes [84].



Plastic thermoforming Process	Metal Fabrication Process
	
Programming	Fixture/ die construction
Tooling construction	Programming
Automated Part Forming	Cutting, bending , welding
Robotic part trimming	Cleaning welds finishing
Part Finishing (bonding attachment points)	Paint preparation and Painting

Table 7: Comparison of Plastic/composites and Metal Manufacturing Process steps

Moreover, Looking at the sheet metal fabrication process one can easily conclude the fact that metals are harder to work with and shape. Metal's inherent characteristics prohibit complex part

designs or shapes, such as compound curves or fluid designs from either the material's capability or cost limitation. Shaping a metal part can require die work, welding, grinding, rework, or bending on each individual part produced to achieve design specifications and required look. In addition to increasing production and lead times as part design complexity increases, part cost increases in an exponential relationship. Now when looking at the same increase in design complexity for a part manufactured with the plastic thermoforming process, it has a relatively minimal impact on the cost of the part. This is due to complex designs, shapes, branding, and surface textures can be incorporated directly into a part's tooling. While this may cause a modest increase in the upfront tooling cost of the part's production, it will not add any additional secondary or shaping labor operations that would affect part cost or production time. The nature of thermoplastic and this method provides a much larger flexibility [84].

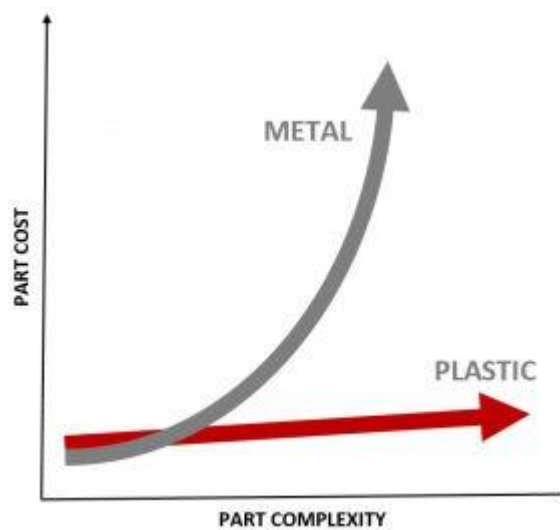


Figure 19: Relationship of part cost with part complexity for plastic and metal [84]

## 2.7. Composite Pipes

Composite pipe body consists of three main constituents; an inner liner, a composite laminate, and an outer cover. The liner, either metallic or polymer, serves mainly as a barricade against the inner fluid. The laminate is the load enduring component. The outer cover is a protective layer from the ambient environment. The inner liner, laminate and cover are all bonded or joined to the laminate. Extra outer layers may be added as special purposes layers for example as local wear protection or fire protection [25]. An epoxy layer is included in the composite pipe to create a polymer matrix which provides reinforcement to the fibers or other fillers. This allows the fabrication of long-lasting parts with high strength-to-weight ratios, compared to conventional materials of construction like metals or wood for example. Epoxy-based polymer composites are resistant to deterioration from corrosion, spalling or rotting [26].

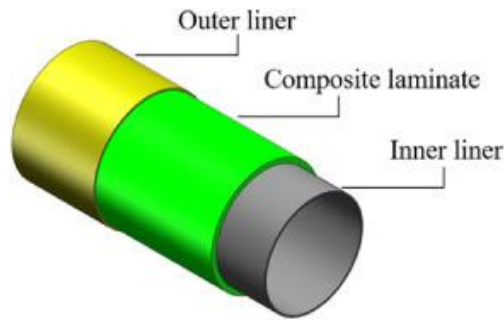


Figure 20: An example of a Glass-fibre reinforced polymer (GFRP) composite [27]

Composite pipes exposed to internal pressure are subjected to both hoop and axial stresses in the case of close-ends tubes with hoop-to-axial stress of two to one. For long open-ends, axial stress due to the internal pressure is zero. Moreover, other stresses can result from the installation, weight, external pressure, etc. In designing composite pipes, the stress and failure analysis is generally performed without taking into account either the internal liner nor the outer cover, as they are assumed to not contribute to the resistance to deformation. The design process of the composite lay-up may include fiber and matrix material selection, overall laminate thickness, the thickness of each lamina, and the fiber orientation of each individual layer [25].

When composite pipes are compared to steel, they have a significantly lower total installed cost. Most composites are malleable, allowing them to handle harder turn radii and grade changes comfortably. Moreover, is the unmatched corrosion endurance and chemical resistance leading to lower maintenance requirements and hence less downtime [29]. In table 8 we can see mechanical properties comparison of CFRP, GFRP and steel.

Property	Material Type		
	CFRP	GFRP	Steel
Density ( $g/cm^3$ )	1.50 – 2.10	1.25 – 2.50	7.85
Tensile Strength (MPa)	600 - 3920	483 – 4580	483 – 690
Young's Modulus (GPa)	37-784	35 – 86	200
Elongation (%)	0.5 - 1.8	1.2 – 5.0	6.0 – 12.0
Coefficient of linear expansion ( $10^{-6}/^{\circ}C$ )	-9.0 – 0.0	6.0 – 10.0	11.7

Table 8: Mechanical properties of some FRP material types and Steel [30]

Composite pipes are used in water transportation for firefighting or cooling systems, sewage and drainage systems, while composite tube wound with filaments are also used in sectors like aerospace, construction and even sport equipment [31]. Typical composite materials used as piping

systems include : PVC (Polyvinyl Chloride), HDPE (High Density Polyethylene) , GRP (Glass Reinforced Plastics) etc [32].

Applications of CFRP composites have been on the rise in recent years especially in applications where material cost is peripheral to performance and weight reduction. This is due to the significant properties and adaptability of fiber reinforcement along load paths to achieve desired composite performance, which is not common in other materials [28].

## 2.8. Pipes under mechanical load

There are 5 main piping stresses that can lead to failure in a piping system: Hoop stress, axial stress, bending stress, torsional stress, and fatigue stress [33].

**Hoop stress** is the outcome of pressure being exerted to the pipe either internally or externally. Since pressure is uniformly applied to the piping system, hoop stress also is accounted to be uniform over a given length of a pipe. Hoop stress varies with the diameter and wall thickness through the piping system [33]. In the coming subchapters derivations of hoop stress formulae and other stresses will be demonstrated.

**Axial stress** which is caused from the restrained axial growth of the pipe. Axial growth (elongation) can be caused by thermal expansion, pressure expansion, and applied forces. Axial stress should not exceed the yield strength of the pipe. When comparing resulting axial growth from pressure, steel pipe growth is less than composite piping [33]. This is mainly due to the higher coefficient of thermal expansion that composite materials have making them sensitive to temperature changes[34].

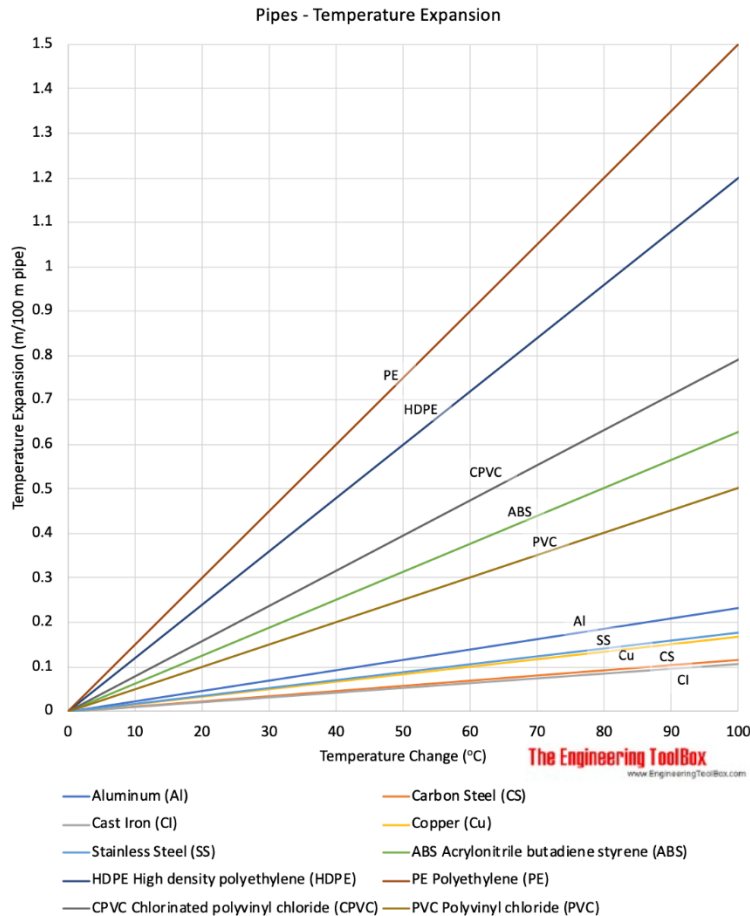


Figure 21: Different Pipe Materials temperature expansion plot[30]

**Bending stress** is the stress resulting from body forces being applied to the piping. Body forces are the pipe and medium weight, concentrated masses like those of valves, flanges. Sporadic forces are included such as seismic, wind, thrust loads and possible forced displacements caused by expansion of adjacent piping and equipment connections. A resultant moment is created from the body forces acting, for which the stress can be represented by moment divided by the section modulus [33].

**Torsional stress** is what results from the rotational moment around the pipe axis and not by body forces like bending stress. Nevertheless, it is much more likely for a pipe to fail in bending stress before torsion therefore usually this stress is neglected [33].

**Fatigue stress** is the continuous cycling of the stresses present in the piping. A good example to demonstrate fatigue stress is turning a water faucet on and off all day as the pressure being released and then built up. In power applications, the cycling of a steam turbine from low pressure to high pressure and temperature develops fatigue stress. Fatigue stress decreases allowable strength of the piping system and can generally be caused by pressure, temperature, vibration, occasional loads [33].

### 2.8.1. Thin wall cylinder stresses

Considering a steel pipe as an example of a tube to distinguish the difference between thick and thin wall tube, from the first look at regular wall (thick) and thin wall stainless steel tubing one may not notice any differences because both types of tubing have an almost similar outside diameter. The difference between thin wall and regular (thick) wall tubing is the thickness of the tubing (walls). This makes the inside diameter of the thin wall tubing larger than the thick wall tubing [35].

Thin-walled pipes are used in the drive technology sector for charge air, coolants, exhaust gas piping and their systems or in a bigger scale thin-walled cylinders are used as boiler shells, pressure tanks and in other low pressure processing equipment.

A pipe is considered to be “thin” if the ratio of the inner diameter to the thickness of the wall is  $>20$  [35]:

$$\frac{D_i}{t} > 20$$

Considering this ratio, one can assume for stress analysis that both the hoop and longitudinal stresses are constant across the wall thickness and the radial stress is of small magnitude in comparison to the hoop and longitudinal stresses therefore we can neglect it. This makes the analysis approximated and, the radial stress will vary between the pressures at the inner and outer diameters i.e., for internal pressure only, the radial stress will vary from zero at the outside surface to a value equal to the internal pressure at the inside surface [36].

$$\sigma_h = \text{constant}$$

$$\sigma_L = \text{constant}$$

$$\sigma_r = \text{constant, negligible}$$

Note that no shear stress is generated.

Now considering Hoop stress ( $\sigma_h$ ) which is the stress generated to resist the force due to the applied pressure as it acts to separate the top and bottom halves of the pipe or cylinder [36].

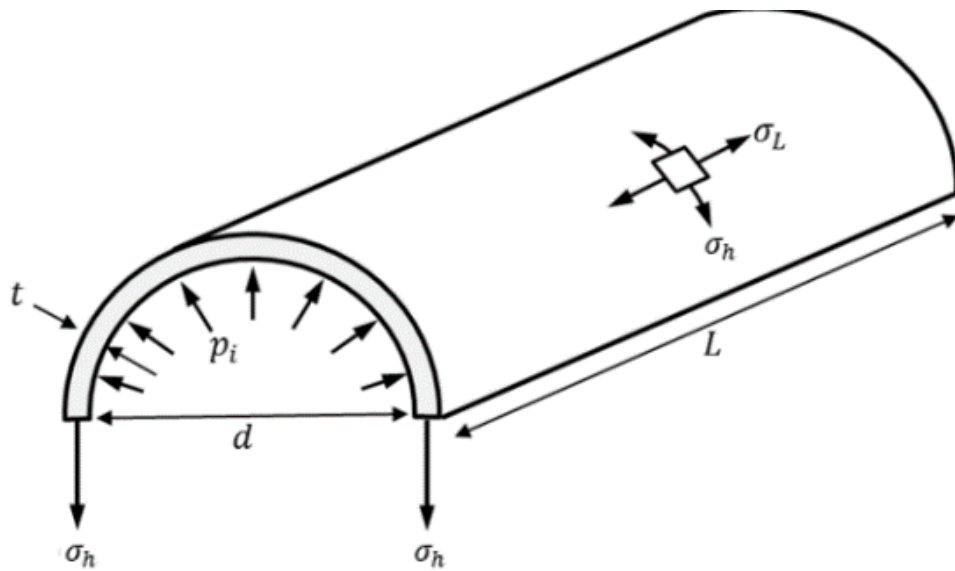


Figure 22: Stresses acting on a tube due to internal pressure[36]

The total resultant force on half of a pipe due to the internal pressure is given by:

$$F = p_i \cdot d \cdot L \quad (1)$$

And the resisting force due to the hoop stress  $\sigma_h$ , forming on the cylinder walls is given by:

$$F_{\sigma_h} = (2\sigma_h) \cdot L \cdot t \quad (2)$$

Equating the above 2 equations gives:

$$p_i \cdot d \cdot L = (2\sigma_h) \cdot L \cdot t \quad (3)$$

rearranging the equation to make hoop stress the subject ( $\sigma_h$ ) we obtain:

$$\sigma_h = \frac{p_i \cdot d \cdot L}{2 \cdot L \cdot t} = \frac{p_i \cdot d}{2 \cdot t} \quad (4)$$

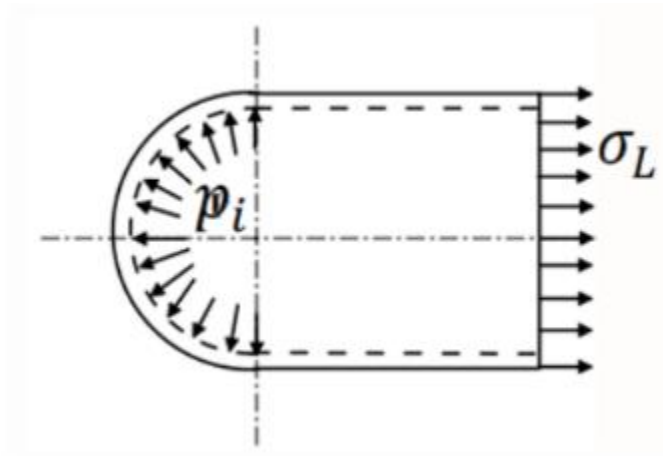


Figure 23: Cross section of a thin cylinder showing longitudinal stress direction[36]

Using the same approach when calculating hoop, the total force acting on the end of the cylinder due to internal pressure is given by [36]:

$$F = \text{pressure} \times \text{area} = p_i \cdot \pi \cdot r^2 = p_i \cdot \frac{\pi d^2}{4} \quad (5)$$

The area of the cylinder material resisting the force acting is given by:

$$\text{Resisting force area} = \pi \cdot d \cdot t \quad (6)$$

Therefore, the longitudinal stress ( $\sigma_L$ ) is obtained by dividing the force acting on the resisting force area which gives us:

$$\sigma_L = \frac{\text{Force}}{\text{Area}} = \frac{p_i \cdot \frac{\pi d^2}{4}}{\pi \cdot d \cdot t} = \frac{p_i \cdot d}{4t} \quad (7)$$

Moreover, the change in length of a thin cylinder can be determined from the longitudinal strain using the following formula that utilizes the material properties using young's modulus of material in use we can obtain :

$$\text{Longitudinal strain } (\varepsilon_L) = \frac{(\sigma_L - \nu \sigma_h)}{E} \quad (8)$$

$$\Delta L = (\varepsilon_L) \cdot \text{Original Length } (L) \quad (9)$$

$$\Delta L = \frac{(\sigma_L - \nu \sigma_h)}{E} (L) = \frac{1}{E} \left( \frac{p_i \cdot d}{4t} - \nu \left( \frac{p_i \cdot d}{2t} \right) \right) L \quad (10)$$

$$\Delta L = \frac{p_i \cdot d}{4 \cdot t \cdot E} (1 - 2\nu) L \quad (11)$$

Where " $\nu$ " is a material property known as poisson's ratio which is the amount of transversal elongation divided by the amount of axial compression, most materials have Poisson's ratio values ranging between 0.0 and 0.5 [93].

Similarly, one can determine the change in diameter from strain acting on the diameter which we can refer to as diametric strain by the following formula [36]:

$$\text{Diametral Strain} = \frac{\text{Change in Diameter}}{\text{Original Diameter}} \quad (12)$$

The change in diameter can be found by considering the circumferential change, which results from the stress acting around the circumference also known as the hoop stress ( $\sigma_h$ ). Giving an increase to the circumferential strain  $\varepsilon_h$  [36].

$$\text{Change in Circumference} = \text{Strain} \cdot (\text{original Circumference})$$

$$\Delta C = \varepsilon_h \cdot (\pi d) \quad (13)$$

Hence the new circumference is given by [36]:



$$\text{New circumference} = \pi d + \pi d(\varepsilon_h) = \pi d(1 + \varepsilon_h) \quad (14)$$

And it can be seen from the equation above that the new diameter is given by:

$$\text{New diameter} = d(1 + \varepsilon_h) \quad (15)$$

This indicates that the change in diameter would be:

$$\Delta d = d \cdot \varepsilon_h \quad (16)$$

$$\therefore \text{Diametral strain} = \frac{d \cdot \varepsilon_h}{d} = \varepsilon_h$$

consequently, exemplifying the diametric strain being equal to the circumferential (hoop) strain.

$$\begin{aligned} \Delta d &= d \cdot \varepsilon_h = \left( \frac{d(\sigma_h - v\sigma_L)}{E} \right) = \frac{d}{E} \left( \frac{p_i d}{2t} - v \frac{p_i d}{4t} \right) \\ \Delta d &= \frac{p_i d^2}{4t} (2 - v) \end{aligned} \quad (17)$$

Another parameter that the deformation due to the stress applied and the strain resulting on the cylinder would be the change in the internal volume which can be derived in a similar approach to what was done above considering the stresses and the strain that is in the cylinder [36].

$$\text{change in volume } (\Delta V) = \text{volumetric strain } (\varepsilon_v) \times \text{original volume } (V)$$

Given:

*Volumetric strain* ( $\varepsilon_v$ ) = *sum of 3 mutually perpendicular strains*

$$\begin{aligned} \varepsilon_v &= \varepsilon_L + 2\varepsilon_h = \frac{1}{E} (\sigma_L - v\sigma_h) + \frac{2}{E} (\sigma_h - v\sigma_L) \\ \varepsilon_v &= \frac{1}{E} (\sigma_L - v\sigma_h + 2\sigma_h - 2v\sigma_L) = \frac{1}{E} (\sigma_L + 2\sigma_h - v(\sigma_h + 2\sigma_L)) \end{aligned} \quad (18)$$

Then plugging in the longitudinal stress, circumferential stress where required and simplifying the equation we end up with:

$$\varepsilon_v = \frac{p_i d}{4 \cdot t \cdot E} (5 - 4v) \quad (19)$$

And to finally get the change in volume due to the stresses experienced, simply we plug in the above equation into the change in volume ( $\Delta V$ ) equation to get [36] :

$$\Delta V = \frac{p_i d}{4 \cdot t \cdot E} (5 - 4v) \cdot V \quad (20)$$

In scenarios where a positive (tensile) force is present, any applied internal pressure would cause an initially bent pipe to bend more. The additional bending will gradually increase till the internal pressure reaches the critical value given by the equation below [37].

$$P_{cri} = \frac{2\pi EDt}{(1-2\nu)l^2} \quad (21)$$

Where  $l$  is the length of the pipe.

Consequent to the gradual increase up to the critical pressure the pipe will become unstable under the internal pressure and buckle [37].

### 2.8.2. Lamé's Theory

Thick-walled pipes are pipes with a ratio of outer diameter to wall thickness of less than 20, mainly used as petroleum geological drilling pipe, cracking pipe for petrochemical industry, boiler pipe, bearing pipe, and high-precision structural pipe for automobile, tractor and aviation [36].

$$\frac{D_i}{t} < 20$$

When we considered thin cylinders, we assumed that the hoop stress was constant across the thickness of the cylinder wall and we ignored any pressure gradient across the wall. Now considering a thick-walled cylinder, these simplifications are no longer valid and one should consider the variation of both hoop and radial stresses. If the cylinder is long in comparison with its diameter, the longitudinal stress is assumed to be uniform throughout the thickness of the cylinder wall [36].

Stress states in a thick wall cylinder :

$$\sigma_h = \text{Varies with radius}$$

$$\sigma_L = \text{constant}$$

$$\sigma_r = \text{Varies with radius}$$

In theory of thick wall cylinder we are interested in sections that are remote from the ends. For sections apart from the ends, the applied pressure is symmetrical and all points on an annular element of the cylinder wall will be subjected to the same displacement. There will exist no shearing stresses set up on transverse planes, which requires stresses on such planes are in fact the acting principal stresses. Similarly, since the radial shape of the cylinder is maintained, there exist no shear stresses on the radial or tangential planes and again the stresses on such planes are principal stresses. Therefore, when considering any element in the wall of a thick cylinder, we will be looking at a mutually perpendicular tri-axial stress system where the 3 stresses are – hoop, longitudinal and radial [36].

In regard to Lamé's theory for thick cylinders, the theorem is based on two assumptions :

1. Material of the cylinder is homogeneous and isotropic ,hence this is not valid for composite materials.
2. Plane sections of the cylinder perpendicular to the longitudinal axis remain plane under the pressure.

The second assumption implies that the longitudinal strain is same at all points meaning the strain is independent of the radius. The cylinder shown in figure 24 has internal and external radii of  $R_i$  &  $R_o$  respectively. the cylinder is subjected to internal and external pressures  $P_i$  &  $P_o$  respectively, consider an element of the cylinder cross section at radius  $r$  and subtending an angle  $\delta\theta$  at the center. Given the radial and hoop stresses on the element are  $\sigma_r$  and  $\sigma_h$  respectively and by equating the radial forces over a unit of axial length for radial equilibrium we obtain [36] :

$$\sigma_r r \delta\theta + 2\sigma_h \delta r \sin \frac{\delta\theta}{2} = (\sigma_r + \delta\sigma_r)(r + \delta)r \delta\theta$$

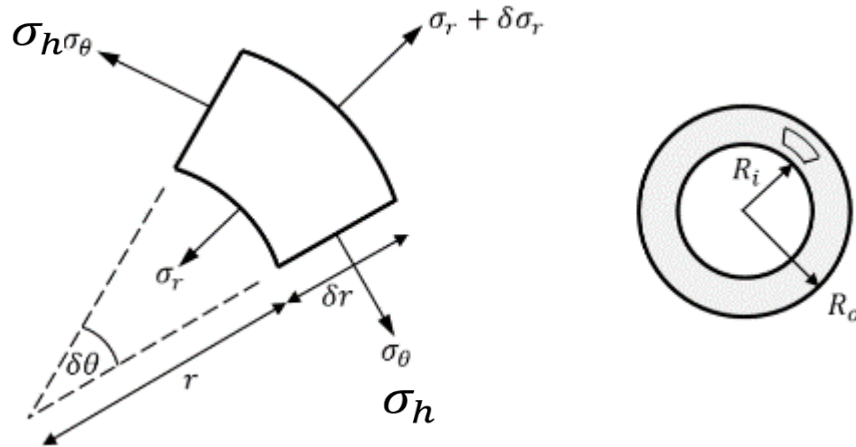


Figure 24: element of cylinder cross section subjected to internal and external pressure[36]

From the equilibrium equation above one can recognize that [36] :

$$\sin \frac{\delta\theta}{2} \rightarrow \frac{\delta\theta}{2}$$

$$\sigma_r r \delta\theta + 2\sigma_h \delta r \frac{\delta\theta}{2} = (\sigma_r + \delta\sigma_r)(r + \delta)r \delta\theta$$

$$\sigma_r r \delta\theta + \sigma_h \delta r \delta\theta = (\sigma_r + \delta\sigma_r)(r + \delta)r \delta\theta$$

Then we divide through by  $d\theta$  :

$$\sigma_r r + \sigma_h \delta r = (\sigma_r + \delta\sigma_r)(r + \delta)$$

$$\sigma_r r + \sigma_h \delta r = \sigma_r r + \sigma_r \delta r + r \delta\sigma_r + \delta\sigma_r \delta r$$

Neglecting small terms :

$$\sigma_r r + \sigma_h \delta r = \sigma_r r + \sigma_r \delta r + r \delta\sigma_r$$

$$\sigma_h \delta r - \sigma_r \delta r = r \delta \sigma_r$$

$$\sigma_h - \sigma_r = r \frac{\delta \sigma_r}{\delta r} \rightarrow \text{Equilibrium Equation} \quad (22)$$

A further step is required to solve for  $\sigma_h$  &  $\sigma_r$ , assuming that plane sections remain plane then :

$$\sigma_L = \text{Constant}$$

$$\varepsilon_L = \text{Constant}$$

$$\varepsilon_L = \frac{1}{E} (\sigma_L - \nu [\sigma_r + \sigma_h])$$

Or :

$$\sigma_r + \sigma_h = \frac{\sigma_L - E \varepsilon_L}{\nu}$$

Since  $\sigma_L$  &  $\varepsilon_L$  are assumed to be constant across the section then we can say :

$$\sigma_r + \sigma_h = \text{constant} = 2A \quad (23)$$

From Equation (22) :

$$\sigma_h = r \frac{d\sigma_r}{dr} + \sigma_r$$

And from Equation (23) we obtain :

$$\sigma_h = 2A - \sigma_r$$

Then by eliminating  $\sigma_h$  and integrating :

$$2A - \sigma_r = r \frac{d\sigma_r}{dr} + \sigma_r$$

$$2 \int \frac{dr}{r} = \int \frac{d\sigma_r}{(A - \sigma_r)}$$

$$2 \ln r = -\ln(A - \sigma_r) + \ln B$$

$$r^2 = \frac{B}{(A - \sigma_r)}$$

Therefore :

$$\sigma_r = A - \frac{B}{r^2} \quad (24)$$

Hence, we plug equation (24) in equation (23) :

$$\sigma_h = 2A - \sigma_r = 2A - \left( A - \frac{B}{r^2} \right)$$

$$\sigma_h = A + \frac{B}{r^2} \quad (25)$$

Our assumption was made considering longitudinal stress ( $\sigma_L$ ) is constant and is given by :

$$\sigma_L = \frac{\text{end load}}{\text{Cross sectional Area}} \quad (26)$$

Equations (24) and (25) are Lamé's equations and by substituting the relevant boundary conditions we are able to determine the constants **A** and **B**. Hence, finding the radial and hoop stresses at any point. Noting that the tensile stresses are regarded to as positive and compressive stresses are regarded as negative [36].

### 2.8.3. Thick cylinders with internal and external pressure

Examining a thick cylinder subjected to an internal pressure  $p_i$  where the external pressure is zero, with the following boundary conditions set as [36]:

$$\text{At } r = R_i, \sigma_r = -p_i$$

$$\text{At } r = R_o, \sigma_r = 0$$

Note that the internal pressure is considered as negative radial stress since it will produce radial compression (thinning) of the cylinder walls and normal stress convention is negative indicating compression.

Using equation (24) with set boundary conditions [36]:

$$\sigma_r = A - \frac{B}{r^2}$$

We obtain :

$$p_i = A - \frac{B}{R_i^2}$$

$$0 = A - \frac{B}{R_o^2}$$

Rearranging the above two equations to get :

$$A = \frac{B}{R_o^2} = -p_i + \frac{B}{R_i^2}$$

$$p_i = \frac{B}{R_i^2} - \frac{B}{R_o^2} = B \frac{(R_o^2 - R_i^2)}{R_i^2 R_o^2}$$

$$B = \frac{p_i R_i^2 R_o^2}{(R_o^2 - R_i^2)}$$

And :

$$A = \frac{B}{R_o^2} = \frac{1}{R_o^2} \frac{p_i R_i^2 R_o^2}{(R_o^2 - R_i^2)} = \frac{p_i R_i^2}{(R_o^2 - R_i^2)}$$

Substituting the above equations of **A** and **B** in the radial stress formula dictated before we obtain :

$$\sigma_r = \frac{p_i R_i^2}{(R_o^2 - R_i^2)} - \frac{1}{r^2} \frac{p_i R_i^2 R_o^2}{(R_o^2 - R_i^2)} = \frac{p_i R_i^2}{(R_o^2 - R_i^2)} \left(1 - \frac{R_o^2}{r^2}\right)$$

$$\sigma_r = \frac{p_i R_i^2}{(R_o^2 - R_i^2)} \left(\frac{r^2 - R_o^2}{r^2}\right) \quad (27)$$

Knowing the above equation we are able to formulate the hoop stress formula which is [36]:

$$\sigma_h = A + \frac{B}{r^2} = \frac{p_i R_i^2}{(R_o^2 - R_i^2)} \left(\frac{r^2 + R_o^2}{r^2}\right) \quad (28)$$

Here we can see that the maximum values of both will only occur at the inside radius, depending on the direction of the pressure gradient. Failure by fracture means that the hoop stress is the dominant principle stress and there are no external loads present. Due to hoop stress failure one can notice the pipe splitting into two halves or rupturing perpendicular to maximum stress. Bursting of the pipe may be encountered if the force created by the internal pressure exceeds the hoop stress's resisting force. In the design process, pipe stresses are appropriately realized, as extreme failure that can result in loss of property, environmental harm or even life. Therefore, Analysis of hoop and other stresses increases life time and is warranted when there are sensitive equipment connections, the existence of external pressure, and elevated temperatures. Inspections, hand calculations or computer modeling are methods of analyzing pipe stresses [38].

Now in order to calculate the longitudinal stress in a thick cylinder with closed ends, subjected to internal and external pressure ( $p_i$  &  $p_o$ ) respectively (see figure 25) [36] :

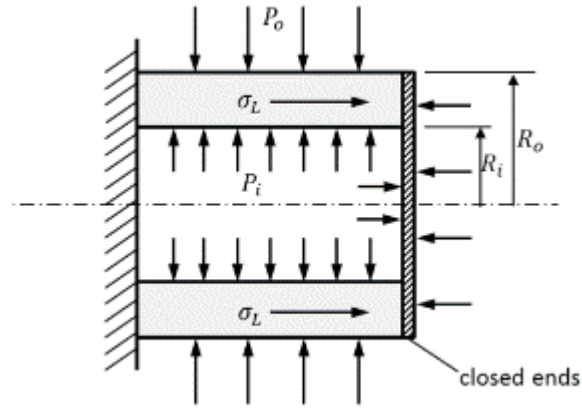


Figure 25: Cross section of thick cylinder with closed ends subjected to internal and external pressure [36]

Formulating the equilibrium equation horizontally where we have longitudinal stress acting we get [36]:

$$\sigma_L \times \pi(R_o^2 - R_i^2) = P_i \times \pi R_i^2 - P_o \times \pi R_o^2$$

Where  $\sigma_L$  is the longitudinal stress formed in the cylinder walls :

$$\sigma_L = \frac{P_i R_i^2 - P_o R_o^2}{(R_o^2 - R_i^2)} = \text{constant}$$

We can see that this constant has the same value as **A** in the Lamé's equations, hence in the case of only internal pressure acting where  $P_o = 0$  this simplifies to :

$$\sigma_L = \frac{P_i R_i^2}{(R_o^2 - R_i^2)} \quad (29)$$

In regard to Maximum shear stress, Stresses on an element at any point in a thick cylinder wall are in fact principal stresses. Therefore, we can see that the maximum shear stress at any point will be given by:

$$\tau_{max} = \frac{\sigma_1 - \sigma_3}{2}$$

The value obtained from the above equation calculating the maximum shear stress would simply be half of the difference between the maximum and minimum principal stresses in case of a thick cylinder [36] :

$$\tau_{max} = \frac{\sigma_h - \sigma_r}{2} \quad (30)$$

Since hoop stress ( $\sigma_h$ ) is normally tensile while the radial stress ( $\sigma_r$ ) is compressive and both are of greater magnitude than longitudinal stress ( $\sigma_L$ ) and so we can write the maximum shear stress formula in terms of **A** and **B** and we can see that we obtain :

$$\tau_{max} = \frac{1}{2} \left[ \left( A + \frac{B}{r^2} \right) - \left( A - \frac{B}{r^2} \right) \right] = \frac{B}{r^2} \quad (31)$$

Thus, the greatest value of  $\tau_{max}$  occurs at the inner radius [36]. Generally, Shear stress tends to cause deformation of a material by slippage along a plane or planes parallel to imposed stress. This stress provides a slipping tendency to one plane against the other mainly caused by the shear forces acting on the pipe cross section or twisting (torsional moments). Since the shear stresses caused by shear forces in a piping system are of small magnitude, this is neglected [39].

#### 2.8.4. Thick Cylinder strain and change in dimensions

Due to the stresses acting on the cylinder three different principle strains form and they are [36]:

$$\varepsilon_r = \frac{\sigma_r - v(\sigma_h + \sigma_L)}{E} \quad (32)$$

$$\varepsilon_h = \frac{\sigma_h - v(\sigma_r + \sigma_L)}{E} \quad (33)$$

$$\varepsilon_L = \frac{\sigma_L - v(\sigma_r + \sigma_h)}{E} \quad (34)$$

Radial strain ( $\varepsilon_r$ ) is not used frequently considering the fact of radial stress being negligible, the change in diameter can be obtained from the hoop strain :

$$\text{Diametral strain} = \frac{\Delta D}{D} = \frac{\Delta \pi D}{\pi D} = \frac{\text{Change in circumference}}{\text{Original Circumference}} = \varepsilon_h = \varepsilon_D \quad (35)$$

We can see from the above equation that the diametric strain on a cylinder is equal to the hoop strain, therefore [36]:

$$\text{Change in Diameter } (\Delta D) = \text{Diametral strain } (\varepsilon_D) \times \text{Original diameter } (D_o)$$

$$\Delta D = \varepsilon_h \times D_o \quad (36)$$

Assuming the principal stresses (hoop, radial and longitudinal) are all tensile, the hoop strain is then :

$$\varepsilon_h = \frac{1}{E} (\sigma_h - v\sigma_r - v\sigma_L) \quad (37)$$

Moreover the change in diameter at any radius r of the cylinder is given by :

$$\Delta D = \frac{D}{E} (\sigma_h - v\sigma_r - v\sigma_L)$$

$$\Delta D = \frac{2r}{E} (\sigma_h - v\sigma_r - v\sigma_L) \quad (38)$$

The change in length of the cylinder is simply calculated by accounting the difference on which the reason behind the change in the length of the tube mainly caused by the longitudinal stress and we are able to use a similar structured formula as above considering difference in the parameter that is changing and the dominant stress causing the change [36] :



$$\Delta L = \frac{L}{E} (\sigma_L - \nu \sigma_r - \nu \sigma_h) \quad (39)$$

Finally we get to determine the change in volume caused by the stresses phenomena and is given by multiplying the original volume by the sum of three mutually perpendicular strains [36]:

$$\text{Change in volume } (\Delta V) = \text{Original Volume } (V_o) \times \text{Volumetric strain } (\varepsilon_V) \quad (40)$$

Where the volumetric strain is the summation of the strains experienced by the cylinder :

$$\begin{aligned} \varepsilon_V &= \varepsilon_D + \varepsilon_h + \varepsilon_L = \varepsilon_L + 2\varepsilon_h \\ \Delta V &= V(\varepsilon_L + 2\varepsilon_h) \end{aligned} \quad (41)$$

Note that the final formula of the change in volume ( $\Delta V$ ) is the change in the internal volume not the change in the cylinder material volume [36].

### 2.8.5. Finite Element Analysis (FEA) for Composites

FEA is the process of simulating the expected reaction of a part or assembly under given circumstances often referred to as conditions so that assesment is done via finite element method (FEM).Engineers often use FEA to to help simulate possible physical phenomena and thereby reduce the need for physical samples, while allowing improvement of components as part of the design process of a project .Mathematical models are used by FEA to acknowledge and quantify effects of real-world conditions on a part of assembly, allowing engineers to locate potential problems in design, stress peaks and weak spots.These simulations that are conducted via specialized software like ABAQUS FEA or ANSYS workbench, use mathematics to understand and quantify structural or fluid behaviour, wave propagation , equivalent stresses and other phenomena [40].

The simulations performed in FEA are created using a mesh of a million smaller elements that combine to create the shape of the structure that is under assesment. Every small element goes through calculations, with mesh refinements combining to output the final result of the structure. These approximate calculations are usually polynomial, with interpolations happening through the small elements, implementing these values can be determined but not at all points.Points where results are determined are known as nodal points and are usually found at the boundary of the element [40].

In this thesis, the stress analysis simulation was performed using ABAQUS. Nevertheless, the finnite element modeling of composites depends on the objective of the analysis. Considering ABAQUS, there are multiple methods of modeling composites such as macroscopic modeling, microscopic modeling , discrete reinforcement modeling, mixed modeling and submodeling. Nevertheless, the most used FEM simulation of composite materials are layered-solids, layered-shells , stacked solid elements and layered continuum shells [94].

Analysis performed in ABAQUS and simulation of different reinforcement materials in composites is simply to predict the mechanical properties and responses of the material whether tensile , compression and thermal response. Where such predicted results can be used for comparison and verification of experimental results. When modeling an anisotropic material which an example for such a material would be the CFC used in this thesis’s experiment the elastic moduli defined in ABAQUS uses linear elasticity.The different anisotropic input selection for linear elastic behavior is shown in table 9 below [94].

*ELASTIC,      TYPE=LAMINA
----------------------------

*Table 9: Linear elastic behavior*

The option shown in table 9 is for orthotropic materials which are materials that have their properties dependant on the direction in which they are measured. This selection is used specifically for plane stress an example for such a case would be a laminated shell. It requires multiple material specification also referred to as elastic constants; like  $E_1$ ,  $E_2$ ,  $\nu_{12}$ ,  $G_{12}$ ,  $G_{13}$  , and  $G_{23}$ . Where  $E_1$  and  $E_2$  represent the longitudinal Modulus and Transverse modulus respectively.  $\nu_{12}$  is major Poisson’s ratio and  $G_{12}$ ,  $G_{13}$  , and  $G_{23}$  are in plane Shear modulus [95 , 94].

Typically, it is not specified that a lamina can be considered as transversely isotropic. For a transversely isotropic lamina, the independent elastic constants become five since  $E_2 = E_3$ ,  $G_{12} = G_{13}$  and  $\nu_{12} = \nu_{13}$ . The value of  $G_{23}$  is needed to run a simulation for an isotropic lamina, which can be obtained from the equation below. When it comes to a two-dimensional analysis, there are only four independent constants required [94].

$$G_{23} = \frac{E_2(1 + \nu_{23})}{2}$$

Furthermore, Boundary conditions and load should be set and will be activated during the simulation. When using ABAQUS, the term load is generally referred to anything that causes a reaction of a structure from its initial condition [94]. In summary, after having already your geometry modeled , material specifications and lay up is set , section definition as they are categorized as solid, shell, beam ,etc with their type selected and assigned. We model the mesh , define analysis type , set boundary conditions , define loads and finally we can then run the analysis [96].

## 2.9. Strain gauge

A strain gauge is simply a resistor that measures strain on an object. Whenever an external force acts on an object, there is a deformation in shape that occurs in response to that force. This

deformation can either be compressive or tensile. When an object deforms within its elastic limit, it either becomes longer and narrower or shorter and thicker. A strain gauge is sensitive to minor changes that occur in the geometry of an object, so due to the change in geometry there is a change in resistance that is measured by the strain gauge and hence the amount of induced stress can be calculated [41].

Strain ( $\epsilon$ ) is defined as the ratio of the change in length ( $\Delta L$ ) of a material to the original length ( $L$ ), as shown in figure 26. When the force on the object leads to elongation of the part strain is positive due to the tensile nature of the force. On the other hand, when the force on the object leads to compression strain is then negative due to the compressive nature of the force. When a material is compressed by a force in one direction, the resistance to this force leads the material to expand in the other two directions perpendicular to the force this phenomenon is known as the Poisson effect. Poisson's ratio ( $\nu$ ) is the scale of this effect and is simply the negative ratio of strain in the transverse direction to the strain in axial direction [42].

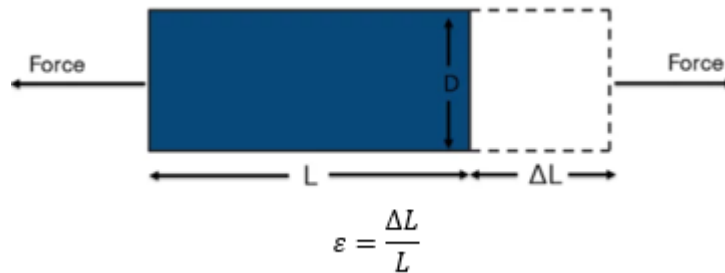


Figure 26: Demonstration of resulting strain due to force applied[42]

From knowing strain, stress can be obtained through Hooke's Law which is given by:

$$\sigma = E \cdot \epsilon$$

Where  $E$  is the Young's modulus of the material with dimensions of force over area just like stress since strain is a dimensionless ratio [44]. The working principle of a strain gauge is based on the change of electrical resistance with deformation. In electrical terminology, a strain gauge is an example of a passive transducer that converts mechanical displacement into an electrical quantity. The formula for the resistance of strain gauge metal is given by [43]:

$$R = \rho \left( \frac{L}{A} \right)$$

Where  $R$  is the resistance in ohms ( $\Omega$ ),  $\rho$  is the resistivity ( $\Omega \cdot m$ ),  $L$  is the length of the conductor or semiconductor element (m) and  $A$  is the cross sectional area ( $m^2$ ).

The most common type of strain gauge used is the bonded metallic strain gauge. The gauge is composed of a metallic foil arranged in a grid pattern. The grid pattern maximizes the amount of metallic foil subjected to strain in the parallel direction. The carrier is the thin backing that the grid is bonded to, which is attached directly to the sample requiring measurement. Hence, the strain

experienced by the sample is transferred directly to the gauge which gives feedback with a linear change in electrical resistance [42].

Considering the functionality of a strain gauge it is used as a precautionary measure in many testing applications where whenever the strain gauge gives a certain reading an alarm would be triggered to inform the user that the capacity has been reached meaning action has to take place before any risk happening.

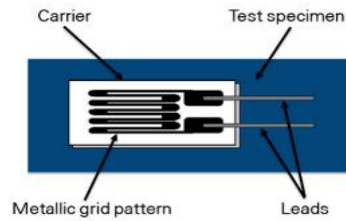


Figure 27: Composition of Bonded metallic strain gauge[42]

### 2.9.1. Selection of a strain gauge

In order to select a suitable strain gauge, the measurement objective needs to be clarified. The main query to be accounted for is whether the gauge is used for experimental tests, resilience or for transducer manufacturing [45].

Experimental / Resilience Tests	Transducer Manufacturing
Experimental test analysis	Force
Residual stress analysis	Mass
Analysis of loading	Torque
Life-time analysis	Pressure
Determining thermal stress	Strain

Table 10: Different Measurements done by strain gauges [45]

In case of experimental tests measurement, the following criteria of selection shown in table 11 should be considered:

<b>Criteria</b>	<b>Description</b>
Geometry	Number and position of grids (pattern)
Strain gauge series	Construction of strain gauge
Connections	Type and position
Temperature response and adaptation	Material to which strain gauge temperature response is matched
Active grid length	In mm
Electrical Resistance	In Ohm ( $\Omega$ )

*Table 11: Strain gauge selection criteria for experimental tests [45]*

Firstly, the geometry of the strain gauge is an essential criterion as they are developed due to stress exerted in different directions. Listed below are some varieties of strain gauge geometries available [46].

### 1) **Linear Strain Gauge**

A linear strain gauge is used to measure strain in a single direction to which the measuring grid is aligned to. Generally, it is mounted to in the direction where the main force is applied. This pattern is favored when measurements are performed in one direction only. Examples for applying this strain gauge can be aircraft component testing, equipment manufacturing etc. [46].

### 2) **Shear Strain Gauge**

A shear strain gauge is composed of two measuring grids arranged at  $45^\circ$  to the strain gauge axis and  $90^\circ$  to each other. This type of pattern is mainly used for measuring torque in a rotating object that includes measurements on torsion bars . They are also used in construction torque transducer [46].

### 3) **Rosette Strain gauge**

Rosettes with 2 or 3 measuring grids are commonly used in several applications. A T-rosette strain gauge has 2 measuring grids arranged on a carrier perpendicular to each other, while a 3-grid geometry has 3 measuring grids spaced at different angles. Multiple strain gauge configurations are suitable for applications where biaxial stress state needs to be determined while not knowing principal direction. Hence, rosette strain gauge allows different directional strain measurements which provides more precise surface strain measurement [46].

### 4) **Chain Strain Gauge**

This type of strain gauges is composed of 10-15 fine evenly spaced grids while all on the same carrier. This configuration is ideal for measuring strain gradient for example the stress curve over a required section or the transfer of peak value due to contact of the load introduced on a moving point.

## 5) Full-bridge Strain Gauge

This type of strain gauge consists of 4 measuring grids that are switched to a Wheatstone full bridge. Every measuring grid is countervailed to the next grid at an angle of 90 °. Common applications for this type of configuration is tension or compression bars and shear stresses happening in shear beams around the neutral fiber. They are also designed to manufacture accurate force transducers while implementing bending beam working principle [46].

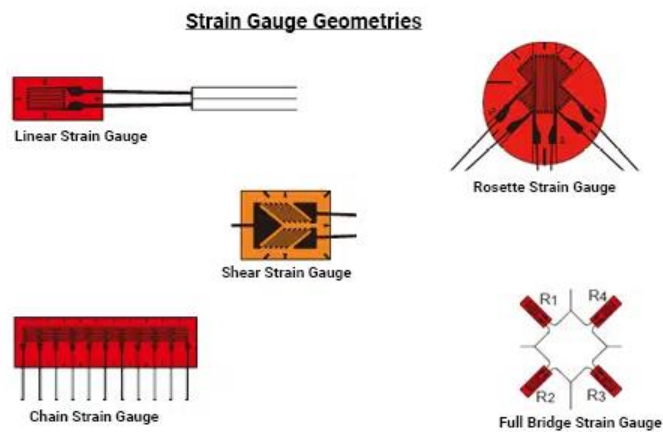


Figure 28: Different Strain gauge pattern geometries[46]

There are different strain gauge series for strain measurement. The strain gauge carrier (e.g., Polyimide) and the measuring grid foil (e.g., Constantan). All strain gauges within a strain gauge series have identical carrier and measuring grid material. Hence, many designations are the same for one strain gauge series. In experimental testing robust and flexible strain gauges, can be used under harsh conditions, have well defined advantages. Strain gauges including the synthetic polyimide, as carrier material for the measuring grid with series identification “Y” are included in this category. The Y series has a wide variety of strain gauges used for different tasks for experimental tests . There exist multiple special types of strain gauges for example used in hole drilling and strain gauge chains for stress distribution investigation for complex structures [45].

The third criterion mentioned above is the connections where different configurations are used on the strain gauge, below are 6 different types of commercially available strain gauge configurations.

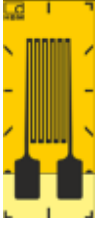
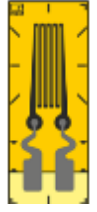



Strain Gauge Connection Configuration	Characteristic
	<p><b>Integrated Solder Tabs (e.g., LY4)</b></p> <ul style="list-style-type: none"> <li>• Allows Direct soldering on the strain gauge</li> </ul>
	<p><b>Big solder tabs with strain relief (e.g., LY6)</b></p> <ul style="list-style-type: none"> <li>• Allows direct soldering on the strain gauge and simultaneously providing nearly full mechanically decoupling of solder tabs and strain gauge carrier</li> </ul>
	<p><b>Ni-plated copper leads, uninsulated, approx. 30 mm (1.18 inch) long (e.g., LY1)</b></p> <ul style="list-style-type: none"> <li>• No direct soldering at the strain gauge.</li> <li>• For full mechanical decoupling of cables and strain gauge.</li> <li>• Use of separate solder terminals directly on the strain gauge required.</li> </ul>
	<p><b>fluoropolymer-insulated connection wires, approx. 50 mm(1.97 inch) long (e.g., K-C LY4)</b></p> <ul style="list-style-type: none"> <li>• No direct soldering at the strain gauge</li> <li>• Fluoropolymer insulation prevents the cable from sticking during installation.</li> <li>• Use of separate solder terminals near the strain gauge required</li> </ul>
	<p><b>Fluoropolymer-insulated connection wires, approx. 50 mm (1.97 inch) long (e.g., K-C LY4)</b></p> <ul style="list-style-type: none"> <li>• cable length as required from 0.5 to 10 m in 2-wire, 3-wire and 4-wire are available.</li> <li>• no direct soldering at the measuring point at all</li> <li>• Fluoropolymer insulation prevents the cable from sticking during installation</li> </ul>

Table 12: Strain gauges with different connection configurations [45]

Now onto the fourth criterion which is the temperature response adaptation, whenever a strain gauge is connected separately in a Wheatstone quarter bridge circuit there will be an output signal if the temperature is altered. This is known as the thermal output, and it is independent to the mechanical load that will act on the test specimen. However, there exists strain gauges that give a very small output signal in case of

temperature change such strain gauges are referred to as self-compensated strain gauges [45].

These strain gauges must be selected to the thermal expansion coefficient of the test specimen to benefit from their matched temperature response [45].

Moreover, the active grid length relies on the objective of the measurements as the output of the measurement using strain gauges will be the mean strain below the measuring grid. Typically, measuring grids have lengths of 3 or 6 mm which provides a good enough solution. Long measuring grids are preferred when dealing with an inhomogeneous specimen, such as concrete or wood. On the other hand, short measuring grids are applicable for detecting the state of strain. Hence, they are fit for determining strain gradients, maximum peak of notch stresses and similar stresses [45].

Finally, the sixth criterion which is the electrical resistance selection. The choice of resistance depends on the constraints of the measurement task, since low resistance and high resistance strain gauges have different characteristics shown in table 13 [45].

Low resistance Strain gauge	High resistance Strain gauge
Lower influence of electromagnetic interferences	Lower influence of electrical resistance in connection paths
Lower influence of a change in isolation resistance	Enhanced antennas in the case of interferences.
Higher power requirement	Higher influence of a change in isolation resistance.
Increased self-heating as a result of high current flow compared to high resistance strain gauge	-

*Table 13: Characteristics of low and high resistance strain gauges[45]*

### 2.9.2. Strain Gauge types

There are different classifications of the strain gauges that one can apply, based on the principle of working strain gauges are classified into Mechanical, Electrical and Piezoelectric. Strain gauges that are directly bonded (pasted/epoxied) on the surface of the structure under strain examination are referred to as bonded strain gauges, the three



types of bonded strain gauges that will be discussed in the following subchapters are [47]:

- Metal Foil Strain gauge
- Fine wire Strain gauge
- Semi-conductor strain gauge

### 2.9.3. Metal foil strain gauge

Metallic foil strain gauge consists of a metal foil of 0.02 mm thick produced via printed circuit technique. This Metal foil is produced on one side of the plastic backing. Leads are soldered to the metal foil for electrical connection of the strain gauge to the Wheatstone bridge [47].

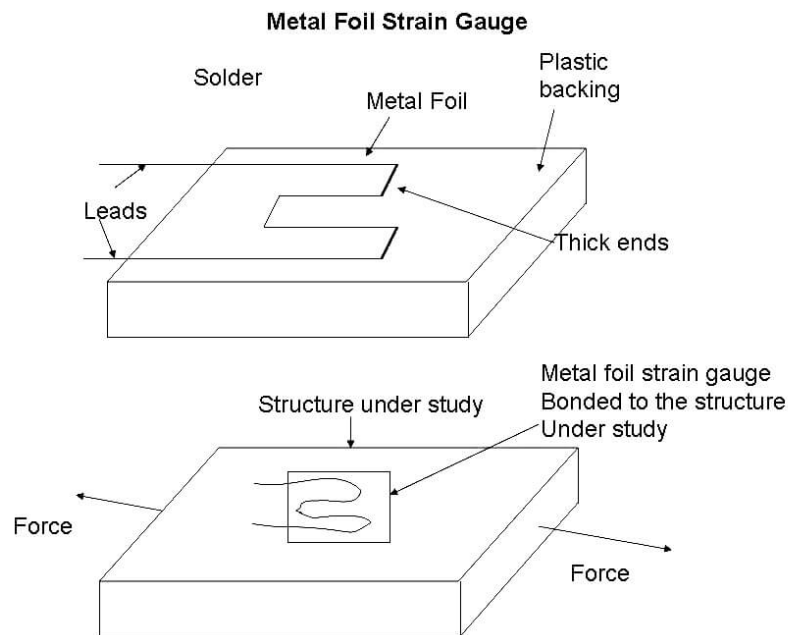


Figure 29: Metal Foil strain gauge arrangement[47]

With the use of an adhesive material, the strain gauge is bonded on the structure under study. Whenever the structure is exposed to a force whether tensile or compressive, due to the force the structure experiences a change in dimension/geometry. Since the strain gauge is bonded to the structure the gauge will also undergo change in both length and cross section indicating that it is strained which leads to change in resistivity that will be recorded by the strain gauge [47].

This deformation (strain) changes the resistance of the strain gauge which is measured using a Wheatstone bridge. The change in resistance of the strain gauge becomes a measure of the extent to which the structure is strained and a measure of the applied force when calibrated [47].

#### **Advantages of Metal foil Strain gauge [48]:**

- For Vibrational and load sensing (static and dynamic load).
- Perfect bondage between the strain gauge and the structure to be examined is achievable.
- The backing can be peeled off and the metal foil with leads can be used directly on the structure under examination. Usually, a ceramic adhesive can be used.
- These Gauges have a better fatigue life, good sensitivity, and stability even at high temperatures.

#### **Disadvantages of Metal foil Strain gauge [48]:**

- Susceptibility to creep error, since they are highly sensitive and are directly bonded to structure under examination
- Accuracy will decrease overtime due to wear of the adhesive.

#### **2.9.4. Fine Wire strain gauge**

The Fine wire strain gauge consists of a fine resistance wire with diameter of 0.025 mm which is bent repeatedly as shown in figure 30. This is done to increase the length of the wires so that permits uniform distribution of stress. The resistance wire is placed between the two carrier bases (paper, Bakelite, or Teflon) which are cemented to each other. The carrier base protects the gauge from damages and the leads provide the electrical connection between the strain gauge and Wheatstone bridge [48].

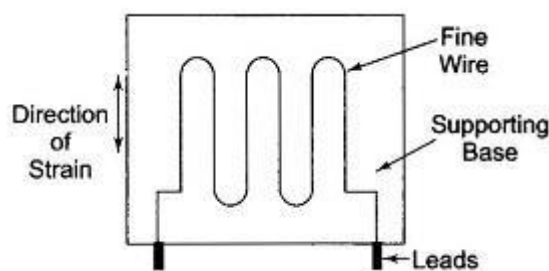


*Figure 30: Fine wire strain gauge arrangement[48]*

Just like the metallic foil strain gauge, the fine wire strain gauge is bonded to the structure under study. Whenever the structure is subjected to a force whether tensile or compressive, due to the force the structure will deform. This deformation will change the resistance of the strain gauge since the strain gauge is bonded to it, in both length and cross section. The change in resistance becomes

the measure of the extent to which the structure is strained and a measure of the applied force when scaled [48].

**Advantages of Fine wire Strain gauge [48]:**

- The range of this gauge is +/- 0.3% of strain.
- High accuracy.
- Has a linearity of +/- 1%.

**Disadvantages of Fine wire Strain gauge [48]:**

- The gauges are not reusable (cannot be detached and used again)
- Higher cost compared to other strain gauges.

### 2.9.5. Semiconductor strain gauge

Semiconductor strain gauge utilizes the property of piezo resistivity possessed by doped silicon or germanium. The resistivity of those such materials changes whenever they are under stress due to the load acting on the materials. This difference in resistivity (resistance) is as a measure of strain which can be scaled to different units per requirement [49].

These gauges are produced in the form of wafers of thickness 150  $\mu\text{m}$ , material used may be silicon or germanium in which exact amounts of contaminants such as Boron or Phosphorous have been added to achieve certain desired properties. This process is known as doping and the crystals formed are referred to as doped crystals [49].

A typical Semiconductor strain gauge consists of semiconductor materials and leads enclosed in a protective casing. Bonded on suitable insulating material such as Teflon. These types of gauges have negative temperature coefficient resistance, which enables very large change in length as compared to other strain gauges, such as wire and foil type gauges. Electrodes are from gold wires as they are utilized as one arm of the Wheatstone bridge [49].

There are two types of the sensing element (wafer) [50]:

1. Negative or n-type, where resistance decrease with respect to tensile strain.
2. Positive or P-type, where resistance increase with respect to tensile strain.

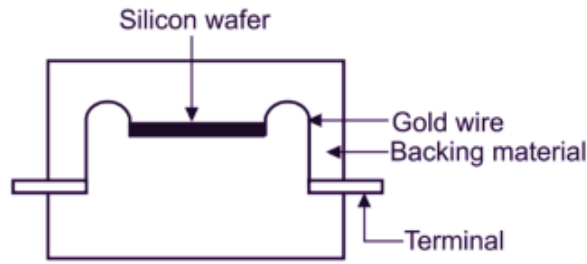


Figure 31: Semiconductor type bonded strain gauge [49]

As the strain gauge is bonded to the structure, the strain gauge will undergo change in both length and cross section (that is strained). When the sensing element (crystal) of the semiconductor strain gauge is strained its resistivity changes contributing to the change in resistance of the strain gauge. The difference in the resistance of the strain gauge is measured via the Wheatstone bridge, this difference becomes a measure of the extent in which the structure is strained and a measure of the applied force when calibrated [49].

**Advantages of semi-conductor Strain gauge [49]:**

- High gauge factor in the range of 100 to 200 as compared to metallic wires having a gauge factor 2. Therefore, very small strains or deformations can be detected.
- More life under fatigue loading.
- Low hysteresis.

**Disadvantages of Semi-conductor Strain gauge [49]:**

- It is highly sensitive to change in temperature, so it is difficult to obtain reliable reading
- It is more expensive and difficult to attach to the object under examination compared to other available strain gauges.
- It has a nonlinear characteristic relationship of output voltage with strain.

**2.9.6. Strain Gauge configurations**

A foundational parameter of a strain gauge is its sensitivity to strain, expressed quantitatively known as the gage factor (GF), GF is the fractional change in electrical resistance to the fractional change in length, or strain [51]:

$$GF = \frac{\Delta R/R}{\Delta L/L} = \frac{\Delta R/R}{\epsilon}$$

Generally, GF for metallic strain gauges is usually around 2. GF of a certain strain gauge can be known from the specification documentation provided from the manufacturer or vendor [51].

Strain gauge measurements rarely involve quantities larger than a few milli strain ( $\epsilon \times 10^{-3}$ ). For that reason, to measure strain, very small changes in resistance must be precisely measured. In order to measure small changes of resistance, strain gauge configurations are based on the conceptualization of a Wheatstone bridge. The general Wheatstone bridge circuit is shown in figure 32, which is a network of four sensitive arms with an excitation voltage ( $V_{EX}$ ) that is applied across the bridge [51].

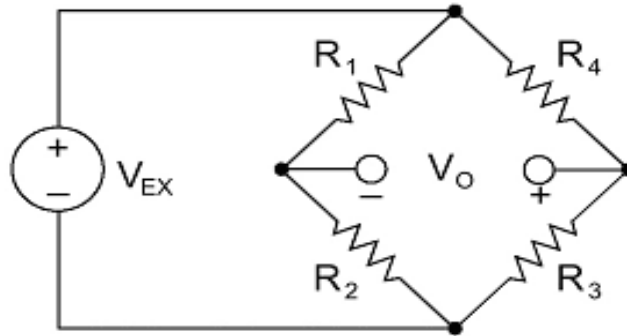


Figure 32: General Wheatstone bridge[51]

The Wheatstone bridge is equivalent to two parallel voltage divider circuits. Where  $R_1$  and  $R_2$  constitute one voltage divider circuit, while  $R_3$  and  $R_4$  constitute the second voltage divider circuit. The output of a Wheatstone bridge is measured between the middle nodes of the two voltage dividers [51].

$$V_o = \left[ \frac{R_3}{R_3 + R_4} - \frac{R_2}{R_1 + R_2} \right] \cdot V_{EX}$$

From the equation above, we can see that  $R_1/R_2 = R_3/R_4$ , where the voltage output ( $V_o$ ). Considering these conditions, the bridge can be called balanced. Any fluctuations in resistance of any arm of the bridge results in a nonzero output voltage. Therefore, when replacing  $R_4$  in figure 32 with an active strain gauge, any fluctuations in the strain gauge resistance unbalance the bridge and produce a nonzero output voltage which is a function of strain. There are three types of strain gauge configurations, quarter-, half-, and full-bridge, which are determined by the number of active elements in the Wheatstone bridge, the inclination of the strain gauges, and the type of strain being measured [51].

### 2.9.7. Quarter-bridge strain gauge Type I and II

Quarter bridge strain gauge configuration type I measures axial or bending strain and requires a passive quarter bridge completion resistor referred to as a dummy resistor. Moreover, this configuration also requires a half bridge completion resistor to complete the

wheat stone bridge.  $R_4$  is the active strain gauge measuring tensile strain ( $+\epsilon$ ), strain gauges set in moment strain configuration are used to measure vertical load [51].

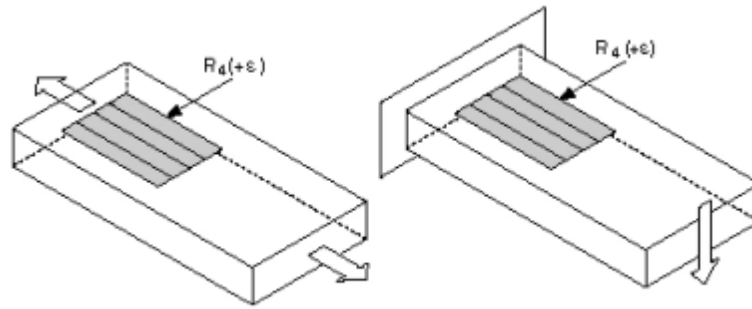


Figure 33: quarter bridge strain gauge configurations[51]

In configuration type II, the resistance of the strain gauge varies only in reaction to applied strain. Nevertheless, strain gauge material, as well as the sample material to which the gauge is applied, also responds to changes in temperature. Quarter-bridge strain gauge configuration type II helps decreasing the effect of temperature by using two strain gauges in the bridge as shown in figure 34, generally one strain gauge ( $R_4$ ) is active and a second strain gauge ( $R_3$ ) is mounted in close thermal contact, but not bonded to the sample and placed transversely to the principal axis of strain. For this reason, there is a small effect on the dummy gauge, but any temperature changes affect both gauges similarly. Since the temperature changes are identical in the two strain gauges, the ratio of their resistance does not get altered, the output voltage does not change, and the effect of temperature is decreased [51].

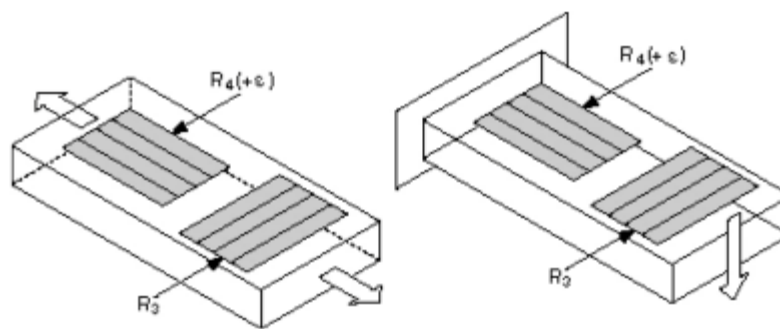


Figure 34: Dummy strain gauges eliminating effect of temperature on measurement[51]

### 2.9.8. Half-bridge strain gauge Type I and II

In half bridge strain gauge configuration, the bridge's sensitivity to strain can be doubled by making both strain gauges active in a half-bridge configuration. Type I configuration measures axial or bending strain and requires half-bridge completion resistors to complete

the Wheatstone bridge.  $R_4$  is the active strain gauge measuring tensile strain ( $+\epsilon$ ) and  $R_3$  is an active strain gauge compensating for Poisson's effect ( $-\nu\epsilon$ ). This configuration is often confused with eh quarter bridge type II, but the difference is that the half bridge type I has an active  $R_3$  element that is bonded to the strained sample.

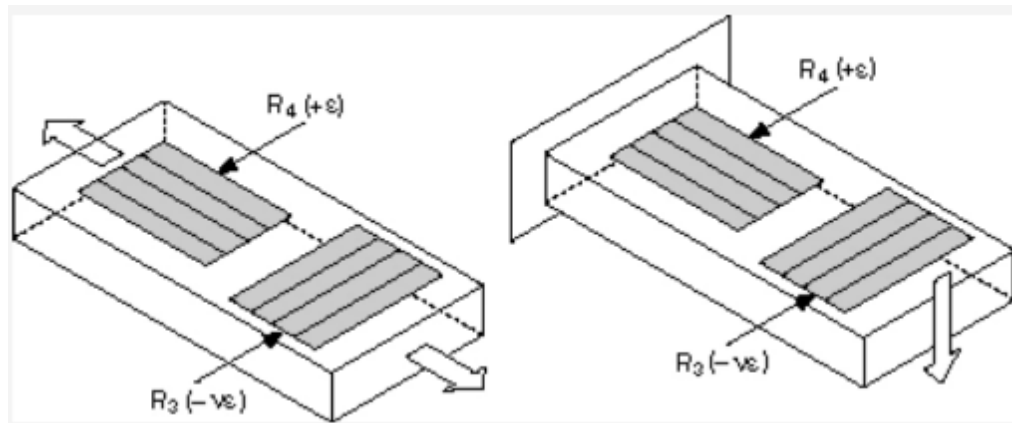


Figure 35: Half bridge strain gauge Type I[51]

Configuration Type II measures bending strain only and it requires half-bridge completion resistors to complete the Wheatstone bridge.  $R_4$  is an active strain gauge measuring the tensile strain ( $+\epsilon$ ) while  $R_3$  is an active strain gauge measuring compressive strain ( $-\epsilon$ ) [51].

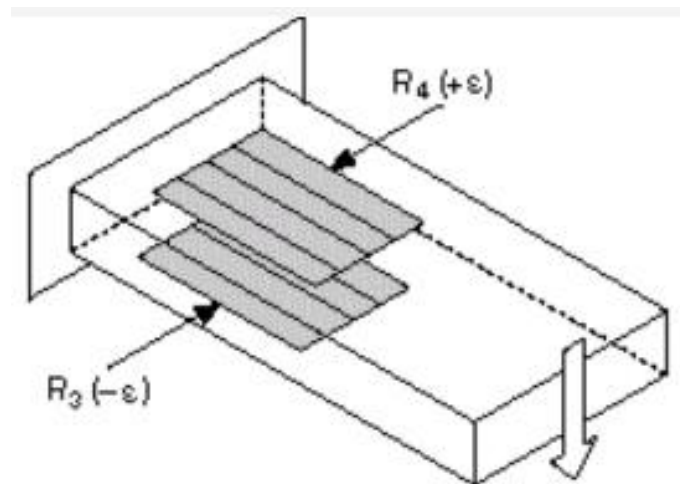


Figure 36: Half bridge strain gauge Type II[51]

### 2.9.9. Full-Bridge Strain gauge

In full-bridge strain gauge configuration four active strain gauges are available in different types. Type I and II measure bending strain while type III measures axial strain. All three configurations compensate the effects of temperature but only type II and III compensate the Poisson effect [51]. Configuration Type I is highly responsive to bending strain

only.  $R_1$  and  $R_3$  are active strain gauges measuring compressive strain ( $-\varepsilon$ ) while  $R_2$  and  $R_4$  are active strain gauges measuring tensile strain ( $+\varepsilon$ ) [51].

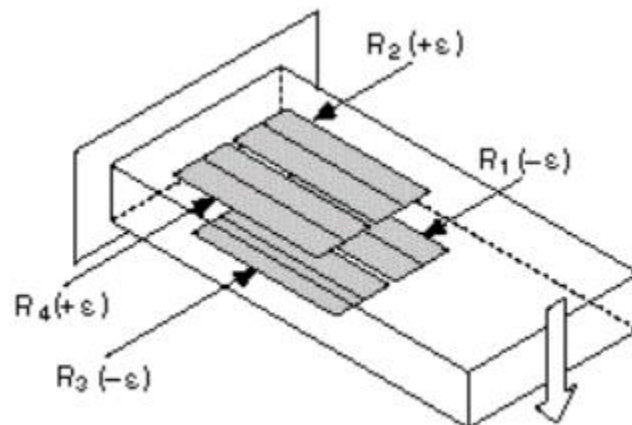


Figure 37: Full-bridge strain gauge Type II [51]

Configuration Type II measures bending strain only while having  $R_1$  and  $R_2$  active strain gauges measuring compressive Poisson effect ( $-\nu\varepsilon$ ) and tensile Poisson effect ( $+\nu\varepsilon$ ) respectively. On the other hand,  $R_3$  and  $R_4$  as active strain gauges as well measuring compressive strain ( $-\varepsilon$ ) and tensile strain ( $+\varepsilon$ ) respectively [51].

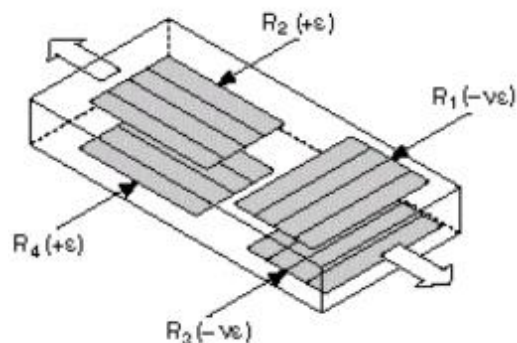


Figure 38: Full-bridge strain gauge Type III [51]

Configuration type III measures axial strain while having  $R_1$  and  $R_3$  as active strain gauges measuring the compressive Poisson effect. On the other hand,  $R_2$  and  $R_4$  are active strain gauges measuring tensile strain ( $+\varepsilon$ ) [51].

### 2.9.10. Compensation of Temperature drift of sensor

For minimization of sensitivity of the strain gauge, manufacturers attempt processing the gauge material to compensate for the thermal expansion of the specimen material for which the gauge is intended. While compensated gauges reduce the thermal sensitivity, they do not totally remove it.



A residual error in the order of  $10 \text{ me}/^\circ\text{C}$  is possible using such a technique. Using a half bridge or a full bridge Wheatstone bridge is the simplest way of correction for temperature drift [52].

When all strain gages in a bridge are at the same temperature and mounted on the same material, any fluctuations in temperature affects all gauges in the same way since the temperature changes are identical in the gauges. The ratio of their resistance does not change nor does the output voltage of the gage [52].

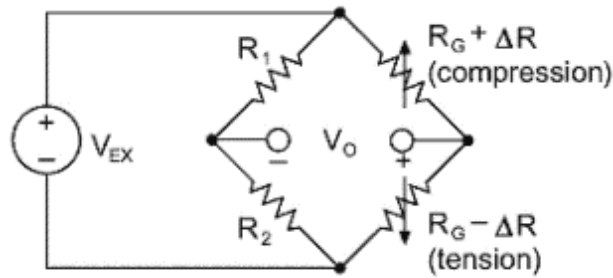


Figure 39: Half-Bridge Configuration [52]

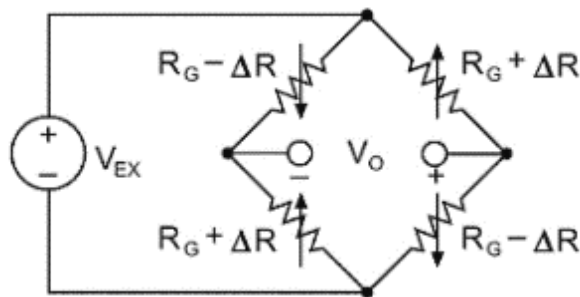


Figure 40: Full-Bridge Configuration [52]

Additional correction is achievable by measuring temperature using a correction curve to correct the data. Manufacturers print the polynomial coefficients of this curve (Figure 41) to the fourth order on each package of gauges. With the given coefficients one can apply temperature correction in applicable software. An error as small as  $1 \text{ me}/^\circ\text{C}$  is possible using this technique [52].

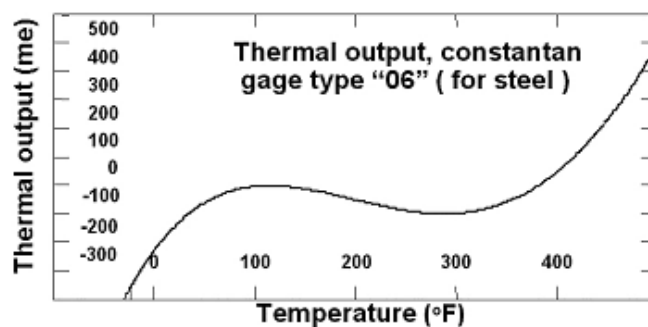


Figure 41: Thermal Output rating[52]

Strain gauges applied in nuclear environments are subjected to tempering of their basic characteristics like sensitivity, electrical resistance, insulation resistance, signal drift, signal noise

and structural integrity. As such alterations result from physical phenomena in the gauge grid metal under radiation, including loss of electrical insulation of the grid carrier, embrittlement of the grid carrier, degradation of the attachment or bonding applied or even degradation of the solder pads and cable connections [53].

Previous experiments performed involving strain gauges in radioactive environment listed the following precautions to ensure optimal performance of strain gauge under irradiation exposure [53] :

- The manufacturing of the gauge should not involve any biological materials.
- Even for applications involving ambient temperature, high-temperature gauges should be used.
- Similarly, to temperature compensation, measurement techniques should provide compensation of calibration shift and drift therefore, the half-bridge or full-bridge connections should be applied.
- In case of neutron dose of radiation, Constantan or platinum/tungsten are to be used for their smaller resistance change when irradiated. Hence, material selection of strain gauge should be chosen carefully per the radiation level.

### 2.9.11. Errors Caused by Lead resistances

An electrical connection consisting of a length of wire, or a metal pad (surface mount technology) designed to connect two locations is referred to as lead [53], the wires connecting the leads of the strain gauge within the Wheatstone bridge have their own resistances and are known as lead wire resistance  $R_l$  [52].

Lead wire resistances also change with temperature and can have an adverse effect on the precision of strain gauge measurements. Even if the system was initially balanced, differences in the lead wire resistance with temperature can impose large errors in static measurements. This can occur even though the lead wire resistance is much smaller than the bridge resistance, considering the temperature coefficient of copper typically being two orders of magnitude greater than the temperature coefficient of the gauges. Even though connecting the gauge with two wires in a quarter bridge circuit, drift caused by lead wire temperature difference would be huge. Therefore, static measurements are performed using the three-wire circuit, shown in figure 42. The bridge remains balanced if lead wire resistances  $R_l$  track with temperature [52].

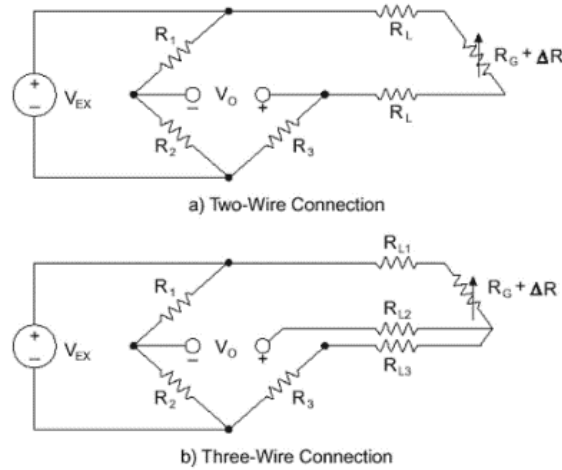


Figure 42: 2 wire and 3 wire connections for quarter bridge sensors [52]

In radioactive environments, whenever a beam of radiation is subjected to a target with a strain gauge applied for a period the accumulated doses of radiation eventually increase the temperature of the target which will affect the strain gauge. With increasing temperature, the resistance of the wires increases as collisions within the wire increase and reduce the flow of current [52]. Therefore, selection of a wire with low resistance will minimize such an effect [53].

### 3. Experiments

This chapter deals with the methodology , equipment and data processing of the experiments performed on the 3 carbon fiber composite pipes. There are several conditioning elements that any part endures during its service lifetime that have effects on the part's life. In our experiment the elements taken into consideration are the effect of radiation on the aging of the part and the mechanical stability of the carbon composite pipes in vacuum , as such elements are typical in ion research facilities. The following 2 hypothesis were set before the experiment:

- A. There are no significant difference between the mechanical responses of the evacuated pipe exposed to radiation compared to the control pipe.
- B. There are no significant changes in the response of strain gauges after exposing them to high radiation.

### 3.1. Methodology

This chapter demonstrates the procedure performed in the preparation of the experiment, given below is the list of instructions followed:

1. Application of strain gauge to cover expected principal stresses.
2. Assembly of the pipes per the sample assembly drawing: including all O-rings, costume rings, sample tube with rail, caps (covers) and bolts with cylinder head and inner Allen.
3. Insertion of the sample assembly inside the irradiation chamber while keeping electronics out of the target range using 10 m connection wires (from strain gauge up to the compensation circle).
4. Connection of strain gauges to the compensation circle (DEWETRON data Acquisition system).
5. Test the set up for functionality and distinguish output responses given from the 3 pipes.
6. Connection of vacuum pump through KF-40 flange as shown in figure 43 and start recording responses of the strain gauges through DEWETRON data acquisition system.
7. Evacuation of the composite pipe down to  $10^{-2}$  mbar (1 mBar = 100 Pa) at ambient conditions.
8. Start Irradiating the pipe in the region shown in figure 43 for 30 minutes using TR-24 cyclotron in Institute of Nuclear physics(UJF , CAS ) labs.
9. Store sample for 40 days or more till the radiation level is safe to handle.
10. Apply New pairs of strain gauges in case of detachment or evaporation of adhesive on any of the samples and set up the connection of compensation circle .check responses of strain gauges after radiation exposure to confirm set hypothesis.
11. Before evacuation of the pipe ensure functionality of the strain gauges and start recording on the DEWETRON data acquisition system then start evacuating to check responses of strain gauges after exposure to confirm hypothesis B.
12. After evacuation for and disassembly off the turbomolecular pump from the sample tubes assembly, cut the sample in the  $1\text{ cm}^2$  samples for light and electron microscopy.

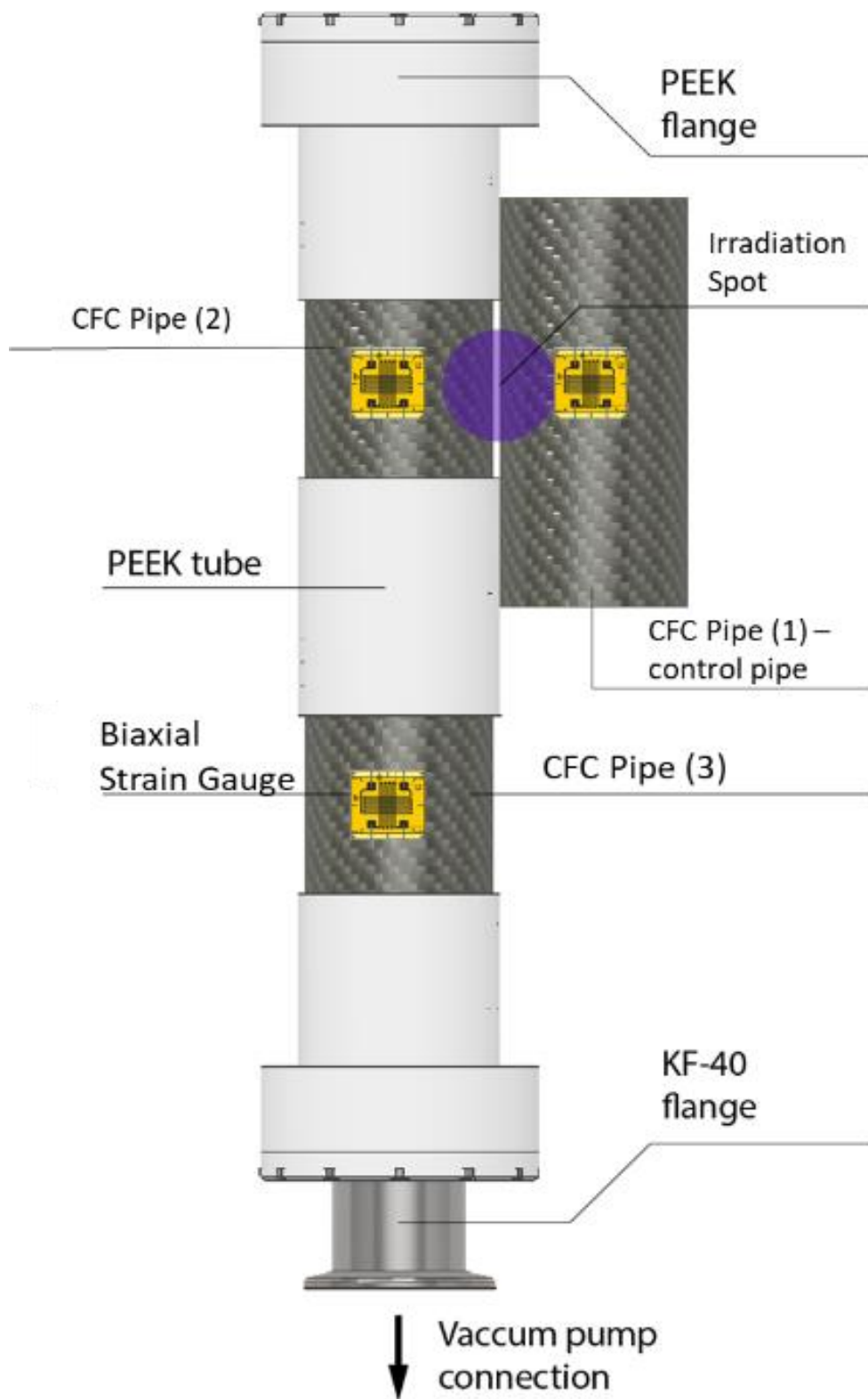


Figure 43: Schematic of experimental setup

### 3.1.1. Preparing the mounting Surface

To understand the stresses that the pipes will endure due to the conditioning elements of the environment that they are being subjected to strain gauges are applied onto our 3 sample tubes. The strain gauge applied is a biaxial strain gauge that measures axial and circumferential (hoop) stress, type 6/120 XY91 from HBM with resistance  $120 \Omega \pm 0.50 \%$ .

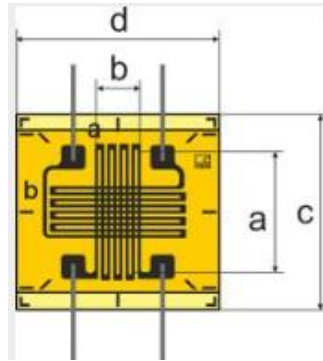


Figure 44: Schematic of type of strain gauge used (XY9 Stacked grid with leads)[85].

Initially, the most important step is to avoid any contaminants that might affect the ability of the adhesive to transmit strain from the pipes to the strain gauge. So, cleaning the surface with the use of a solvent such as acetone or alcohol to remove any grease or oils from the surface to which the strain gauge will be bonded to was done. This prevents any contaminants from being driven into the surface while performing subsequent steps. Hence, by cleaning an area larger than the gauge helps in avoiding any contaminants being introduced to the gauge area [98].

Moreover, Abrading the surface to remove any oxidation, or coating from surface finishing. The abrading is done using sand paper to ensure proper smooth texture for adhesion. Keeping in mind to not over-brade the surface resulting in alteration of either dimensions or mechanical properties of the pipe. After the surface has been prepared, we do not let it stand for more than few minutes and apply the gauge to it [98].

### 3.1.2. Bonding the Strain gauge and Functionality test

Preparing the gauge to be applied should be done in a careful and smooth way, firstly with the use of a tweezer we grasp the gauge and place it on the clean working area with the bonding side down. Then with the use of proper length approximately 15 cm of cellutape to pick up the strain gauge and transfer it to the gauging area of the pipe. Aligning the strain gauge in such a way that makes the gauge plane parallel to the axis of the pipe. Then by pressing one end of the tape to the part, following that we smoothly place the whole tape and the gauge into position [98].

We then apply the catalyst by lifting one end of the tape such that the gauge is not in contact with the gauging area and the bonding site is exposed. After spreading the catalyst evenly on the area and the gauge we then apply enough adhesive to guarantee coverage under the gauge for proper adhesion. Figuring out what is enough adhesion required some trial and error iterations as the adhesive we used was Z90 adhesive solution which did not spread evenly under the surface of the gauge in the first attempts. After applying the adhesive, the strain gauge was under gentle thumb pressure to guarantee the bonding as much as possible, so applying pressure for 4-5 minutes fulfilled the adhesion process.

The above procedure of surface preparation and bonding of the strain gauge was done before the assembly of the covers and the rest of the apparatus to our 3 sample pipes we received from Compotech . In Figure 45, we can see the strain gauges applied on the pipes.



*Figure 45: Applied Strain gauges on pipes*

Following the application of the strain gauge on the pipes, the lead wires are then soldered onto solder terminals between the connecting cables and the strain gauge itself (see figure 46). This will facilitate perfect solder joint and provide strain relief for the strain gauge connections. In this experiment the connection used is a 3 wire sensor connection which means that every grid leads will be connected to a total of 3 wires that facilitates the connection between the strain gauge and the data acquisition system. Moreover, benefits acquired from such a connection include automatic compensation for the effects of leadwire temperature changes on bridge balance and increased measurement sensitivity compared to the two-wire configuration. In figure 47 we can see the circuit of the 3 wire connection and general specification of the DAQP-STG data acquisition system used.

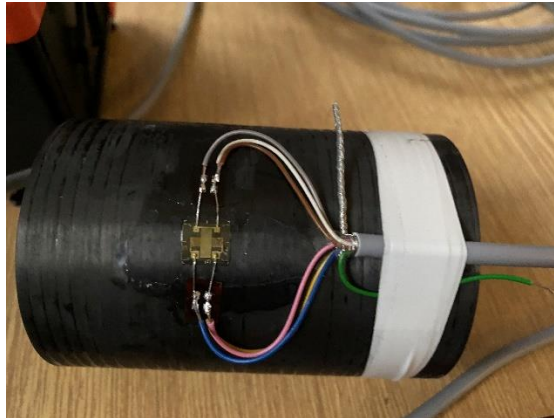


Figure 46: Control Pipe , soldered strain gauge lead wires and connection to wheatstone bridge

## Quarter bridge signal connection

### 3-wire sensor connection

(Sense+ is connected to EXC+ at the connector)

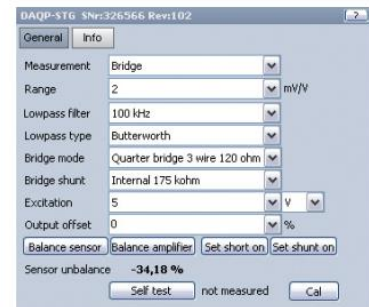
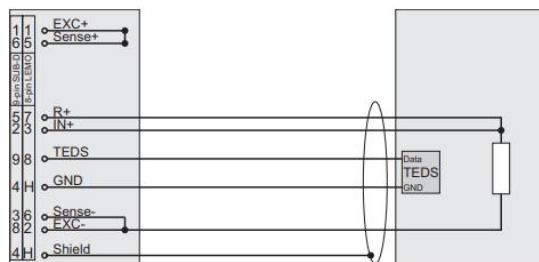


Figure 47: connection of strain gauge to DAQP-STG 3 via connector scheme and general specification [86]

Measurements depend on the right connection cables, they have to transfer the measurement signals from the strain gauge to the DAQ system and also have to avoid interference signals and resist stress during their use.



Figure 48: Six DB9 connectors connected to DAQ to complete compensation circle of the three strain gauges



The connection cable wires were soldered to the DB9 connector (covered with the plastic hood cover as shown in figure 48) per the 3 wire connection schematic shown in figure 48. A DB9 connector is an analog socket with 9 pins from the D-subminiature's connector family [87], after performing the connections the set up was tested for functionality through a computer software called DEWESOFTX and following the setting up given initial settings as the 3 wire connection, output obtained is a plot of strain gauge (mV/V) against time in seconds as shown in figure 49. Any stress applied by hand on the pipe would show a different pattern of increased fluctuations indicating the successful response of the strain gauge.

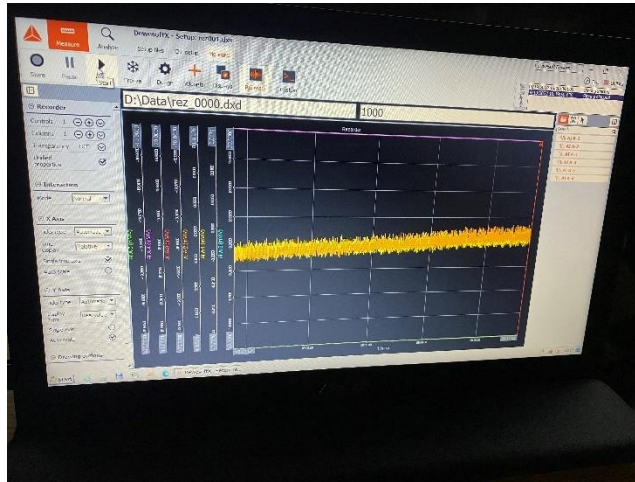


Figure 49: Strain gauge functionality check and plotting of Output (mV/V) against time (s)

### 3.1.3. Cyclotron TR 24 and Turbomolecular pump

In order to provide the conditioning elements taken into account for the environment that the composite pipes will be in the Cyclotron TR 24 is used as a radiation source directed onto the pipes and a turbomolecular pump is for pipe evacuation.



Figure 50: Cyclotron TR-24 of the canadian company ACSI (Advanced cyclotron systems Inc.) in the Czech academy of sciences irradiation chamber.

This cyclotron provides proton beams with energies ranging from 18 MeV to 24 MeV. Equipped with an axial injection system with an external ion source of the CUSP (cyclotron up scattering process) type which enhances the reachable current of the accelerated beams up to 300  $\mu\text{A}$  [88].

TR 24 – Advanced Cyclotron System Inc. (canada)	
Protons energy range	18- 24 MeV
Max. beam current	300 $\mu\text{A}$
Accelerating frequency	85 MHz
Aceelerating voltage	50 kV
Ion source	Multi-CUSP
Simultaneous beams	2
Weight	25 t
Size	1.8 x 1.8 x 2.5 m
Power consumption	180 kW
Average magnetic field	1.4 T

Table 14 : Parameters of cyclotron TR-24[88]

The sample assembly of the pipes was subjected to a beam with an energy of 24 MeV , monitored at a thin carbon foil which detects the particles. The EPR (Electron paramagnetic resonance)

current of the beam is 2  $\mu\text{A}$  and pipes were exposed for almost 30 minutes. Figure 51 and Figure 52 show the resonating trend of the beam's EPR current plotted against the irradiation period and report showing other current parameters from the monitoring system respectively.



Figure 51: TR-24 EPR current plot through irradiation period

Operator: ACSI-TR24\AC		Date & Time: April-20-22 12:00:55	
Beam on date: 4/ 5/2022		Beam on time 10 : 38 : 20 Elapsed time: 0 : 26 : 02	
<b>SIDE 2 Branch C</b> EPR: Radius: 508.2mm Azimuth: 2.20 Energy 24.0MeV Current: 2.0μA EBF: L: -0.1 μA R: 0.0 μA CM: -1.8 A -1.5 A CBF: L: -0.0 μA R: -0.0 μA BST2: 0.0 A 10.3 A PSL: -0.0 -0.0 0.0 BQ21: 89.3 A 89.2 A BQ22: 101. A 101. A SM: 82.5 A 82.5 A BBF: L: -0.0 μA R: 0.0 μA  Beamline loss: -0.0 μA		<b>SIDE 1</b> TGT: 1C Dummy EPR: Radius: 598.2mm Azimuth: 0.66 Energy 33.9MeV Current: -0.0μA  TS: X: 1.44 mm Y: 1.24mm PCL: L: 0.0 μA R: -0.1 μA TBF: -0.0 μA TCL: -0.0 -0.0 -0.0 0.0 TCL sum: 0.0 μA  Target current: -0.1 μA Transmission: 39.0 % Pressure: 68.1 Bar Beam counter: 0.0 μAmin	
<b>CURRENT SUMS</b>		EPR Sum	2.0
		TGT+TCL+TBF Sum	-0.1
		Target Sum	512.5
		Transmission Total %	*****
<b>CURRENTS</b>	XV0	2.8μA	
	PPR	0.3μA	
<b>MAGNET</b>	478.60 A	480.24 A	
<b>RF</b>	AmpRef	50.00 kV	50.03 kV
	RefP		0.05 kW
	Coupler	3.95	3.98
	Tuner	5.95	5.77
	Phase	5.95	
	Pwid	40.0	
<b>VACUUM</b>			
Temperatures:		Pressures:	
CP01	11.7 K	IG01	89.33 μPa
CP2	18.5 K	IG32	249.3 μPa
		IG2	2.4E7 μPa
<b>SITE WATER</b>		18.6 °C	
		1.9 M-Ohm	
<b>FILAMENT USAGE</b>		103 hours	
<b>ION SOURCE</b>			
Inflector (-)	7.50 kV	2.25 μA	
(+)	7.50 kV	1.22 μA	
IQ02	3.49 A	3.47 A	
IQ01	3.27 A	3.23 A	
YST01	-0.21 A	-0.16 A	
XST01	0.72 A	0.58 A	
Extract supply	0.66 kV	0.66 kV	
		3.97 mA	
Plasma supply	3.90 V	3.97 V	
		3.17 A	
Filament supply	221.5 A	221.2 A	
		3.43 V	
Arc supply	95.00 V	91.96 V	
	4.45 A	4.47 A	
Bias supply	28.00kV	27.92 kV	
		1.17 mA	
Flow controller	5.50 sccm	4.49 sccm	

Figure 52: Experiment's Irradiation Report from the TR-24 monitoring system

The second conditioning element taken into account in this experiment is vacuum where vacuum pressures have to be achieved inside the sample pipes when assembled through a vacuum sealing centering O-ring in between the KF flanges from the pipes sample assembly and the pump tube restrained together by a clamp to ensure contact. The pump used is the Scrollvac SC 5D shown in figure 53, the sample pipes were evacuated down to  $10^{-2}$  measured using pressure sensor PCG55x ATM to Medium Vacuum Gauge.



Figure 53: Vacuum pump connected to pressure sensor through valve top flange

### 3.1.4. Sealing Covers assembly and set up in Irradiation Chamber

The experiment is mainly based on the testing of the three carbon composite pipes. Two of the three pipes have two shoulders on the ends with three rail patterns forming a diameter slightly bigger than the nominal diameter see figure 54, where O-rings are fitted with the use of DOW CORNING high vacuum grease to smoothen the fit. After the O-rings are mounted (see figure 55) the two tubes are facing each other and are fitted onto a costume ring in between the bottom pipe (Pipe no.3) that is connected to the vacuum pump through the KF 40 flange. The top pipe is only covered by the flange and top cover bolted by 12 bolts with cylinder head and inner allen on each end as shown in figure 56.

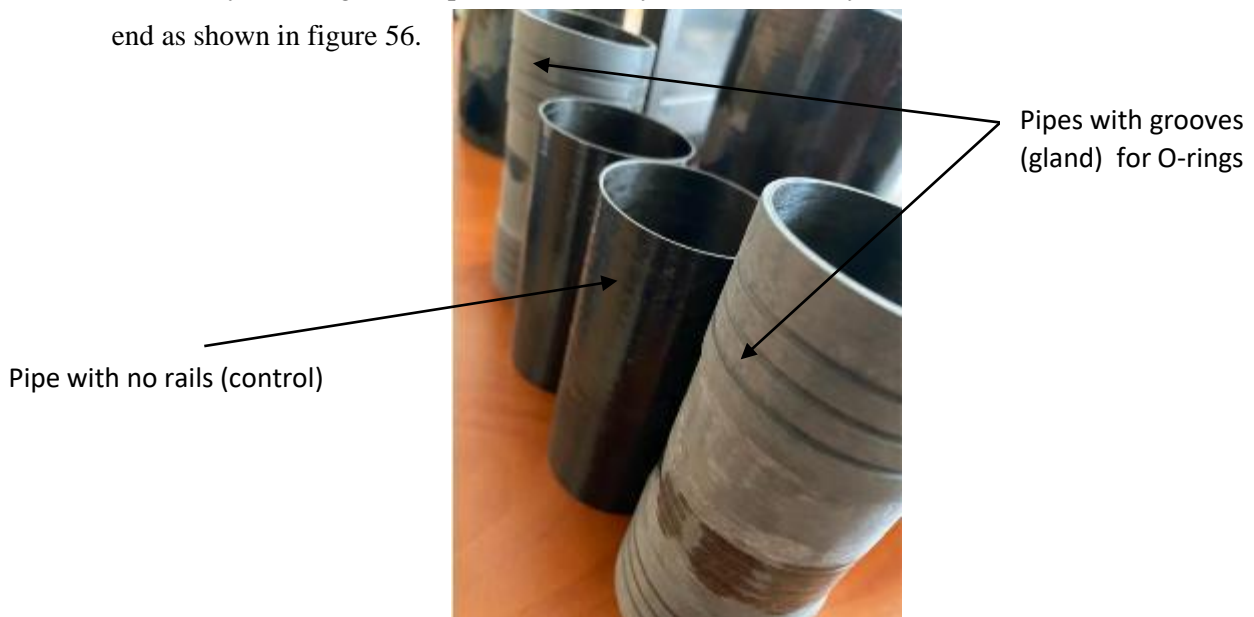


Figure 54: CFC experiment pipes





Figure 55: O-rings mounted on railed pipes

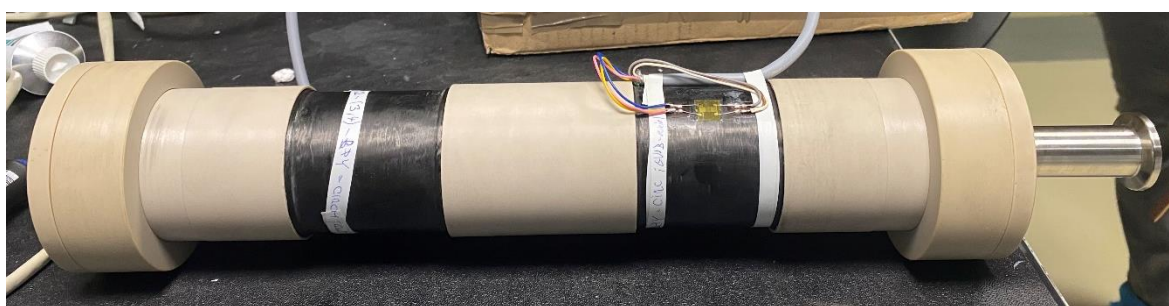
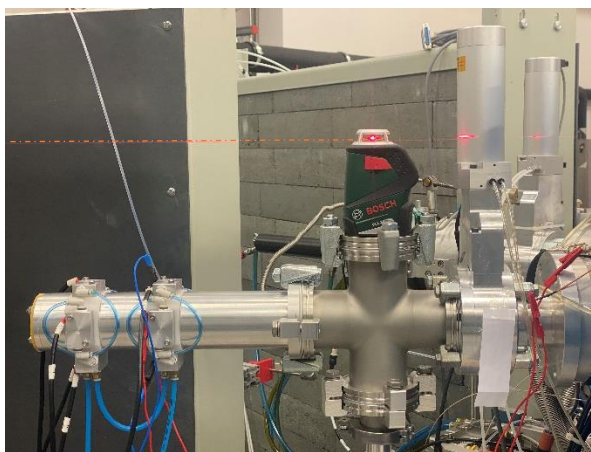


Figure 56: Assembly of railed pipes with costume ring, covers and flanges

In order to be able to distinguish the output readings obtained from the three strain gauges the pipes were numbered in the following order by the white cellulose tape around them :

1. Control pipe that is taped to the assembly parallel to the Irradiated pipe.
2. Evacuated Irradiated pipe (top pipe) that is irradiated on the mid-section by the beam
3. Evacuated pipe (bottom pipe) which is connected to turbomolecular pump through a KF40 flange.

Following the assembly of the pipes as shown in figure 56 , we had to position them vertically in such a way the beam from the source is hitting the target which is the pipes in a direction perpendicular to the center axis of the pipes. To ensure the beam of particles hitting the target, BOSCH line laser PLL 360 (see figure 57) was used to mark the path of the particles and therefore we are able to guarantee the beam striking the desired target region on the pipes. A metallic extruded framing with rails was used to level the sample assembly with the target path of the particles by taping the costume ring in the middle of the assembly to the framing and the rails are used to mount the KF-40 flange clampgripping the hose of the vacuum pump in contact with the framing.



*Figure 57: BOSCH line laser on TR 24 (cyclotron)*



*Figure 58: Pipes sample assembly taped to metallic framing and connected turbomolecular pump hose.*

Following the fixation of the pipes sample assembly and alignment with the target location, the strain gauges were checked for functionality again and the Pipe (No.3) connection through the KF40 flange was tightened and locked by the clampover the vacuum pump hose where it started evacuation through the vacuum pump. The irradiation chamber is then evacuated from the staff and the recording of the strain gauges started through the software DEWESOFTX and the samples were left in the chamber for approximately 90 minutes since the irradiation started.

### 3.1.5. Strain Gauge Data

Recorded responses of applied strain gauges were labelled in the order listed below, as each strain gauge provides two sets of values. One for axial stress and the another for circumferential stress.

- Control Pipe No.1 : Filtered Axial Stress (FA1), Filtered Circumferential Stress (FC1)
- Top Pipe No.2 : Filtered Axial Stress (FA2) ,Filtered Circumferential Stress (FC2)

- Bottom Pipe No.3 : Filtered Axial Stress (FA3), Filtered Circumferential Stress (FC3)

The Data obtained was very large approximately up to 7 million data points were recorded as the data saved included readings with part of a second. The Data acquisition system has a feature of providing filtered readings from the noise of the signals perceived. Below is a snippet of the data columns obtained in .txt format from DEWESOFTX program.

```
Data info
File name: D:\data\rez_0004.dxd
Start time: 4/28/2022 11:06:07.000
Number of channels: 13
Sample rate: 1000
Store type: always fast

Data1
Time (s) 1A (mV/V) 1C (mV/V) 2A (mV/V) 2C (mV/V) 3A (mV/V) 3C (mV/V) vac (V) 1A/Filter (-) 1C/Filter (-) 2A/Filter (-) 2C/Filter (-) 3A/Filter (-) 3C/Filter (-)
0 0.106609464 0.018956196 0.035648104 -0.003556907 0.001790728 -0.009762328 9.993896484 0.106609464 0.018956199 0.035648108 -0.003556907 0.001790732 -0.009762332
0.001 0.107998252 0.020937454 0.03582811 -0.003382862 0.001793113 -0.00983147 9.993906975 0.106609464 0.018956199 0.035648108 -0.003556907 0.001790732 -0.009762332
0.002 0.106719136 0.018617641 0.036022421 -0.003088415 0.00186583 -0.009559672 9.993967056 0.106609464 0.018956199 0.035648108 -0.003556907 0.001790732 -0.009762332
0.003 0.108490586 0.019977819 0.037318226 -0.002170503 0.002591815 -0.00853328 9.993991852 0.106609464 0.018956199 0.035648108 -0.003556907 0.001790732 -0.009762332
0.004 0.10697782 0.01085354 0.045464989 0.00536114 0.006737914 -0.002019685 9.993905067 0.106609464 0.018956199 0.035648108 -0.003556907 0.001790732 -0.009762332
0.005 0.104278922 0.000512134 0.044724699 0.005067885 0.005845036 -0.00261031 9.993927002 0.106609464 0.018956201 0.035648108 -0.003556907 0.001790732 -0.009762332
0.006 0.106391311 0.000757434 0.042880531 0.003550351 0.004465785 -0.004037898 9.9939394 0.106609464 0.018956203 0.035648108 -0.003556906 0.001790733 -0.009762331
0.007 0.106727481 0.000719558 0.042283293 0.003102124 0.003832784 -0.004347842 9.993917465 0.106609471 0.018956203 0.035648111 -0.003556902 0.001790734 -0.009762329
0.008 0.106937173 0.004424583 0.03767943 -0.00115484 0.001367535 -0.00160155 9.993983269 0.106609479 0.018956203 0.035648122 -0.003556893 0.001790738 -0.009762322
0.009 0.108284354 0.013386738 0.033576246 -0.005182922 -0.000486169 -0.01132993 9.994004425 0.106609486 0.018956196 0.035648145 -0.003556872 0.001790748 -0.009762307
0.01 0.109060943 0.02258135 0.029537436 -0.008939207 -0.002113376 -0.014577191 9.993953705 0.106609508 0.018956166 0.035648189 -0.00355683 0.001790768 -0.009762274
0.011 0.10943234 0.029896932 0.029337164 -0.00946492 -0.001796279 -0.01455931 9.993979454 0.106609538 0.018956097 0.035648271 -0.003556754 0.001790803 -0.009762214
0.012 0.108321309 0.033273231 0.026432034 -0.012430847 -0.00325401 -0.017090123 9.993935585 0.106609575 0.018955957 0.035648409 -0.003556624 0.001790863 -0.00976211
0.013 0.109804273 0.03651334 0.02918696 -0.010264814 -0.00142673 -0.014989655 9.993938446 0.106609628 0.018955708 0.035648629 -0.003556417 0.001790957 -0.009761945
0.014 0.107768178 0.030126106 0.033942219 -0.005789697 0.001194682 -0.01122145 9.993947983 0.106609702 0.018955296 0.035648957 -0.003556107 0.001791096 -0.009761697
0.015 0.106599927 0.023952257 0.036531445 -0.003177822 0.002370806 -0.009078067 9.994012833 0.106609792 0.018954663 0.035649426 -0.00355662 0.001791291 -0.009761341
0.016 0.106285214 0.020459425 0.035397764 -0.004024288 0.001440253 -0.010026973 9.993951797 0.106609918 0.018953739 0.035650071 -0.003555052 0.001791554 -0.00976085
```

Figure 59: Snapshot of Output data .txt file

14 data columns are present in the .txt files where we considered only 8 of them as we plotted time in minutes against the filtered data of each gauge ( Axial and circumferential stress) signal output given in (mV/V) for the three pipes. In addition to the readings gathered from the pressure sensorlabelled in the .txt file as Vac (V). The plots were done in MATLAB R2019a after importing the columns to the workspace and labeling them accordingly, where the following equations (39) and (40) were used to convert the strain gauge signal outputs into strain ( $\epsilon$ ) and pressure sensor output to pressure unit (mBar) respectively. Thus, a multiaxis plot including pressure in mBar, strain (in the order of  $10^{-5}$ ) and time in minutes was scripted to show the readings throughout the experiment.

$$\epsilon = \frac{(mV/V) \cdot 2}{1000} \quad (39)$$

$$P = 10^{0.778(U-c)} \quad (40)$$

Where in equation (40) , ‘P’ is pressure in mBar, ‘U’ is the output signal in V and c is 6.143 obtained from operating manual of the pressure sensor. Since the columns provided different values where the strain gauge responses were of similar magnitude but the output from the pressure sensor was of a much bigger magnitude the plot must be limited on the y-axis starting it from zero to 1.5. This way we can notice changes as they occur to the strain gauge responses with reference to the time measured and the values recorded from the pressure sensor. Note that the time column was divided by 60 to give time in minutes. The plots are shown next with description on what we interpreted from the bumps, peaks and fluctuations observed. Note that all the filtered data columns



got subtracted from the initial reading value present at time being 0 to ensure compensation of any existential readings before irradiation. We should also state that the left y-axis has been scaled down so that the strain gauges plots are comparable to that of the pressure sensor as they are of higher magnitude.

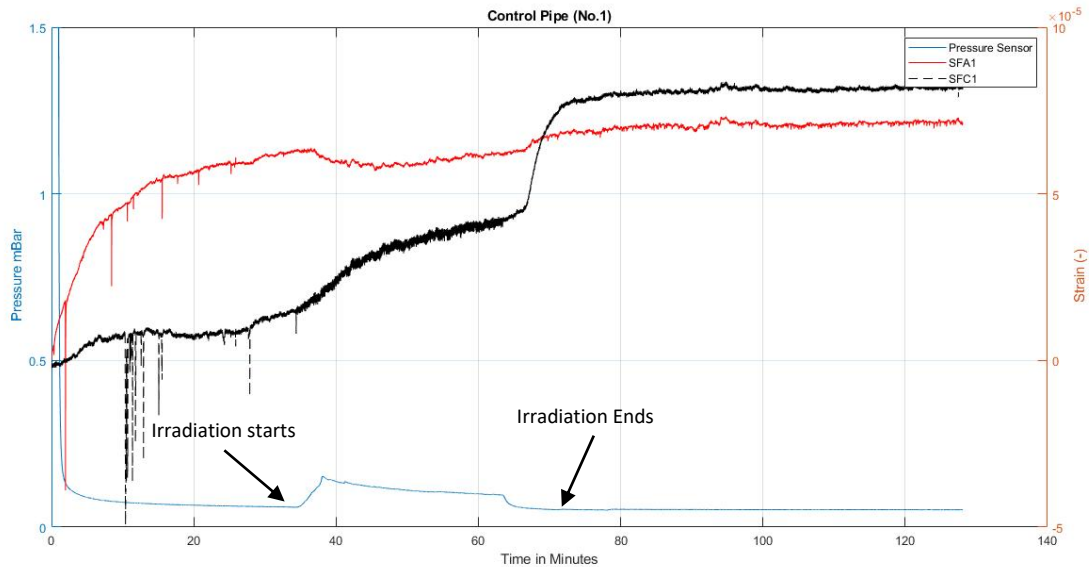


Figure 60: Control Pipe Plot

In figure 60, we can see 3 plots labelled as SFA1 (Axial strain) , SFC1 (Circumferential strain) and Pressure sensor. SFA1 showed a positive strain characteristic indicating the nature of the stress experienced being tensile, as we know that the Irradiation approximately started in the 33<sup>rd</sup> minute of the plot duration we can notice a gradual decrease of axial strain during the period of irradiation followed by normal steady fluctuations in the cooling down period. The circumferential stress (SFC1) showed increasing fluctuations pattern during the irradiation period as the temperature increases leading it to an eventual higher magnitude than the axial stress after the irradiation stopped and thus the set up was left to cool down. This plot tells us that the response of circumferential (hoop ) stress is sensitive to temperature as it leaves residual stresses increasing the overall magnitude of circumferential stress due to thermal loading as the pipe was not subjected to internal vacuum pressure. Moreover, the spikes noted in the beginning of the plot of the strains can be due to transient surges that the strain gauges experienced at the start.

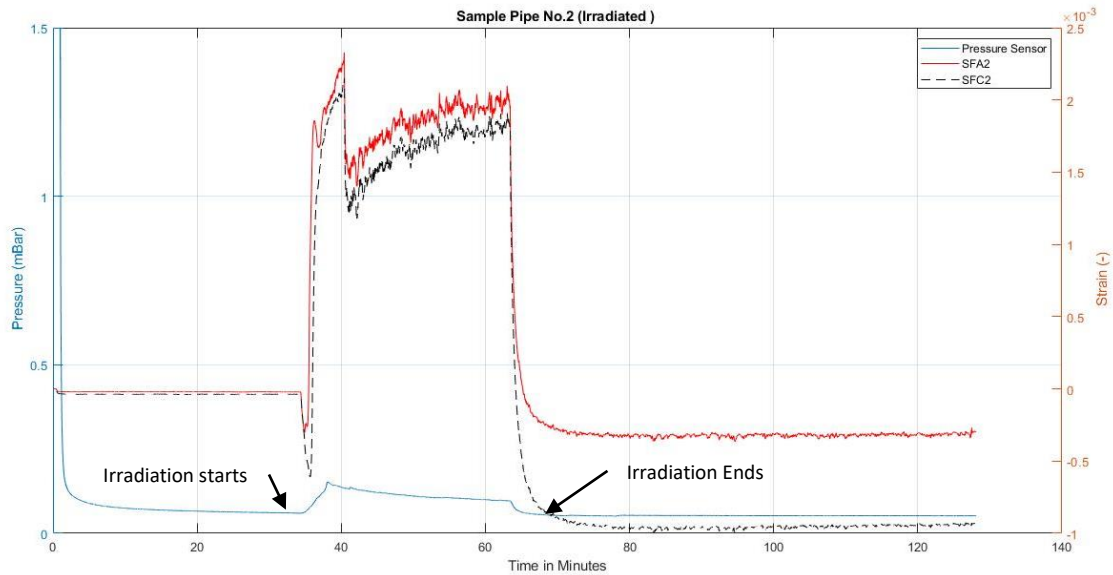


Figure 61: Sample Pipe No.2 Plot

In figure 61, the plot of the top pipe (No.2) strain gauge responses is shown. Initially, as this pipe is connected to the sample assembly that is evacuated through the vacuum pump down to  $10^{-2}$  mBar. The strains had a steady pattern with no fluctuations on either axial (SFA2) nor circumferential (SFC2) strain below zero indicating a negative value due to compression experienced from evacuation but the fact that the output was showing steady horizontal line with no fluctuations is an odd unexpected behavior. When the irradiation started a small drop followed by a rapid increase of both strains experienced by the pipe, differing in magnitude is the axial strain having the highest peak on the plot. This indicates that the heat caused by the irradiation is inducing more axial stress on the pipe, that can be due to micro expansion of the molecules of the pipe due to thermal loading building up. Furthermore, after the peak fluctuations during the irradiation period the strains decreased rapidly back to lower levels of strain with higher magnitude than initial indicating the pipe being under compression again with no much fluctuations which might tell us that the strain gauges experienced some sort of detachment due to the lack of readings and steady non rapid output. By the end of the recording, the circumferential strain that had significantly higher compression magnitude compared to the axial strain, showing us its sensitivity towards heating being more than axial strain. Moreover, the magnitude of the strain measured is in the order of  $10^{-3}$  which is bigger than the other two strain gauge data obtained hence the possibility of detachment causing bigger strain output can be valid.

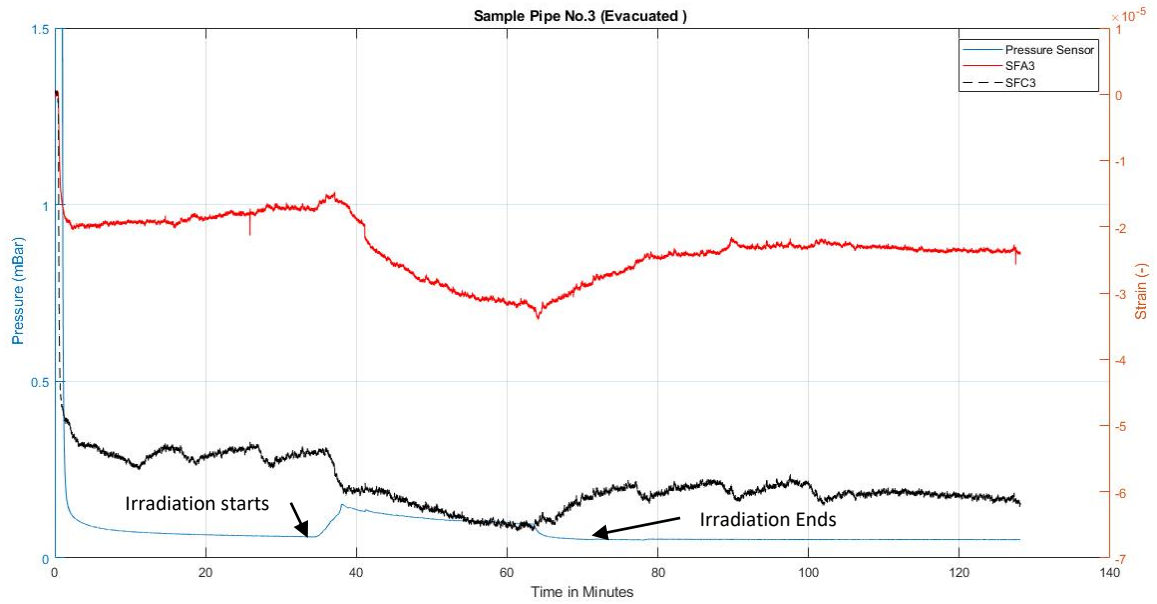


Figure 62: Sample Pipe No.3 Plot

In figure 62, the plot of the bottom pipe (No.3) strain gauge responses is shown. The plot is mostly showing negative values of strain indicating that the stress experienced by the pipes as compressive. Since the bottom pipe is connected to the vacuum pump through the KF40 flange, therefore it is experiencing internal compression due to the evacuation that took place. We can notice that during the irradiation period the strain magnitude increased in the compressive manner indicating possible effects of temperature gradient (increased temperature), even though the target source was aimed at the top region between the top and control pipe. We should also mention that the connection of our strain gauges was the quarter bridge configuration and it does not compensate temperature effects that can also be leading to the significant presence of the dip on the strain plots during the irradiation period. Moreover, in all of the 3 plots we can say that the magnitude of the circumferential stress is always bigger than that of the axial, confirming the thin wall cylinder theory formulae.

### 3.1.6. Strain Gauge responses after irradiation

After Irradiation of the pipes, they were stored for 40 days or more till their radiation level is safe to handle. Where after, we would like to check the functionality and responses of the strain gauges after radiation exposure. Some observations were made as we can notice the top sample pipe (no.1) biaxial strain gauge was peeled off, including one of the solder pads which can be due to the adhesive evaporating, the connection wires experienced discoloration as well as the solder color did change which might indicate changes in the resistance of the wire causing possible alterations in the signal outputs.



*Figure 63: Irradiated Sample pipe (No.2), peeled off strain gauge*

In figure 63, we can notice the discoloration that seems like a burning effect of the white tape around the pipe indicating the elevated temperatures that can probably cause full degradation of the tape if it was kept for a longer period. Moreover, is the discoloration of the stranded wire covers as they were brown, white, and gray before irradiation. After exposition, the color changed to black due to the burning caused by the ionizing radiation. In addition to the puffy looking solder with a brighter color than its initial silver look that it had before exposure (see figure 64), this might have affected the resistances of the wires in a way giving either higher or lower output responses.



*Figure 64: Sample pipe (No.2) , Before Irradiation*

In order to confirm the hypothesis B, the experiment was repeated in CTU Labs using an older turbomolecular pump that does not reach as low levels as the one used in the Irradiation chamber. Similar procedure was followed as the first experiment. Hence, the pipes were assembled and a rosette Strain gauge was connected instead of the peeled off biaxial strain gauge on the sample pipe (No.1). The cables were connected and their functionality was checked via the DEWETRON DAQ.



*Figure 65: Sample Assembly Set up in CTU*



*Figure 66: Vacuum pump used in CTU*

To check whether the strain gauge responses differs before and after irradiation, we will consider the biaxial strain gauge that is still attached correctly on the sample pipe (No.3) as the plot we obtained from the first experiment seemed like the most reasonable one. Therefore, from the second experiment we will check what is the lowest achievable pressure by the pump from the pressure sensor reading and check the output value obtained from the biaxial strain gauge that was applied on the bottom pipe. Then considering this lowest value of pressure achieved by the older vacuum pump , we check the closest value to that pressure that was achieved on the first experiment in the irradiation chamber and hence check the strain gauge outputs perceived and compare the values.

As the evacuation started we were keeping track of the readings on the pressure sensor and waited till the value was not fluctuating no more. This is where we assumed that the pipeswere evacuated to the pump's limit. In order to induce some stresses considering that the element of radiation was not there. We altered the valve between the hose and the pipe to induce some stresses caused by the pressure differences to see if the strain gauges will catch the responses due to the valve being opened and closed. The plot of the sample pipe (No.3) strains included the vacuum pump being started and turned off twice. In figure 67, the plot of sample pipe (No.3) is shown. We can see 6 bumps on the pressure sensor plot caused by the following order :

1. Initial Evacuation.
2. Stopping the Pump.
3. Opening the Valves.
4. Starting the pump.
5. Stopping the Pump again.



## 6. Opening the valves.

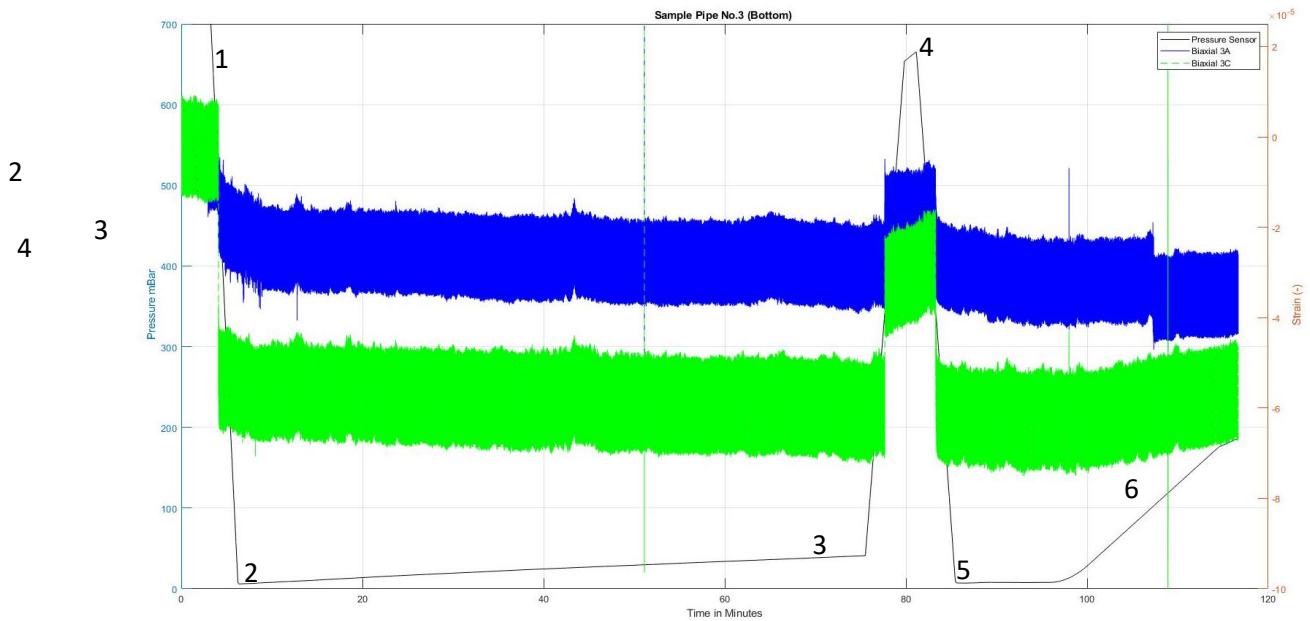


Figure 67: Sample Pipe (No.3) 2<sup>nd</sup> experiment plot.

Now according to the data file that was used to plot the output of the biaxial strain gauge on the sample pipe (No.3) from the **second** experiment:

- $P_{2nd\ Experiment} = 5.1674\ mBar$ ; is the lowest pressure achieved.

The strain values obtained from the two grids of the Biaxial strain gauge at that pressure is :

- $\varepsilon_{Circumferential} = -5.422 \times 10^{-5}$
- $\varepsilon_{Axial} = -1.829 \times 10^{-5}$

Both values of strain are negative indicating compression experienced by the pipe at that pressure.

Now according to the data file obtained to plot the output of the biaxial strain gauge on the sample pipe (No.3) from the **first** experiment:

- $P_{1st\ Experiment} = 5.1641\ mBar$  ; is the pressure closest to the lowest pressure obtained in the **second** experiment.

The strain gauge response values obtained from the two grids of the Biaxial strain gauge at that pressure is :

- $\varepsilon_{Circumferential} = -4.676 \times 10^{-5}$
- $\varepsilon_{Axial} = -1.557 \times 10^{-5}$

Both readings of strain output have a negative value indicating compressive strain which is the state the pipe is at when being evacuated down to the range of 5.16 mBar (516 Pa) , this can

substantiate hypothesis B where we can notice no significant differences in the strain gauge responses before and after irradiation.

### 3.1.7. Finite Element Analysis (FEA) simulation

To check the stresses and expected deformation caused by vacuum on the structural integrity of the composite pipe, FEA analysis was performed including stress and critical buckling analyses were performed on ABAQUS. The model was simplified to a thin wall cylinder of thickness 0.91 mm, internal diameter 52 mm and length of 130 mm. Since our pipe is a CFC composite, we obtained the following data from the manufacturer (COMPOTECH).

Composite Mechanical Property	Magnitude (MPa)
Effective Axial Modulus ( $E_x$ )	21913
Effective Tangential Modulus ( $E_y$ )	124603
Effective Shear Modulus ( $G_{xy}$ )	4837

Table 15: CFC sample Mechanical Properties.

Layer Number	Orientation of fiber	Layer thickness	Volume Fraction ( $V_f$ )	Fiber type
-	°	mm	%	-
1	89	0.27	63	Hypersensitive Carbon
2	+/- 21.7	0.45	63	Hypersensitive Carbon
3	89	0.19	63	Hypersensitive Carbon

Table 16: CFC sample Layers Composition.

Knowing the simplified pipe parameters, a circle with radius 26 was extruded up to a height of 130 mm. Given this provided information the model of the composite chosen is that of a Lamina. Where material properties required by the software are  $E_1$ ,  $E_2$ ,  $G_{12}$ ,  $\nu_{12}$ ,  $G_{13}$  and  $G_{23}$ . Where  $G_{12}$  refers to the In-plane shear modulus,  $G_{13}$  and  $G_{23}$  refer to the transverse shear modulus. Hence, for simplification the following assumptions were set:

- $E_1 = 21913$  MPa
- $E_2 = 124603$  MPa
- $\nu_{12} = \text{Poisson's ratio} = 0.3$
- $G_{12} = 4837$  MPa
- $G_{13} = 4837$  MPa



- $G_{23} = 3100 \text{ MPa}$

Moreover, the material properties set up, using the composite layup manager the composition of the lamina is set according to Table 16 . The Lamina layers stack up is shown in figure 68. Following the layer composition , the assembly is set by selecting the part through the program where we move forward to the step manager to set the type of analysis we would like to perform. Static (General) is the procedure selected to perform the analysis of stress where the loads are due to inside vacuum pressure down to ( $10^{-2} \text{ mBar} = 1 \text{ Pa}$ ) and outside ambient pressure being 101325 Pa. The pipe is then referenced, and the boundary conditions are fixed supports on the end faces. The software meshes the part bearing in mind that the student version of ABAQUS is limited to 1000 nodes. Hence, the job is created and submitted to obtain results of the stress conditions set.

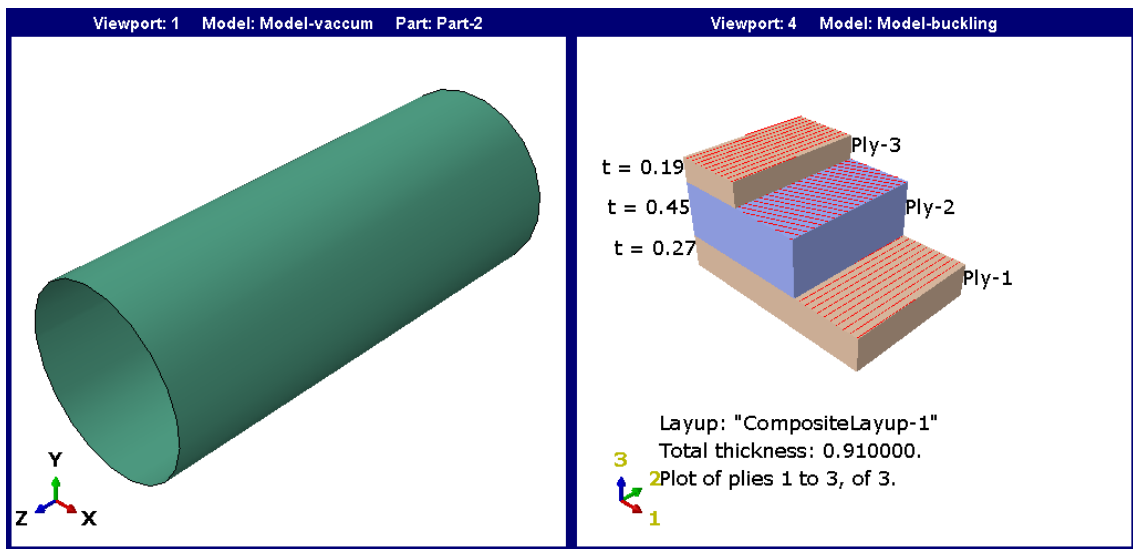


Figure 68: Modeled pipe , Lamina lay-up composition thickness in mm

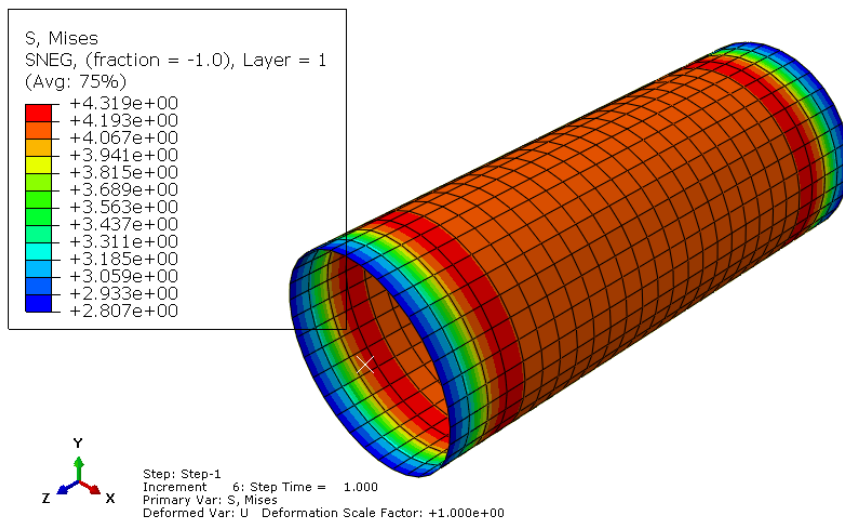


Figure 69: Modeled pipe, Equivalent Von-mises stress (MPa)

In figure 69, we can see the equivalent stress state of the pipe due to internal vacuum and external ambient pressure. The lowest equivalent stress magnitudes are those present on the end faces of the

pipe as they are constrained with fixed support and the maximum is in the mid-section of the pipe. Most of the mid-section of the pipe is experiencing an average equivalent stress approximately 4.19 MPa.

To be able to tell the nature of most of the stress experienced by the pipe due to the conditioning elements being the vacuum internally and externally ambient pressure. A plot of Maximum principal stress is shown in figure 70. We can notice that the color scale has only negative values which tells us that the pipe is under compression. Which makes sense considering the smaller number of air molecules when internally there is vacuum pressure and the pressure exerted by the ambient pressure molecules loading up the pipe with compression. As the pipe is loaded with compressive stress there will exist some deformation even though it is of small values. In figure 71 we can see the deformation on the pipe due to the compressive stresses being experienced, especially in the mid-section is where the maximum magnitude of deformation exists up to a maximum of 0.000561 mm and the ends having minimal as they are fixed.

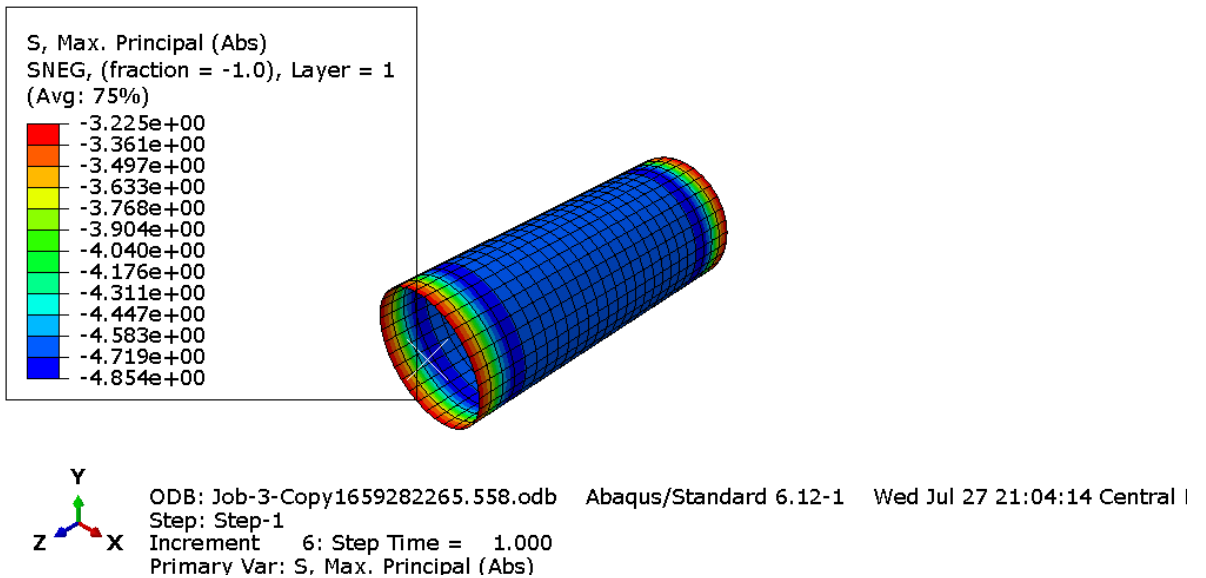


Figure 70: Modeled pipe , Maximum Principal stress (MPa)

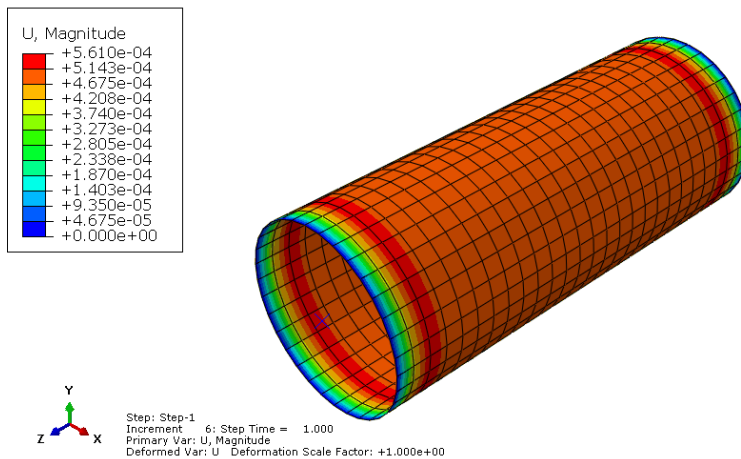


Figure 71: Modeled pipe, Magnitude of deformation (mm)

To check the structural integrity of the pipe under axial loading, buckling analysis will be performed. Similar set up steps that was done for the vacuum analysis is done again for the buckling analysis up until selection of procedure, where we change it to linear perturbation and pick “Buckle”. Thus, we then set the load considering the axis of the pipe as this is where it will be acting on which is the z axis in our model’s case. Furthermore, the 1<sup>st</sup> mode of buckling is what we are interpreting as we are considering fixed supports on both ends. In figure 72, we can see the deformation of the pipe under the 1<sup>st</sup> mode of buckling.

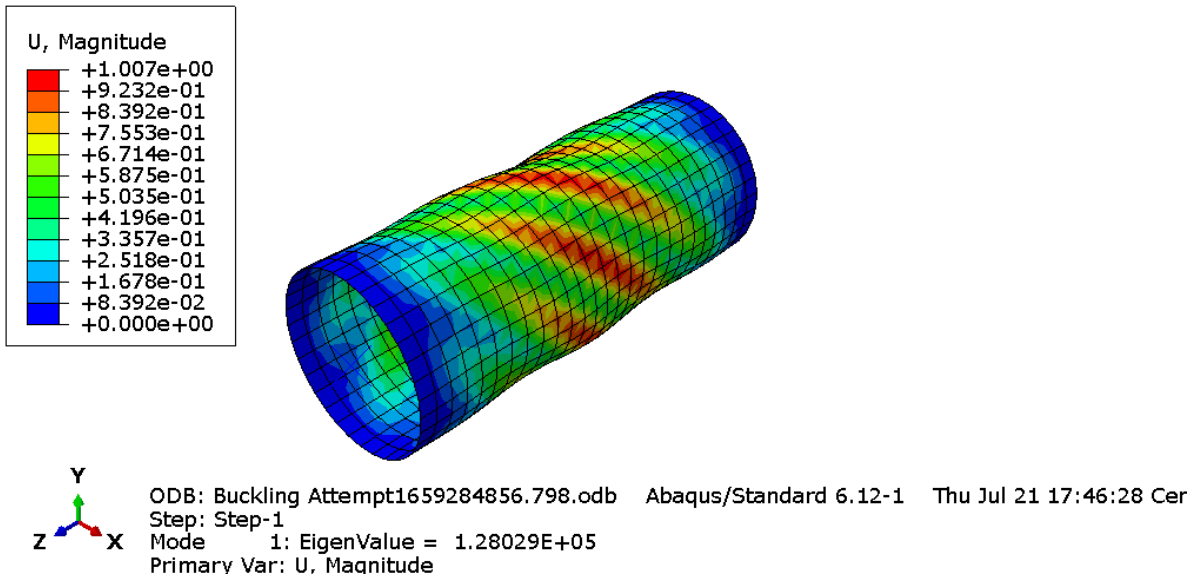


Figure 72: Modeled pipe, Magnitude of Buckling deformation (mm)

To quantify the buckling stress that leads to this deformation shown in figure 72 we can simply take the Eigen value shown in the plot and divide it by the surface area of the pipe and this value would be the critical buckling pressure for the 1<sup>st</sup> mode as shown below :

$$Area_{(pipe)} = \frac{\pi(D^2 - (D - 2t)^2)}{4}$$

Where ‘D’ is the outside diameter of the pipe being 52.91 mm and t is the wall thickness which is 0.91mm

$$Area_{(pipe)} = \frac{\pi(52.91^2 - (52.91 - 2(0.91))^2)}{4} = 148.7 \text{ mm}^2$$

$$\sigma_{Buckling} = \frac{Eigen \ Value}{Area_{(pipe)}} = \frac{1.28029 \times 10^5 \ N}{148.7 \ \text{mm}^2} = 861 \ \text{MPa}$$

### 3.1.8. Theoretical deformation due to internal Vacuum pressure

Considering our CFC pipe as an orthotropic material we can use the generalised Hooke's law for a linear elastic material theory and inverting it giving us the general strain-stress relationship for a 3D body in a 1-2-3 orthogonal cartesian coordinate system which is [89] :

$$\begin{bmatrix} \varepsilon_1 \\ \varepsilon_2 \\ \varepsilon_3 \\ \gamma_{23} \\ \gamma_{31} \\ \gamma_{12} \end{bmatrix} = \begin{bmatrix} S_{11} & S_{12} & S_{13} & S_{14} & S_{15} & S_{16} \\ S_{21} & S_{22} & S_{23} & S_{24} & S_{25} & S_{26} \\ S_{31} & S_{32} & S_{33} & S_{34} & S_{35} & S_{36} \\ S_{41} & S_{43} & S_{43} & S_{44} & S_{45} & S_{46} \\ S_{51} & S_{52} & S_{53} & S_{54} & S_{55} & S_{56} \\ S_{61} & S_{62} & S_{63} & S_{64} & S_{65} & S_{66} \end{bmatrix} \begin{bmatrix} \sigma_1 \\ \sigma_2 \\ \sigma_3 \\ \tau_{23} \\ \tau_{31} \\ \tau_{12} \end{bmatrix}$$

Where we can simplify and redefine the elements subscripted in the matrix to the given assumptions, we have to determine the deformation caused due to internal vacuum pressure and so we will write the same equation as :

$$\begin{bmatrix} \varepsilon_x \\ \varepsilon_y \\ \gamma_{xy} \end{bmatrix} = \begin{bmatrix} S_{11} & S_{12} & 0 \\ S_{12} & S_{22} & 0 \\ 0 & 0 & S_{66} \end{bmatrix} \begin{bmatrix} \sigma_x \\ \sigma_y \\ \tau_{xy} \end{bmatrix}$$

Where :

- $\sigma_x$  is the stress acting on the x-plane being the longitudinal stress on the pipe.
- $\sigma_y$  is the stress acting on the y-plane being the circumferential (hoop) stress on the pipe.
- $\tau_{xy}$  is the shear stress induced on the xy plane.
- $\varepsilon_x$  and  $\varepsilon_y$  is the strain due to the stress acting on x and y planes respectively.
- $\gamma_{xy}$  is the shear strain due to the shear stress acting on the xy plane.
- $S_{ij}$  are elements of the compliance matrix.

Given :

- $p_i = 1 \text{ Pa}$
- $E_x = 21913 \text{ MPa}$
- $E_y = 124609 \text{ MPa}$
- $G_{xy} = \text{shear modulus in } xy \text{ - plane} = 4837 \text{ MPa}$
- $d_i = 52 \text{ mm}, t = 0.91 \text{ mm}$  and  $L = 130 \text{ mm}$
- Assuming Poisson's for our pipe  $\nu = 0.3$

Hence for thin- wall pipes we can calculate :

$$\sigma_y = \frac{P_i d_i}{2t} = \frac{(1)(52)}{2(0.91)} = 28.60 \text{ Pa}$$

$$\sigma_x = \frac{P_i d_i}{4t} = \frac{(1)(52)}{4(0.91)} = 14.30 \text{ Pa}$$

$$\tau_{xy} = \frac{\sigma_y - \sigma_x}{2} = \frac{28.6 - 14.3}{2} = 7.15 \text{ Pa}$$

Thus we can quantify the elements of the compliance matrix ( $S_{ij}$ ) using the given mechanical properties where :

- $S_{11} = \frac{1}{E_x} = \frac{1}{21913 \times 10^6} = 4.56 \times 10^{-11} \text{ Pa}^{-1}$
- $S_{12} = \frac{\nu}{E_x} = \frac{0.3}{21913 \times 10^6} = 1.369 \times 10^{-11} \text{ Pa}^{-1}$
- $S_{22} = \frac{1}{E_y} = \frac{1}{124603 \times 10^6} = 8.025 \times 10^{-12} \text{ Pa}^{-1}$
- $S_{66} = \frac{1}{G_{xy}} = \frac{1}{4837 \times 10^6} = 2.067 \times 10^{-10} \text{ Pa}^{-1}$

Now we plug in the quantities calculated in the matrix :

$$\begin{bmatrix} \varepsilon_x \\ \varepsilon_y \\ \gamma_{xy} \end{bmatrix} = \begin{bmatrix} 4.56 \times 10^{-11} & 1.369 \times 10^{-11} & 0 \\ 1.369 \times 10^{-11} & 8.025 \times 10^{-12} & 0 \\ 0 & 0 & 2.067 \times 10^{-10} \end{bmatrix} \begin{bmatrix} 14.3 \\ 28.6 \\ 7.15 \end{bmatrix}$$

$$\begin{bmatrix} \varepsilon_x \\ \varepsilon_y \\ \gamma_{xy} \end{bmatrix} = \begin{bmatrix} 4.56 \times 10^{-11}(14.3) & 1.369 \times 10^{-11}(28.6) & 0 \\ 1.369 \times 10^{-11}(14.3) & 8.025 \times 10^{-12}(28.6) & 0 \\ 0 & 0 & 2.067 \times 10^{-10}(7.15) \end{bmatrix}$$

$$\begin{bmatrix} \varepsilon_x \\ \varepsilon_y \\ \gamma_{xy} \end{bmatrix} = \begin{bmatrix} 4.56 \times 10^{-11}(14.3) + 1.369 \times 10^{-11}(28.6) \\ 1.369 \times 10^{-11}(14.3) + 8.025 \times 10^{-12}(28.6) \\ 2.067 \times 10^{-10}(7.15) \end{bmatrix}$$

So , the induced strain due to internal vacuum pressure gives the following values :

$$\begin{bmatrix} \varepsilon_x \\ \varepsilon_y \\ \gamma_{xy} \end{bmatrix} = \begin{bmatrix} 1.04 \times 10^{-9} \\ 4.25 \times 10^{-10} \\ 1.48 \times 10^{-9} \end{bmatrix}$$

And we know that :

$$\Delta C = \varepsilon_h \cdot (\pi d)$$

Where  $\varepsilon_h = \varepsilon_y$  is caused by  $\sigma_y$  and we can therefore compute the change in circumference :

$$\Delta C = (4.25 \times 10^{-10}) \cdot (\pi(52)) = 6.94 \times 10^{-8} \text{ mm} = 6.94 \times 10^{-5} \mu\text{m}$$

The change in length due to the longitudinal stress can be simply computed by :

$$\Delta L = L \cdot \varepsilon_x = (130)(1.04 \times 10^{-9}) = 1.35 \times 10^{-7} \text{ mm} = 1.35 \times 10^{-4} \mu\text{m}$$

Thus, we can notice that the possible deformation due to internal vacuum is of negligible magnitude.

To compute the buckling pressure due to a compressive load we can use the Euler buckling equation developed for Isotropic materials but modified to consider the influence of material orthotropy, the following formula can be used [97]:

$$\sigma_b = \frac{\pi^2 \cdot E_x}{\left[\left(\frac{Kl}{r}\right)^2 + 1.2\pi^2\left(\frac{E_x}{G_{xy}}\right)\right]}$$

Where :

- $E_x$  is the axial stiffness in the direction of the compressive loading (21913 MPa)
- $G_{xy}$  is the shear stiffness in the direction of buckling (4837 MPa)
- $l$  is the length of the pipe , assuming the fixed support ends being the end faces. (L = 130 mm)
- $K$  is the constraint factor which is 1 for the case of fixed supports. (k=1)
- $r$  is the radius of gyration of the pipe's cross section , where :

$$r = \sqrt{\frac{\text{Area Moment of Inertia for a pipe}}{\text{Area of pipe}}} = \sqrt{\frac{\left(\frac{\pi(52.91^4 - 52^4)}{64}\right)}{\left(\frac{\pi(52.91^2 - 52^2)}{4}\right)}} = 18.5 \text{ mm}$$

Hence we plug in the given in the buckling stress formula to we obtain :

$$\sigma_b = \frac{\pi^2 \times (21913 \times 10^6)}{\left[\left(\frac{(1)(0.13)}{(0.0185)}\right)^2 + 1.2\pi^2\left(\frac{21913 \times 10^6}{4837 \times 10^6}\right)\right]} = 2.1 \text{ GPa}$$

#### 4. Discussion and Conclusion

In general , composite material buckling theory is not quite commonly investigated. As applications that include buckling analysis are mostly done on conventional materials that have been studied thoroughly. Considering the application of the CFC pipe in an accelerator facility, such pipes would be of much bigger dimensions than the samples we investigated in this thesis. Therefore, the susceptibility of buckling is definitely one of the failure modes that should be digged into deeper during the material selection stage of design.

The irradiated evacuated sample pipe (No.2) showed some minor discoloration or could be a gassing phenomena. This finding should be studied considering the type of resin in the pipe used by the manufacturer and the possibility of different types of resin might have different reactions to irradiation at various doses. Another remark, would be the questioning the effectivity of the resin or how long can it endure irradiation and not cause any internal defects affecting the structural integrity of the pipe as the irradiation might be changing the internal structure of the resin.

Moreover, the fact that for the irradiated evacuated pipe (No.2) strain gauge peeled off after irradiation puts some doubts on the reliability of readings obtained from the strain gauge responses as the magnitude of strain measured was in the order of  $10^{-3}$  which is bigger than the other two pipes measured being  $10^{-5}$ . As initially when the pipes were assembled the strain gauge backing strip seemed to be in tight contact with the pipe and did not have any gaps that might lead it to peel off. This can be due to the adhesive becoming more ductile as the temperature increases making it weaker. Adding to that, the solder of the strain gauge that peeled off had a different brighter color than its initial silver color this might lead to alterations in the resistance of the wires giving different responses either in higher or lower magnitudes.

In regard to the FEA performed we should bear in mind that the ABAQUS version used is the student edition one which is limited to 1000 nodes. Hence, more accurate results would be achieved if the number of nodes is increased as results are dependant on the number of nodes that the software uses to perform calculations giving us results. Nevertheless, the models simulated give a good idea about what can be expected when subjected to internal vacuum pressure .

1) From the modeled FEA analysis the following results were obtained :

- 1) The equivalent stress when the pipe is subjected to internal vacuum (1 Pa) and external ambient pressure (101325 Pa) has a maximum of 4.192 MPa , majorly located in the mid section of the pipe.
- 2) The Principal stress acting on the pipe is of compressive nature with a maximum of 4.85 MPa , also majorly located in the mid section of the pipe.
- 3) Maximum deformation due to the internal vacuum pressure (1 Pa) is majorly in the mid section of the pipe with a magnitude of  $5.61 \times 10^{-4}$  mm.

- 4) Maximum deformation from 1<sup>st</sup> mode of buckling has a magnitude of 1mm , and critical stress computed from eigen value obtained from model is 861 MPa.
- 2) From the theoretical deformation due to internal vacuum pressure calculations , the following results were obtained :
  - 1) Circumferential stress generated due to 1 Pa of vacuum pressure is 28.6 Pa.
  - 2) Longitudinal Stress generated due to 1 Pa of vacuum pressure is 14.3 Pa.
  - 3) Circumferential strain generated is equal to  $4.25 \times 10^{-10}$
  - 4) Longitudinal strain generated is equal to  $1.04 \times 10^{-9}$ .
  - 5) Change in circumference due to circumferential stress is of negligible magnitude being  $6.94 \times 10^{-8}mm$ .
  - 6) Change in length due to Longitudinal stress is also of negligible magnitude being  $1.35 \times 10^{-7}mm$  .
  - 7) Buckling stress calculated using modified Euler buckling equation is 2.1 GPa.

The results obtained gave an overview of what the material can experience when subjected to such conditions, the deformation theoretical deformation calculated is of negligible magnitude when compared to that of the FEA model. The major difference being the magnitude of the buckling stress, where the theoretical value calculated gives a value more than double the modeled result through abaqus. Other equations can be applied neglecting some of the assumptions might improve the results obtained to give a similar value calculated theoretically to that of the FEA simulation. Moreover , the experimental results measured from the strain gauges and plotted in MATLAB gave strains of a bigger magnitude than the theoretical calculation where it was in the order of  $10^{-5}$ .

Hypothesis B was confirmed as we checked the lowest achievable pressure in the 2<sup>nd</sup> experiment in CTU which is 5.167 mBar and the closest pressure sensed in the 1<sup>st</sup> experiment was 5.1641 mBar. Nevertheless, even though the values differ by 0.0029 mBar the strains measured at that interval were of a negative value indicating compressive nature with magnitudes close to each other as shown in the table below.

Strain (-)	2 <sup>nd</sup> experiment (after Irradiation) P = 5.167 mBar = 516.70 Pa	1 <sup>st</sup> experiment (with Irradiation) P = 5.1641 mBar = 516.41
Circumferential	$-5.422 \times 10^{-5}$	$-4.67 \times 10^{-5}$
Axial	$-1.829 \times 10^{-5}$	$-1.557 \times 10^{-5}$

Table 17: Responses of strain gauge at similar pressure level after radiation and with radiation



In conclusion, with regard to discussing points of interest in this thesis. The experiment needs to be repeated to be able to ensure qualitative results are obtained. Considering hypothesis A, we weren't able to confirm as we can clearly see two different plots when comparing control pipe (No. 1) to the sample pipe (No.2). The sample pipe (No.2) was subjected thoroughly to radiation more than any other pipe in the assembly and it is the only pipe that had its strain gauge gets peeled off and largest strain magnitude, so this keeps a speculation on the output responses obtained by it not being as reliable as the sample pipe (No. 3) for example.

To promote more buckling, we would recommend retrying the experiment using a pipe with bigger diameter and longer length. Doing so might help strain measurements to be caught easily by the strain gauge as it might be possible to have some remarks noticed on the eye level. Additionally, different type of solder can be used and even the same type just to check whether there are significant changes in the outputs obtained from the normal solder and the changed one after irradiation. Another potential replacement would be welding. Furthermore, to check in case of any structural changes occurring in the pipe, samples can be cut into smaller pieces and checked via Light and electron microscopy for further micro and macroscopic investigation.

## 5. References

- [1] Marsh, Harry, and Francisco Rodríguez-Reinoso. 2006. "CHAPTER 9 - Production and Reference Material." Pp. 454–508 in *Activated Carbon*, edited by H. Marsh and F. Rodríguez-Reinoso. Oxford: Elsevier Science Ltd.
- [2] "Carbon fibers," *Wikipedia*. Jun. 27, 2022. Accessed: Jul. 23, 2022. [Online]. Available: [https://en.wikipedia.org/w/index.php?title=Carbon\\_fibers&oldid=1095270709](https://en.wikipedia.org/w/index.php?title=Carbon_fibers&oldid=1095270709)
- [3] "Van der Waals forces Definition & Meaning - Merriam-Webster." <https://www.merriam-webster.com/dictionary/van%20der%20Waals%20forces> (accessed Jul. 23, 2022).
- [4] Bhatt P, Goe A. Carbon Fibres: Production, Properties and Potential Use. *Mat.Sci. Res.India*;14(1). Available from: <http://www.materialsciencejournal.org/?p=5641>
- [5] P. César, B. Queiroz, and D. Zouain, "THE CARBON FIBER DEVELOPMENT FOR URANIUM CENTRIFUGES: A BRAZILIAN COOPERATIVE RESEARCH," Jul. 2022.
- [6] S. Kurbanoglu, B. Uslu, and S. A. Ozkan, "Chapter 28 - Carbon-based nanostructures for electrochemical analysis of oral medicines," in *Nanostructures for Oral Medicine*, E. Andronescu and A. M. Grumezescu, Eds. Elsevier, 2017, pp. 885–938. doi: 10.1016/B978-0-323-47720-8.00029-8.
- [7] M. Minus and S. Kumar, "The processing, properties, and structure of carbon fibers," *JOM*, vol. 57, no. 2, pp. 52–58, Feb. 2005, doi: 10.1007/s11837-005-0217-8.
- [8] E. Fitzer, A. Gkogkidis, and M. Heine, "Carbon Fibers and their Composites (A Review)," *High Temp.-High Press.*, vol. HTHP, pp. 363–392, Aug. 1984.
- [9] H. Khayyam *et al.*, "PAN precursor fabrication, applications and thermal stabilization process in carbon fiber production: Experimental and mathematical modelling," *Prog. Mater. Sci.*, vol. 107, p. 100575, Jan. 2020, doi: 10.1016/j.pmatsci.2019.100575.
- [10] J. A. Auer and J. A. Stick, Eds., "Copyright," in *Equine Surgery (Fourth Edition)*, Fourth Edition., Saint Louis: W.B. Saunders, 2012, p. iv. doi: <https://doi.org/10.1016/B978-1-4377-0867-7.00105-8>.
- [11] N. Saba and M. Jawaid, "3 - Epoxy resin-based hybrid polymer composites," in *Hybrid Polymer Composite Materials*, V. K. Thakur, M. K. Thakur, and A. Pappu, Eds. Woodhead Publishing, 2017, pp. 57–82. doi: 10.1016/B978-0-08-100787-7.00003-2.
- [12] P. S. K. Reddy, C. Nagaraju, and T. H. Krishna, "Optimum Design And Analysis Of Filament Wound Composite Tubes In Pure And Combined Loading," *International Journal of Engineering Research*, vol. 1, no. 8, p. 4, 2012.
- [13] M. F. Ashby, Ed., "Copyright," in *Materials and the Environment (Second Edition)*, Second Edition., Boston: Butterworth-Heinemann, 2013, p. iv. doi: <https://doi.org/10.1016/B978-0-12-385971-6.00017-8>.
- [14] M. Chowdhury, *Manufacturing processes of Carbon Fiber Reinforced Polymer and its beneficial approach to retrofitting and strengthening of structural elements*. 2019.
- [15] H. Hocheng, Ed., "Copyright," in *Machining Technology for Composite Materials*, Woodhead Publishing, 2012, p. iv. doi: <https://doi.org/10.1016/B978-0-85709-030-0.50019-9>.

- [16] “How to Manufacture Carbon Fiber Parts,” Formlabs.  
<https://formlabs.com/blog/composite-materials-carbon-fiber-layup/> (accessed Jul. 24, 2022).
- [17] M. Raji, H. Abdellaoui, H. Essabir, C.-A. Kakou, R. Bouhfid, and A. el kacem Qaiss, “3 - Prediction of the cyclic durability of woven-hybrid composites,” in *Durability and Life Prediction in Biocomposites, Fibre-Reinforced Composites and Hybrid Composites*, M. Jawaid, M. Thariq, and N. Saba, Eds. Woodhead Publishing, 2019, pp. 27–62. doi: <https://doi.org/10.1016/B978-0-08-102290-0.00003-9>.
- [18] N. Nordin, “INTRODUCTION TO COMPOSITE PIPING SYSTEM (With PDF),” *What is Piping*. <https://whatispiping.com/composite-piping-system/> (accessed Jul. 24, 2022).
- [19] Q. Ma, R. Rejab, B. Zhang, M. Merzuki, and N. Manoj Kumar, Wireless technology applied in 3-axis filament winding machine control system using MIT app inventor, vol. 469. 2019. doi: 10.1088/1757-899X/469/1/012030.
- [20] “Filament Winding - Open Molding,” *CompositesLab*.  
<http://compositeslab.com/composites-manufacturing-processes/open-molding/filament-winding/> (accessed Jul. 24, 2022).
- [21] U. Uygun, “Explanation Of Filament Winding Process,” ML - Best Engineering Blog, Apr. 29, 2021. <https://mechanicalland.com/explanation-of-filament-winding-process/> (accessed Jul. 24, 2022).
- [22] Ö. Özbek, “DETERMINATION OF MECHANICAL BEHAVIORS OF FILAMENT WOUND HYBRID COMPOSITE PIPES,” 2019.
- [23] "Advantages and Disadvantages of Carbon Fibre Reinforcement Polymer," StudyMoose, 15-Oct-2016. [Online]. Available: <https://studymoose.com/advantages-and-disadvantages-of-carbon-fibre-reinforcement-polymer-essay>. [Accessed: 24-Jul-2022]
- [24] D. Ho, T. H. T. Phan, R. J. Mobbs, and R. Reddy, “The use of radiolucent (carbon fibre-reinforced polymer) pedicle screw fixation for serial monitoring of clear cell meningioma: a case report,” *J Surg Case Rep*, vol. 2020, no. 12, p. rjaa510, Dec. 2020, doi: 10.1093/jscr/rjaa510.
- [25]“(PDF) Design of Composite Pipes with Different Fiber Orientations Evaluation of the Internal Pressure Capacity.”  
[https://www.researchgate.net/publication/329272620\\_Design\\_of\\_Composite\\_Pipes\\_with\\_Different\\_Fiber\\_Orientations\\_Evaluation\\_of\\_the\\_Internal\\_Pressure\\_Capacity](https://www.researchgate.net/publication/329272620_Design_of_Composite_Pipes_with_Different_Fiber_Orientations_Evaluation_of_the_Internal_Pressure_Capacity) (accessed Jul. 25, 2022).
- [26] Dianhydrides, “What are Epoxy Composites?” Dianhydrides.com, Jul. 01, 2021.  
<https://dianhydrides.com/what-epoxy-composites/> (accessed Jul. 25, 2022).
- [27] Y. Zhu et al., “Design, fabrication and stiffness analysis of a novel GFRP sandwiched pipe with stiffened core,” *Thin-Walled Structures*, vol. 156, p. 106982, 2020, doi: <https://doi.org/10.1016/j.tws.2020.106982>.
- [28] J. Hodgkinson, S.-R. Shamsuddin, L. Asp, R. Langstrom, and A. Bismarck, Carbon fibre reinforced PVDF pipe. 2013

- [29] B. Hughes, "Composite Pipe vs. Steel." <https://www.thermoflexpipe.com/academy/composite-pipe-vs-steel> (accessed Jul. 25, 2022).
- [30] A. Ahmed, S. Guo, Z. Zhang, C. Shi, and D. Zhu, "A review on durability of fiber reinforced polymer (FRP) bars reinforced seawater sea sand concrete," *Construction and Building Materials*, vol. 256, p. 119484, 2020, doi: <https://doi.org/10.1016/j.conbuildmat.2020.119484>.
- [31] "What is a Composite Pipe?" <https://www.twi-global.com/technical-knowledge/faqs/what-is-a-composite-pipe.aspx> (accessed Jul. 25, 2022).
- [32] lessoadmin, "Ultimate Guide to Composite Pipes," LESSO Blog, Nov. 08, 2021. <https://en.lesso.com/blogs/composite-pipes/> (accessed Jul. 25, 2022).
- [33] "Consulting - Specifying Engineer | How to perform a pipe stress analysis," *Consulting - Specifying Engineer*, Sep. 21, 2017. <https://www.csemag.com/articles/how-to-perform-a-pipe-stress-analysis/> (accessed Jul. 26, 2022).
- [34] "Piping Materials - Temperature Expansion Coefficients." [https://www.engineeringtoolbox.com/pipes-temperature-expansion-coefficients-d\\_48.html](https://www.engineeringtoolbox.com/pipes-temperature-expansion-coefficients-d_48.html) (accessed Jul. 26, 2022).
- [35] "What Is the Difference Between Regular Wall and Thin Wall Stainless Steel Tubing?" <https://componentsupplycompany.com/blog/tag/what-is-the-difference-between-regular-wall-and-thin-wall-stainless-steel-tubing/> (accessed Jul. 26, 2022).
- [36] "Advanced Structural Analysis EGF316 , 4.Cylinders Under pressure" <https://chennachaos.github.io/website/teaching/2017-2018/EGF316/week2/EGF316%20Thin%20and%20Thick%20Cylinders%20-%20notes.pdf/> (accessed Jul. 26, 2022)
- [37] A. Catinaccio, "PIPES UNDER INTERNAL PRESSURE AND BENDING," p. 8. <https://cds.cern.ch/record/1224245/files/?docname=PH-EP-Tech-Note-2009-004&version=all/> (accessed Jul. 26, 2022)
- [38] "What is Hoop Stress? - Definition from Trenchlesspedia." <http://www.trenchlesspedia.com/definition/2799/hoop-stress> (accessed Jul. 26, 2022).
- [39] "Types of Stresses in a Piping System (With PDF) – What Is Piping." <https://whatispiping.com/types-of-stresses-in-a-piping-system/> (accessed Jul. 26, 2022).
- [40] "What is Finite Element Analysis (FEA)?" <https://www.twi-global.com/technical-knowledge/faqs/finite-element-analysis.aspx> (accessed Jul. 26, 2022).
- [41] "Strain Gauge: Working Principle & Diagram | Electrical4U," <https://www.electrical4u.com/>. <https://www.electrical4u.com/strain-gauge/> (accessed Jul. 26, 2022).
- [42] "Measuring Strain with Strain Gages." <https://www.ni.com/en-gb/innovations/white-papers/07/measuring-strain-with-strain-gages.html> (accessed Jul. 26, 2022).
- [43] I. Engineer, "Bonded and Unbonded Strain Gauges," Nov. 19, 2020. <https://instrumentationapplication.com/2020/11/19/bonded-and-unbonded-strain-gauges/> (accessed Jul. 26, 2022).

- [44] “Strain gauge.” <https://www.brown.edu/Departments/Engineering/Courses/En123/Lectures/StrainFromCyber.htm> (accessed Jul. 26, 2022).
- [45] “How to Select the Right Strain Gauge,” HBM, Dec. 15, 2020. <https://www.hbm.com/en/7164/how-to-find-the-right-strain-gauge/> (accessed Jul. 26, 2022).
- [46] “Different Types of Strain Gauge Geometries,” Bestech Australia, Apr. 14, 2020. <https://www.bestech.com.au/blogs/different-types-of-strain-gauge-geometries/> (accessed Jul. 27, 2022).
- [47] E. Staff, “Metal Foil Strain Gauge Principle,” *Inst Tools*, Apr. 01, 2018. <https://instrumentationtools.com/metal-foil-strain-gauge-principle/> (accessed Jul. 27, 2022).
- [48] E. Staff, “Fine Wire Strain Gauge Principle,” *Inst Tools*, Apr. 01, 2018. <https://instrumentationtools.com/fine-wire-strain-gauge/> (accessed Jul. 27, 2022).
- [49] A. E. Workbook, “What is Semiconductor Strain Gauge? Working, Construction & Applications,” *ElectricalWorkbook*, Jul. 27, 2021. <https://electricalworkbook.com/semiconductor-strain-gauge/> (accessed Jul. 27, 2022).
- [50] E. Staff, “Semi-Conductor or Piezo Resistive Strain Gauge Principle,” *Inst Tools*, Apr. 01, 2018. <https://instrumentationtools.com/semi-conductor-or-piezo-resistive-strain-gauge-principle/> (accessed Jul. 27, 2022).
- [51] “Measuring Strain with Strain Gages.” <https://www.ni.com/en-gb/innovations/white-papers/07/measuring-strain-with-strain-gages.html> (accessed Jul. 26, 2022).
- [52] “How Is Temperature Affecting Your Strain Measurement Accuracy?” <https://www.ni.com/en-gb/innovations/white-papers/06/how-is-temperature-affecting-your-strain-measurement-accuracy-.html> (accessed Jul. 27, 2022).
- [53] “Lead (electronics) - Wikipedia.” [https://en.wikipedia.org/wiki/Lead\\_\(electronics\)](https://en.wikipedia.org/wiki/Lead_(electronics)) (accessed Jul. 27, 2022).
- [54] “How does resistance of a conductor vary with temperature?” Toppr Ask. <https://www.toppr.com/ask/question/how-does-resistance-of-a-conductor-vary-with-temperature/> (accessed Jul. 27, 2022).
- [55] “How Particle Accelerators Work,” *Energy.gov*. <https://www.energy.gov/articles/how-particle-accelerators-work> (accessed Jul. 28, 2022).
- [56] “(PDF) Machine Protection and Interlock Systems for Circular Machines - Example for LHC.” <https://www.researchgate.net/publication>
- [57] “44.4 Particle Accelerators and Detectors - University Physics - OpenStax CNX.” <https://cnx.org/contents/dP0ocxV9@5.329:p3nizZII@5/44-4-Particle-Accelerators-and-Detectors> (accessed Jul. 28, 2022).
- [58] N. Marquardt, “INTRODUCTION TO THE PRINCIPLES OF VACUUM PHYSICS,” p. 24. <https://cds.cern.ch/record/582156/files/p1.pdf> (accessed Jul. 28, 2022)
- [59] “Absolute, Gauge, Atmospheric, and Vacuum Pressures.” <https://instrumentationapplication.com/different-types-of-pressures/> (accessed Jul. 28, 2022).

- [60] “Modern vacuum physics (Book, 2005) [WorldCat.org].”  
<https://www.worldcat.org/title/modern-vacuum-physics/oclc/55000526> (accessed Jul. 28, 2022).
- [61] Senior Lab - Experiments "Vacuum Techniques - Vacuum.Pdf"  
<http://web.physics.ucsb.edu/~phys128/experiments/vacuum/> (accessed Jul. 28, 2022)
- [62] “Types of Industrial Vacuum Pumps | Knowledge Hub,” gardnerdenver.  
<https://www.gardnerdenver.com/en-in/knowledge-hub/articles/types-of-vacuum-pumps>  
 (accessed Jul. 28, 2022).
- [63] T. Lish, “Vacuum Pressure: What is it & how do you measure it?”  
<https://www.setra.com/blog/vacuum-pressure-what-is-it-how-do-you-measure-it> (accessed Jul. 28, 2022).
- [64] “Vacuum pressure gauges - How they work | Tameson.com,” Tameson.  
<https://tameson.com/vacuum-pressure-gauge.html> (accessed Jul. 28, 2022).
- [65] “Pressure Sensor Applications: What Are They Used For? | The Design Engineers’ Guide | Avnet Abacus.”  
<https://www.avnet.com/wps/portal/abacus/solutions/technologies/sensors/pressure-sensors/applications/> (accessed Jul. 28, 2022).
- [66] Electricalterminology, “How does a pressure sensor work?,” Electricalterminology, Dec. 01, 2021. <http://www.electricalterminology.com/how-does-a-pressure-sensor-work/> (accessed Jul. 28, 2022).
- [67] Henry E. Frankel "Effect of Vacuum on Materials"  
<https://ntrs.nasa.gov/api/citations/19690026573/downloads/19690026573.pdf>  
 (accessed on Jul.28, 2022)
- [68] “An Introduction to Vacuum Pumps,” Vacaero, Jan. 13, 2016.  
<https://vacaero.com/information-resources/vacuum-pump-technology-education-and-training/1039-an-introduction-to-vacuum-pumps.html> (accessed Jul. 28, 2022).
- [69] F. Bradaschia, “Components of electromagnetic spectrum,” Radio2Space, Jul. 15, 2013.  
<https://www.radio2space.com/components-of-electromagnetic-spectrum/> (accessed Jul. 28, 2022).
- [70] “Primary Radiation Damage in Materials,” Nuclear Energy Agency (NEA).  
[https://www.oecd-nea.org/jcms/pl\\_19620/primary-radiation-damage-in-materials?details=true](https://www.oecd-nea.org/jcms/pl_19620/primary-radiation-damage-in-materials?details=true)  
 (accessed Jan. 26, 2022).
- [71] CDC, “Ionizing Radiation,” Centers for Disease Control and Prevention, Jun. 29, 2021.  
[https://www.cdc.gov/ncet/radiation/ionizing\\_radiation.html](https://www.cdc.gov/ncet/radiation/ionizing_radiation.html) (accessed Jul. 28, 2022).
- [72] “What is Man-made Sources of Radiation - Definition,” Radiation Dosimetry, Dec. 14, 2019. <https://www.radiation-dosimetry.org/what-is-man-made-sources-of-radiation-definition/>  
 (accessed Aug. 02, 2022)..
- [73] Robert Percuoco, "Clinical Imaging (Third Edition)"  
<https://www.sciencedirect.com/topics/biochemistry-genetics-and-molecular-biology/particle-radiation>. (Accessed Jul. 28, 2022).
- [74] “Electromagnetic spectrum | Definition, Diagram, & Uses | Britannica.”  
<https://www.britannica.com/science/electromagnetic-spectrum> (accessed May 23, 2022).

- [75] Ryan K. Funk MD , Nadia N Issa Laack MD, MS "Clinical Cardio Oncology",2016 <https://www.sciencedirect.com/book/9780323442275/clinical-cardio-oncology> (accessed May 23, 2022).
- [76] P. Hosemann, D. Frazer, M. Fratoni, A. Bolind, and M. F. Ashby, "Materials selection for nuclear applications: Challenges and opportunities," *Scr. Mater.*, vol. 143, pp. 181–187, 2018, doi: <https://doi.org/10.1016/j.scriptamat.2017.04.027>.
- [77] O. US EPA, "Particle Accelerators and Radiation Research," Nov. 30, 2018. <https://www.epa.gov/radtown/particle-accelerators-and-radiation-research> (accessed Jul. 29, 2022).
- [78] K. Ammigan, B. D. Hartsell, P. Hurh, and R. M. Zwaska, "Experimental Results of Beryllium Exposed to Intense High Energy Proton Beam Pulses," p. 4, 2016. <https://accelconf.web.cern.ch/napac2016/papers/mopob14.pdf> (accessed Jul. 29, 2022).
- [79] R. Veness, G. Simmons, and C. Dorn, "Development of Beryllium Vacuum Chamber Technology for the LHC," Jan. 2011. [https://www.researchgate.net/publication/241772154\\_Development\\_of\\_Beryllium\\_Vacuum\\_Chamber\\_Technology\\_for\\_the\\_LHC](https://www.researchgate.net/publication/241772154_Development_of_Beryllium_Vacuum_Chamber_Technology_for_the_LHC) (accessed Jul.29,2022).
- [80] "The European Physical Journal C," Springer. <https://www.springer.com/journal/10052> (accessed Jul. 29, 2022).
- [81] D. R. Paschotta, "Beam Collimators." [https://www.rp-photonics.com/beam\\_collimators.html](https://www.rp-photonics.com/beam_collimators.html) (accessed Jul. 29, 2022).
- [82] "Tungsten Alloy Development as Advanced Target Material for High-Power Proton Accelerator - CERN Document Server." <https://cds.cern.ch/record/2799870/files/> (accessed Jul. 29, 2022).
- [83] "Metals Designed for Particle Accelerators," AZoM.com, Jun. 22, 2018. <https://www.azom.com/article.aspx?ArticleID=16206> (accessed Jul. 29, 2022)
- [84] "Metal vs. Plastic Thermoforming - How to Choose? | Productive Plastics." <https://www.productiveplastics.com/metal-vs-plastic-thermoforming-5-key-comparisons/> (accessed Jul. 05, 2022).
- [85] "XY T Rosettes with 2 Measuring Grids for Analyzing Biaxial," HBM, Dec. 16, 2021. <https://www.hbm.com/en/3443/xy-t-rosettes-with-measuring-grids-for-analyzing-biaxial-stress/> (accessed Apr. 24, 2022).
- [86] "DAQP-STG Module Technical reference manual," studylib.net. <https://studylib.net/doc/18653703/daqp-stg-module-technical-reference-manual> (accessed Jul. 29, 2022).
- [87] "DB9 Connector – 9 PIN D-Sub | EDAC Interconnect Solutions | EDAC." <https://edac.net/products/db9-connector/145> (accessed Jul. 29, 2022).
- [88] "Cyclotron TR-24 - Ústav jaderné fyziky AV ČR." <http://www.ujf.cas.cz/en/departments/department-of-accelerators/TR-24/> (accessed Jul. 29, 2022).
- [89] "Mechanics of Composite Materials - 2nd Edition - Autar K. Kaw - Frank." <https://www.routledge.com/Mechanics-of-Composite-Materials/Kaw/p/book/9780849313431> (accessed Aug. 01, 2022).

- [90] S. Rogers, "Radiation exposure: a quick guide to what each level means," the Guardian, Mar. 15, 2011. <http://www.theguardian.com/news/datablog/2011/mar/15/radiation-exposure-levels-guide> (accessed Aug. 02, 2022).
- [91] "Polymer Materials Selection for Radiation-Sterilized Products," mddionline.com, Feb. 01, 2000. <https://www.mddionline.com/materials/polymer-materials-selection-radiation-sterilized-products> (accessed Aug. 02, 2022).
- [92] IUPAC, Compendium of Chemical Terminology, 2nd ed. (the "Gold Book") (1997). Online corrected version: (2006–) "chain scission". doi:10.1351/goldbook.C00961
- [93] "The expression for the determination of Poisson's ratio class 11 physics JEE\_Main." <https://www.vedantu.com/question-answer/the-expression-for-the-determination-of-poissons-class-11-physics-jee-main-5f911f3da88cd54016e41d51> (accessed Aug. 02, 2022).
- [94] M. Nurhaniza, M. K. A. Ariffin, A. Ali, F. Mustapha, and A. W. Noraini, "Finite element analysis of composites materials for aerospace applications," *IOP Conference Series: Materials Science and Engineering*, vol. 11, p. 012010, May 2010, doi: 10.1088/1757-899x/11/1/012010.
- [95] "Isotropic and Orthotropic Materials - 2012 - SOLIDWORKS Help." [https://help.solidworks.com/2012/english/solidworks/cworks/isotropic\\_and\\_orthotropic\\_materials.htm](https://help.solidworks.com/2012/english/solidworks/cworks/isotropic_and_orthotropic_materials.htm) (accessed Aug. 03, 2022).
- [96] Dr. Savvas Triantafyllou, "Quick guide to Abaqus/ CAE" [https://ethz.ch/content/dam/ethz/special-interest/baug/ibk/structural-mechanics-dam/education/femII/ABAQUS\\_Guide.pdf](https://ethz.ch/content/dam/ethz/special-interest/baug/ibk/structural-mechanics-dam/education/femII/ABAQUS_Guide.pdf) (accessed Aug. 03, 2022).
- [97] Dr. Donald F. Adams, "Buckling of composite material compression specimens." <https://www.compositesworld.com/articles/buckling-of-composite-material-compression-specimens> (accessed Aug. 04, 2022).
- [98] MADGETECH Inc, "Introduction to Strain and Strain Gages" [http://www.synergy-mi.com/uploads/3/9/6/2/39627747/strain\\_gage\\_app\\_note.pdf](http://www.synergy-mi.com/uploads/3/9/6/2/39627747/strain_gage_app_note.pdf) (accessed Aug. 04, 2022)



## List of Abbreviations

- 1) CF - Carbon Fiber
- 2) CFC - Carbon Fiber Composite
- 3) CFRP - Carbon Fiber Reinforced Polymer
- 4) GFRP - Glass Fiber Reinforced Polymer
- 5) RF - Radio Frequency
- 6) DNA - Deoxyribonucleic Acid
- 7) FEA - Finite Element Analysis
- 8) FRP - Fiber Reinforced Polymer
- 9) UHM- Ultra high Modulus
- 10) HM- High Modulus
- 11) IM - Intermediate Modulus
- 12) LM - Low Modulus
- 13) HT - High Tensile
- 14) SHT - Super High Tensile
- 15) PAN - Polyacrylonitrile
- 16) HHT - High Heat Treatment
- 17) IHT - Intermediate Heat Treatment
- 18) LHT - Low Heat Treatment
- 19) PVC - Polyvinyl Chloride
- 20) ABS -Acrylonitrile butadiene styrene
- 21) HDPE - High Density Polyethylene
- 22) GRP - Glass Reinforced Plastics
- 23) PEEK - Polyether ether ketone
- 24) DAQ - Data Acquisition systems
- 25) CUSP - cyclotron up scattering process
- 26) EPR - Electron paramagnetic resonance
- 27) KF - Klein Flansche

## List of Tables

1) Table 1: Figures of Merit for Transparent Beampipes.....	20
2) Table 2:Classification of carbon fiber types based on Mechanical Properties.....	26
3) Table 3:Classification of carbon fiber types based on final heat treatment.....	26
4) Table 4:Classification of carbon fiber based on precursor fiber material.....	26
5) Table 5:Physical and Mechanical properties of Carbon fiber.....	27
6) Table 6:Metals and Plastic different specific gravity indicating difference in weight.....	31
7) Table 7:Comparison of plastic/composites and Metal Manufacturing Process steps.....	33
8) Table 8:Mechanical properties of some FRP material types and Steel.....	35
9) Table 9: Linear elastic behavior.....	49
10) Table 10:Different Measurements done by strain gauges.....	51
11) Table 11:Strain gauge Selection criteria for experimental tests.....	52
12) Table 12:Strain gauges with different connection configurations.....	54
13) Table 13: Characteristics of low and high resistance strain gauges.....	55
14) Table 14:Parameters of Cyclotron TR-24.....	73
15) Table 15: CFC Sample Mechanical Properties.....	87
16) Table 16: CFC Sample Layers Composition.....	87
17) Table 17: Responses of strain gauge at similar pressure level after radiation and with radiation.....	97

## List of Figures

1) Figure 1: Typical components of a circular accelerator, RF (Radio-frequency) cavities.....	10
2) Figure 2: Linear accelerator with charged tubes.....	10
3) Figure 3: Absolute, Gauge, Atmosphere, and vacuum pressure.....	12
4) Figure 4: Classification of vacuum pumps.....	13
5) Figure 5: Typical Industrial vacuum pumps.....	14
6) Figure 6: Components of electromagnetic spectrum.....	16
7) Figure 7: Comparison of radiation exposure levels.....	17
8) Figure 8: Displacement cascade initiated by neutron or ion impact.....	18
9) Figure 9: Classification of polymer composites.....	21
10) Figure 10: Hand lay-up schematic.....	23
11) Figure 11: Schematic diagram of filament winding technique.....	23
12) Figure 12: Schematic representation of three types of winding patterns.....	24
13) Figure 13: Schematic diagram of injection molding and reaction injection molding process.....	25
14) Figure 14: Short term strength (stress), of Carbon materials including CFRC compared with C/epoxy and metals.....	28
15) Figure 15: Manufacturing Process of Carbon Fiber (PAN-based).....	29
16) Figure 16: Industrial Carbon Fiber Manufacturing process.....	30
17) Figure 17: Material comparison strength.....	32
18) Figure 18: Specific stiffness comparison.....	32
19) Figure 19: Relationship of part cost with part complexity for plastic and metal.....	34
20) Figure 20: An example of a Glass-fiber reinforced polymer (GFRP) composite.....	34
21) Figure 21: Different pipe materials temperature expansion plot.....	36
22) Figure 22: Stresses acting on a tube due to internal pressure.....	38
23) Figure 23: Cross section of a thin cylinder showing longitudinal stress direction.....	39
24) Figure 24: Element of cylinder cross section subjected to internal and external pressure.....	42
25) Figure 25: Cross section of thick cylinder with closed ends subjected to internal and external pressure.....	46
26) Figure 26: Demonstration of resulting strain due to force applied.....	50
27) Figure 27: Composition of Bonded metallic strain gauge.....	51
28) Figure 28: Different Strain gauge pattern geometries.....	53
29) Figure 29: Metal Foil strain gauge arrangement.....	56
30) Figure 30: Fine wire strain gauge arrangement.....	57
31) Figure 31: Semiconductor type bonded strain gauge.....	58
32) Figure 32: General Wheatstone bridge.....	60
33) Figure 33: quarter bridge strain gauge configurations.....	61
34) Figure 34: Dummy strain gauges eliminating effect of temperature on measurement.....	61
35) Figure 35: Half bridge strain gauge Type I.....	62
36) Figure 36: Half bridge strain gauge Type II.....	62
37) Figure 37: Full-bridge strain gauge Type II.....	63
38) Figure 38: Full-bridge strain gauge Type III.....	63

39) Figure 39: Half-Bridge Configuration.....	64
40) Figure 40: Full-Bridge Configuration.....	64
41) Figure 41: Thermal Output rating.....	64
42) Figure 42: 2 wire and 3 wire connections for quarter bridge sensors.....	66
43) Figure 43: Schematic of experimental setup.....	68
44) Figure 44: Schematic of type of strain gauge used (XY9 Stacked grid with leads).....	69
45) Figure 45: Applied Strain gauges on pipes.....	70
46) Figure 46: Control Pipe , soldered strain gauge lead wires and connection to Wheatstone bridge.....	71
47) Figure 47:connection of strain gauge to DAQP-STG 3 via connector scheme and general specification.....	71
48) Figure 48:Six DB9 connectors connected to DAQ to complete compensation circle of the three straingauges.....	71
49) Figure 49: Strain gauge functionality check and plotting of Output (mV/V) against time (s).....	72
50) Figure 50: Cyclotron TR-24 of the Canadian company ACSI (Advanced cyclotron systems Inc.) in the Czech academy of sciences irradiation chamber.....	72
51) Figure 51: TR-24 EPR current plot through irradiation period.....	74
52) Figure 52: Experiment's Irradiation Report from the TR-24 monitoring system.....	75
53) Figure 53: Vacuum pump connected to pressure sensor through valve top flange.....	76
54) Figure 54:CFC experiment pipes.....	76
55) Figure 55:O-rings mounted on railed pipes.....	77
56) Figure 56: Assembly of railed pipes with costume ring, covers and flanges.....	77
57) Figure 57: BOSCH line laser on TR 24 (cyclotron).....	78
58) Figure 58: Pipes sample assembly taped to metallic framing and connected turbomolecular pump hose.....	78
59) Figure 59: Snapshot of Output data .txt file.....	79
60) Figure 60: Control Pipe Plot.....	80
61) Figure 61: Sample Pipe No.2 Plot.....	81
62) Figure 62: Sample Pipe No.3 Plot.....	82
63) Figure 63: Irradiated Sample pipe (No.2) , peeled off strain gauge.....	83
64) Figure 64: Sample pipe (No.2) , Before Irradiation.....	84
65) Figure 65: Sample Assembly Set up in CTU.....	84
66) Figure 66: Vacuum pump used in CTU.....	85
67) Figure 67: Sample Pipe (No.3) 2nd experiment plot.....	86
68) Figure 68: Modeled pipe, Lamina lay-up composition thickness in mm.....	88
69) Figure 69: Modeled pipe, Equivalent Von-mises stress (MPa).....	88
70) Figure 70: Modeled pipe, Maximum Principal stress (MPa).....	89
71) Figure 71: Modeled pipe, Magnitude of deformation (mm).....	89
72) Figure 72: Modeled pipe, Magnitude of Buckling deformation (mm).....	90

